Czech Technical University in Prague

Faculty of Nuclear Sciences and Physical Engineering

Doctoral Thesis

Carriers of Therapeutic and Diagnostic Radionuclides for Nuclear Medicine

Prague 2022

Ekaterina Kukleva

Bibliographic Entry

Author	Ing. Ekaterina Kukleva Czech Technical University in Prague Faculty of Nuclear Sciences and Physical Engineering Department of Nuclear Chemistry
Title of Dissertation	Carriers of therapeutic and diagnostic radionuclides for nuclear medicine
Degree Programme	Applications of Natural Sciences
Field of Study	Nuclear Chemistry
Supervisor	Asoc. Prof. RNDr. Ján Kozempel, Ph.D. Czech Technical University in Prague Faculty of Nuclear Sciences and Physical Engineering Department of Nuclear Chemistry
Academic Year	2021/2022
Number of Pages	106
Keywords	hydroxyapatite, HAp, nanoparticles, nanomaterials, sorption, ^{99m}Tc, ^{223}Ra, ^{18}F, ^{68}Ga

Bibliografický záznam

Autor	Ing. Ekaterina Kukleva České vysoké učení technické v Praze Fakulta jaderná a fyzikálně inženýrská Katedra jaderné chemie
Název práce	Nosiče terapeutických a diagnostických radionuklidů pro nukleární medicínu
Studijní program	Aplikace přírodních věd
Studijní obor	Jaderná chemie
Školitel	Doc. RNDr. Ján Kozempel, Ph.D. České vysoké učení technické v Praze Fakulta jaderná a fyzikálně inženýrská Katedra jaderné chemie
Akademický rok	2021/2022
Počet stran	106
Klíčová slova	hydroxyapatit, HAp, nanočástice, nanomateriály, sorpce, ^{99m}Tc, ^{223}Ra, ^{18}F, ^{68}Ga

Abstract

Hydroxyapatite (HAp) is a material used in a number of branches. Due to its beneficial properties, such as radiation stability, biocompatibility, low toxicity, large specific surface area and other, it can be applied as a carrier for medicinal radionuclides for diagnostics and therapy. First of all, the HAp preparation method was developed and the material was characterised in detail. Then sorption of four radionuclides on HAp nanoparticles was investigated: ^{18}F, ^{68}Ga, ^{99m}Tc, and ^{223}Ra. Labelling yields for all four radionuclides were over 95 % and further stability studies have shown retained activity over 80 % for the majority of tested samples in biologically relevant media, such as bovine serum, bovine plasma, saline, and albumin solutions for approx. 5 half-lives for each radionuclide. Achieved results proved the assumption to use HAp as a radionuclide carrier for medicine approach.

Abstrakt

Hydroxyapatit (HAp) je materiál používaný v řadě odvětví. Díky svým příznivým vlastnostem, jako je radiační stabilita, biokompatibilita, nízká toxicita, velký specifický povrch a dalším, může být použit jako nosič pro medicinální radionuklidy pro diagnostiku a terapii. V dané práci nejprve byla vyvinuta metoda přípravy HAp, který byl dále detailně charakterizován. Poté byla zkoumána sorpce čtyř radionuklidů na nanočástice HAp: ^{18}F, ^{68}Ga, ^{99m}Tc a ^{223}Ra. Výtěžky značení pro všechny čtyři radionuklidy přesahovali 95 % a další studie stability prokázaly zachování aktivity na HAp přes 80 % u většiny testovaných vzorků v biologicky relevantních médiích, jako hovězí sérum, hovězí plazma, fyziologický roztok a roztoky albuminu po dobu cca. 5 poločasů pro každý radionuklid. Dosažené výsledky potvrdily předpoklad využití HAp jako radionuklidového nosiče vhodného pro nukleární medicínu.

Declaration of Honour

I, Ekaterina Kukleva, declare that I independently prepared the present work and that I did not use any literature or resources other than those indicated. Verbatim or non-verbatim citations are all marked and their origin is specified. This also applies to figures, tables and illustrations, as well as to online sources. This thesis contains no material that has been submitted previously, in whole or in part, for the award of any other academic degree or diploma. Except where otherwise indicated, this thesis is my work.

Additionally, I declare that the digital version submitted matches invariably the printed version in content and wording.

In Prague,

Acknowledgement

I would like to express my gratitude to my supervisor, Ján Kozempel, who guided me throughout this project. The assistance provided by Martin Vlk and Petra Suchánková was greatly appreciated. I wish to extend my special thanks to Karel Štamberg for data modelling. I wish to acknowledge the help provided by the technical and support staff in the Nuclear chemistry department.

I would like to show my deep appreciation to Miroslav Šlouf from the Institute of Macromolecular Chemistry, Czech Academy of Sciences for TEM measurements. I would also like to thank my friends and family who supported me and offered deep insight into the study.

This work was supported by the grants:

- ČVUT SGS: SGS16/251/OHK4/3T/14
- ČVUT SGS: SGS19/194/OHK4/3T/14
- AZV ČR: 16-30544A
- MŠMT - LK21310

Table of Content

Abbreviation List

BRB	Britton-Robinson Buffer
CERT	Contrast-Enhanced Radiotherapy
ClAp	Chlorapatite
CT	Computed Tomography
DOTA	2,2′,2′′,2′′′-(1,4,7,10-Tetraazacyclododecane-1,4,7,10-tetrayl) tetraacetic Acid
EMA	European Medicines Agency
EPR	Enhanced Permeability And Retention
FAp	Fluorapatite
FDA	U.S. Food And Drug Administration
FDG	[^{18}F]-2-Deoxy-2-Fluoro-D-Glucose
HAp	Hydroxyapatite
HEPES	4-(2-Hydroxyethyl)-1-Piperazineethanesulfonic Acid
HPMA	Hydroxypropyl Methacrylate
i.v.	Intravenously
MRI	Magnetic Resonance Imaging
NO2APBP	1,4,7-Triazacyclononane-1,4,7-N,N′,N′′-triacetic Acid
NODAGA	2,2′-(7-(1-Carboxy-4-((2,5-dioxopyrrolidin-1-yl)oxy)-4-oxobutyl)-1,4,7-triazonane-1,4-diyl)diacetic Acid
NPs	Nanoparticles
PBS	Phosphate Buffer Saline
PEG	Polyethene Glycol
PET	Positron Emission Tomography
PSMA	Prostate-Specific Membrane Antigen
QDs	Quantum Dots
RN	Radionuclide
RPh	Radiopharmaceutical
SPC	Summary Of Product Characteristics
SPECT	Single Photon Emission Computed Tomography
SPIONs	Superparamagnetic Iron Oxide Nanoparticles
tBU-DO3A	1,4,7-Tris(Tert-butoxycarboxymethyl)-1,4,7,10-tetraa-zadodecane

Introduction

Nanomaterials have been well known since ancient times, however, the word itself appeared in the ´90s. The first nanoparticles were made of gold and were used as red glass dyes, and no one knew anything about the process. In the ’50s R. Feynman provided a hypothesis about molecule-scale world perspectives and his prediction could be taken as the beginning of the nanotechnology era.

Nanomaterials and nanotechnology applications are extremely wide and can be found in any area of life. As examples can serve sunscreens with nano-titanium dioxide, composites reinforcement with carbon nanotubes, water-resistant amorphous silica nanolayer, computer chips with 65 and 32 nm transistors, and many others.

Branches studied in the current thesis are nanomedicine and applications of nanoparticles for nuclear medicine and cancer treatment particularly. Today cancer treatment includes a variety of diagnostic and therapeutic methods, but due to the wide range of complications in surgery and side effects of chemotherapy, they cannot be used as a treatment in any case.

The existence of various cancer types, which can differ in many aspects, and the lack of sufficient diagnostic and treatment methods lead research to look for new drugs, therapy systems or even new approaches. The idea of radionuclide usage for noninvasive cancer treatment is not new, however, nuclear medicine is still lacking an exhaustive list of proper targeting vectors for many cancer types. Thus the alpha and beta particles often destroy not just the cancer cells but also surrounding healthy tissues.

Due to the danger of alpha and beta particle irradiation especially inside a human body, direct usage is usually highly restricted. The exceptions are self-targeting radionuclides such as ^{131}I and ^{223}Ra. So a new approach, such as nanoparticles, which can carry everything needed and be targeted with biomolecules or linkers, is welcome.

The theranostic approach has been discussed for several decades, but with the development of sciences, it seems to have become real. Nanoparticles can

deliver both diagnostic and therapeutic agents, carry passive or active targeting agents and show minimal negative impact on a whole organism.

Nanoparticle application for cancer treatment is theoretically possible due to a better understanding of the differences between normal and tumour tissues. This difference leads to an opportunity for particle infiltration and simultaneous targeting. An effect that covers both points is enhanced permeability and retention (EPR). Furthermore, excess excretion of some hormones increases the permeability of tumour tissue.

The high specific surface area belongs among nanoparticle benefits and can be used for bonding and transport of various substances like DNA, RNA, proteins, low-weight molecules or radionuclides. Nanoparticles synthesised from biocompatible materials such as lipids, chitosan, hydroxyapatite, metal oxides and many others lead to non-toxic and biocompatible products. Moreover, the nanoparticle surface can be modified to increase distribution specificity, colloidal stability or radiochemical stability.

At the current time, the development of radionuclide carriers for nuclear medicine is an issue of the day especially due to the increasing number of cancer appearances. This disease is very diverse, which leads to the complexity of drug development and enlarges the number of drugs needed.

There are several ways to create cancer either diagnostic or treatment drugs. One of them discussed in the current thesis is the use of radionuclides which can be delivered to the target tissue. In order to transfer radioactive isotope to the required place, nanoparticles of biocompatible and non-toxic hydroxyapatite were chosen. Nanoparticles themself have good sorption properties for many molecules and ions and can be prepared in a diverse size and shape scale. Therefore, the combination of hydroxyapatite nanoparticles with diagnostic (^{18}F, ^{68}Ga, ^{99m}Tc) or therapeutic (^{223}Ra) radionuclide seems to be potential and beneficial.

State-of-the-Art

Brief History of Nanoparticles

The first idea of the nano-scale world was presented by Richard Feynman in 1959. In his lecture, he described an idea, that machines could construct smaller machines and down to the molecular level [Bayda 2020]. Later in 1974 N. Taniguchi published the first article operating with the term nanotechnology to describe nanometer-scale film deposition. He defined the term as: “nanotechnology mainly consists of the processing of separation, consolidation, and deformation of materials by one atom or one molecule” [Taniguchi 1974]. Term nanomaterials appeared later to describe materials, which have at least one side sized from 1 to 100 nm (named 1D to 3D).

According to the 7th International Conference on Nanostructured Materials held in Wiesbaden, Germany [Nano 2004], there are the following types of nanomaterials:

- nanoporous structures
- nanoparticles (3D)
- nanotubes and nanofibers, nanosheets (2D)
- nanodispersions
- nanostructured surfaces and nanolayers (1D)
- nanocrystals and nanoclusters.

However, today newly appeared quantum dots (0D) also belong to nanomaterials.

It is impossible to describe the general nanomaterial properties of any type of material except their size. Final properties highly depend on initial material, type, size, shape etc, however, due to usually higher surface area, nanomaterial properties differ from initial material properties. [Guisbiers 2012] Nonetheless, there are some similarities in their biological interactions at a cellular level

including blood circulation, membrane penetration, uptake, accumulation and biotransformation [Zhu 2013].

Nanoparticles are materials where each dimension is sized from 1 to 100 nm. They are being used widely, but only a biological approach is relevant for the current work. Nanoparticles in medicine are conceived as any drug delivery system, which can simultaneously provide direct transport, save the drug from preliminary biotransformation and provide controlled release.

Nanoparticles in Medicine

Nanomedicine is a rather new branch combining nanotechnology, pharmacy, medicine, biology and chemistry. It aims to develop drugs with higher efficacy and lower risk levels. Nano-drugs could be defined as diagnostic or therapeutic agents whose main parts are nanoparticles that improve biodistribution, efficacy or reduce the toxicity of the drug. [Bobo 2016] The interaction of nanomaterials with their biological environment at any level depends on the controllable properties of the particles, such as size, shape, and material used, as well as on the uncontrollable properties of the surrounding media (plasma protein concentrations, sugar, etc.). [Ikeda 2011, Zhu 2013]

Nanomaterial parameters are also important for sufficient efficacy. The material must be biocompatible, should not interact with blood components, be inert for an immune system. Furthermore, the surface charge should be slightly negative for better stabilisation (approx. -30 mV). The material should also be colloidally stable enough to remain in the blood circulation for satisfactory distribution and stable in the tissue during the exposure (a total of days to weeks, in exceptional cases months). [Maeda 2013]

The size plays a key role in the uptake and excretory mechanisms. Particles sized from 4 to 10 nm can pass through the cell membrane, bigger particles from 90 nm up to 1 μm usually undergo active transport and require functionalization. Considering excretion, particles below about 10 nm in size are excreted by the kidneys, larger particles are excreted by the liver and remain in circulation for a longer period. The possible route of uptake and desired route of excretion must be taken into account in drug design. For example, small, actively targeted

particles are rapidly removed if they are not accumulated in the target organ after the first pass through the liver. On the other hand, passively targeted particles should be larger and resist biotransformation in the liver to stay in the bloodstream longer due to prolonged uptake. [Ikeda 2011, Zhu 2013]

Nanoparticles are often conjugated with already used low molecular weight drugs to upgrade the drug's targeting, pharmacokinetics and/or pharmacodynamics. In most cases, the effect is achieved by passive targeting controlled by the chemical properties of the nanoparticle. Active targeting is controlled by binding a ligand or antigen that is related to a receptor. For example, there is a nanodrug approved by the FDA in 1999 (Ontak®) that operates based on active targeting and is used to treat cutaneous T-lymphoma. It is a recombinant cytotoxic protein with a molecular weight of 58 kDa, which consists of the amino acid sequence of diphtheria toxin (fragments A and B, drug agent here) to which protein produced by T-lymphocytes is bound (active targeting agent) [Ontak 2017, Turturro 2011].

Classification

Nanoparticles in medicine can be divided into several key categories based on the material used: polymeric, liposomal and inorganic.

Polymer-based nanoparticles are commonly used as drug conjugates. The aims are either to increase biological half-life and bioavailability or to provide control release drug delivery systems [Hruby 2006]. One of the most common polymers is polyethene glycol (PEG), which is used for controlled drug release. An example can be the drug Neulasta®, which was approved by the FDA in 2002 for the treatment of chemotherapy-induced neutropenia [Bobo 2016]. Furthermore, polymers can also be used in nuclear medicine, e.g. to capture daughter products of the decay of ^{225}Ac, mainly ^{221}Fr, whose reflection energy significantly exceeds the binding energy [Fitzsimmons 2007].

Liposomal nanoparticles also belong to a broad group of drug delivery materials. They are usually used for drugs that are either highly toxic or poorly bioavailable. The simplest form of liposome is the phospholipid bilayer surrounding the hydrophilic core. Liposomal nanoparticles are often used for

chemotherapy and can also serve as suitable radionuclide carriers, e.g. for ^{223}Ra in targeted alpha therapy [Allen 2013, Jonasdottir 2006, Henriksen 2004] and ^{99m}Tc for diagnostics [Banerjee 2014].

The group of **inorganic materials** is the widest one from the compositional point of view. It includes nanoparticles based on metal oxides, metals and minerals. This type of nanoparticles is very well studied and is widely used not only in medicine but also in many other disciplines. Among examples are nanoparticles based on iron oxides like Fe_2O_3, which are used as contrast agents for MRI, superparamagnetic iron oxide particles (SPIONs) are being developed and their use for nuclear medicine purposes is being under research. SPIONs seem to provide both MRI and SPECT beneficial properties. They were labelled mainly with diagnostic radionuclides ^{99m}Tc [Madru 2012] and ^{18}F [Devaraj 2009], but also ^{223}Ra [Mokhodoeva 2016] and already showed sufficient stability for subsequent use.

Lanthanum phosphate nanoparticles labelled with ^{225}Ac [McLaughlin 2013, Woodward 2011] or ^{223}Ra and ^{225}Ra/^{225}Ac [Rojas 2015] can be used as carriers in targeted alpha therapy. Silver nanoparticles are well known for their bactericidal properties [Ruparelia 2007, Bankura 2012, Gao 2013], and are already used for ages. Their modification with a polyethene oxide coating and further labelling with ^{211}At are studied for nuclear medicine purposes [Kučka 2006] and labelled with ^{105g}Ag serve for environmental studies [Ichedef 2013]. Gold nanoparticles are used in several scientific disciplines. They occur in medicine due to their low toxicity, simple preparation, high stability and the possibility of easy surface modification with biomolecules [Daniel 2004, Boisselier 2009]. They are used as contrast agents for diagnostics and can increase the effectiveness of X-ray irradiation in contrast-enhanced radiotherapy (CERT) [Smith 2012]. They were labelled with ^{111}In [Ng 2014] and ^{99m}Tc [Mendoza-Sánchez 2010] for imaging of cancer and also with ^{211}At for cancer therapy [Janiszewska 2015]. Titanium dioxide plays a key role in nuclear medicine as a sorbent in a recently available ^{68}Ge/^{68}Ga generator. Titanium dioxide based nanoparticles have been labelled with ^{48}V [Abbas 2010], ^{18}F [Pérez-Campaña 2014] and radioactive isotopes of titanium [Hildebrand 2015] to study the transport of nanoparticles in the body. Also, it was labelled with ^{223}Ra and ^{99m}Tc for theranostic purposes [Suchankova

2020 A]. Hydroxyapatite (HAp), which is studied in this work, also appears to be a promising material for the targeted transport of drugs and radionuclides.

Hydroxyapatite (HAp)

HAp properties

The apatite group includes minerals from the phosphate group, which contain varying amounts of hydroxyl, fluorine and chlorine. Their general chemical formula is $Ca_{10}(PO_4)_6(OH,F,Cl)_2$. Apatites are formed by crystallisation from magma or organic residues and are one of the basic components of rocks. It is the most abundant phosphate in the earth's crust. Apatites include fluorapatite (FAp) $Ca_{10}(PO_4)_6F_2$, chlorapatite (ClAp) $Ca_{10}(PO_4)_6Cl_2$, hydroxyapatite (HAp) $Ca_{10}(PO_4)_6(OH)_2$, carbonatapatite $Ca_{10}(PO_4,CO_3)_6(OH,F,Cl)_2$ and others. [BSE 1969]

The hexagonal crystallographic structure of HAp allows the substitution of various ions for Ca^{2+}, PO_4^{3-} and OH^-, which often occurs in nature. Similar changes in composition result in crystallographic changes, and changes in chemical and physical properties, such as crystal lattice parameters, spectral properties, colours, crystal sizes and shapes, solubility, and thermal stability. The changes in properties are proportional to the size of the substituted ion. For example, the complete or partial incorporation of F^- into the crystal lattice causes the growth of larger and thinner crystals with lower water solubility compared to unsubstituted HAp. The thermal stability of apatites decreases in the following order: FAp> HAp> ClAp and, conversely, the solubility increases. [LeGeros 2009]

The incorporation of cations by substitutions for calcium ions is frequent. Some cations such as strontium (Sr^{2+}), barium (Ba^{2+}) and lead (Pb^{2+}) can completely replace calcium in HAp. The incorporation of trace amounts of manganese, copper I, copper II, ferrous, and ferric ions leads to colour changes. The incorporation takes place during the formation of crystals in a solution containing named ions. Radionuclides can be incorporated in the same way.

The ideal HAp, whose general formula is $Ca_{10}(PO_4)_6(OH)_2$, does not fully correspond to natural HAp. The natural material is much more complex, not stoichiometric, usually calcium deficient (Ca/P ratio < 1.67) and contains traces

of CO_3^{2-}, Mg^{2+}, Na^+, F^- and Cl^-. It should be noted that the closer the Ca/P value is to the ideal 1.67, the greater the thermodynamic stability of the material inside the human body is [Kalita 2007, Rivera-Muñoz 2011]. Changes in Ca/P ratio lead to the formation of variable phases (**Tab. 1**).

Tab. 1. Influence of Ca/P ratio on phosphates' formation [Saxena 2019].

Ca/P Ratio	General Name	Chemical Formula
0.50	Monocalcium Phosphate	$Ca(H_2PO_4)_2$
1.00	Dicalcium Phosphate	$CaHPO_4$
1.33	Octacalcium Phosphate	$Ca_8(HPO_4)_2(PO_4)_4$
1.50	Tricalcium Phosphate	$Ca_3(PO_4)_2$
1.67	Hydroxyapatite	$Ca_{10}(PO_4)_6(OH)_2$

HAp in biology, medicine and daily use

Based on X-ray diffraction analysis and simultaneous chemical analysis it was found that the enamel, dentin and bones consist of hydroxyapatite. This invention was made in 1926. Then it was found that mixtures of HAp and other calcium phosphates occur in pathological calcification (e.g. kidney and urinary stones) or dental cases (**Tab. 2**). The first mention of calcium phosphate used for bone repair appeared even in 1920, but the development of HAp and other phosphates in medicine began in the 1980s. [LeGeros 2009, Rivera-Muñoz 2011]

Today, HAp is used as a material for tissue engineering, bone coating and dental implants [LeGeros 2009, Rivera-Muñoz 2011], also as a part of a skin filling in cosmetics [Radiesse 2017], as a remineralizing agent in toothpaste, e.g. Sangi Co., Ltd. (Japan) APAGARAD®, APADENT®; Curaprox® White is black, etc. Also, HAp is called bioceramic and is used for prosthetic applications [Saxena 2019]. Moreover, its beneficial properties such as anti-age, roughness and elasticity effect have placed HAp as an active compound in daily face cream KALILIGHT [Kalilight 2020] and as UV-filter in sun care APALIGHT [Apalight 2020] (both Kalichem Italia s.r.l.). Even in the Baby Powder by Johnson's HAp helps to moisturise and soften skin [Johnson's 2020].

The reason why HAp is so popular and is used almost everywhere is its similarity to human bone crystallography and chemical composition. Another significant advantage of HAp is the possibility to prepare it in diverse forms according to the required application such as dense ceramic, powder, coating material, and porous material. The most interesting application in a term of current work is a delivery system for proteins, peptides, genes, and drugs [Saxena 2019].

Tab. 2. Calcium phosphate appearance in the organism and biological systems [LeGeros 2009].

Calcium phosphate	Chemical Formula	Appearance
Carbonate HAp, Carbonate FAp	$Ca_{10}(PO_4,CO_3)_6(OH,F)_2$	Enamel, dentin, bones, kidney and urinary stones, soft tissue calcification
Octacalcium Phosphate	$Ca_8H_2(PO_4)_6 \cdot 5H_2O$	Urinary stones
Dicalcium Phosphate	$Ca_2HPO_4 \cdot 2H_2O$	Pathological calcification, chondrocalcinosis, enamel, dental caries
Dicalcium Pyrophosphate	$Ca_2P_2O_7 \cdot 2H_2O$	Chondrocalcinosis

Due to HAp's high specific surface area [LeGeros 2010], the material has a variety of applications not just in medicine, but in photovoltaics and environmental science. These implementations are based on such HAp properties as biocompatibility and sorption capacity, which are very important for water decontamination from different pollutants, such as metal ions [Bogatu 2017, Corami 2007, Handley-Sidhu 2016] or organic compounds [He 2018].

Many other possibilities of using HAp are under research. For example, wires and tubes made of HAp as biologically active substances for cell proliferation and osteogenic differentiation [Stojanović 2016], composite nanoparticles based on HAp, Fe_3O_4 and chitosan doped with Ag for orthopaedic and dental applications [Anjaneyulu 2016], a flexible composite material based on polymethacrylate with HAp for tissue engineering [Song 2008], and many others due to its

biocompatibility and low toxicity [Sonmez 2016]. HAp is the subject of many studies and will certainly find more applications in medicine and cosmetics.

Recent studies on HAp cytotoxicity also improve the positive impact on its appearance. Commercially available HAp nanoparticles (HAp-NPs) were tested for cell viability, metabolic activity, mitochondria tracking and apoptosis on human gingival fibroblast cells. It was found that cell viability was not impacted, but metabolic activity even increased in comparison to non-treated samples. Mitochondria tracking showed no changes as well as F-actin cytoskeleton, so the presence of healthy cells was confirmed. No apoptosis caused by the presence of HAp-NPs was observed. [Coelho 2019]

Simultaneously, already mentioned high sorption ability and capacity are also important for medicine, where HAp can serve as a radionuclide carrier for imaging and therapy [Cędrowska 2018, Duan 2018, Rajeswari 2017, Vimalnath 2015]. Inorganic nanoparticles offer an opportunity for both passive and active targeting based on the EPR effect and/or surface functionalization.

Synthesis of HAp nanoparticles

There are various methods published describing the preparation of HAp of different forms and sizes. It is quite hard to demarcate them clearly because newer articles use knowledge from previous ones by combining them. Therefore, the classification presented here is not absolute, but the most synoptic in my opinion.

Extraction from natural sources

Natural HAp extracted from biological sources has non-stoichiometric composition and is more similar to human bones in comparison with synthetic HAp. As a source of HAp serves mammalian bone (e.g. bovine, camel, and horse), marine or aquatic sources (e.g. fishbone and fish scale), shell sources (e.g. cockle, clam, eggshell, and seashell), plants, algae, and also mineral sources (e.g. limestone). Extraction is performed by calcination, alkaline hydrolysis, hydrothermal method, or a combination of mentioned methods. However, to be used in medicine, natural HAp must be carefully purified, therefore synthetic

HAp produced from defined and pure precursors seems to be preferable. [Owusu 2020]

Enzymatic hydrolysis

Enzymatic hydrolysis of calcium glycerophosphate in the presence of alkaline phosphatase belongs among very unconventional methods. The product was mainly spherically shaped HAp and tended to form aggregates. Crystallites sizes were 12–14 nm, however, aggregates were significantly bigger (1.5–2 μm). [Orlova 2018]

Synthesis in water solutions

- **Hydrothermal methods** use elevated temperature and pressure in aqueous solutions. According to the literature, these methods lead to controlled shape HAp crystal synthesis. Changes in pH, temperature, time and initial compounds influence final product size and shape. It was found that higher temperature led to better crystal formation, while lower pH led to longer crystal formation [Liu 2003].

  Either $CaHPO_4 \cdot 2H_2O$ or $Ca(OH)_2$ are usually used as initial compounds, however, other Ca salts can be also utilised. Mixing Ca with phosphoric acid HAp precursor appears. Subsequently, it converts to HAp at elevated temperature and pressure (120 °C, 7 bar, 20 h, resulting size of nanowires 37 x 3700 nm [Stojanović 2016]; 2 h, 180 °C, resulting size of particles 57 ± 13 nm [Kim 2015]).

- **Precipitation** (and co-precipitation) is the most commonly used synthetic method because it does not require any special equipment or conditions. In general, salts containing Ca and PO_4 are dissolved in water and then mixed under a certain pH. Among frequently repeated conditions belongs the Ca/P ratio of 1.67 and pH over 10. In 12–24 hours after mixing, the precipitate is usually washed and then centrifuged/dried/lyophilized. Co-precipitation usually appears as a method to insert other cations and anions into the HAp structure that leads to the product with different parameters. The following methods demonstrate wide spectra of possible synthetic routes:

- The solutions of $Ca(NO_3)_2$ and $(NH_4)_2HPO_4$, both with pH 12, were mixed vigorously. The precipitated HAp was heated for 10 min at 70 °C and then cooled to room temperature. Then it was filtered, washed with water and ethanol, dried, and finally grounded. More than 85 % of the particles had a size ranging from 5 to 20 μm. [Unni 2002]
- Here again $(NH_4)_2HPO_4$ and $Ca(NO_3)_2$ aqueous solutions (Ca/P = 1.66) were used. Reaction occurred at 37 °C, and pH was equal to 11. The precipitate was filtered, repeatedly washed with deionized boiling water, dried at 100 °C, and then grounded. Prepared particles sized 210 μm. [Albernaz 2013]
- Solutions of H_3PO_4 and of $Ca(CH_3COO)_2$ were used. The reaction was performed at a stabilised pH value of 10 by the addition of NH_4OH and stirred at room temperature overnight. The precipitate was centrifuged, washed with water and finally suspended in ultrapure water. Prepared nanoparticles were also modified with citrate by adding $Na_3(Cit)$ and purified with dialysis. The method resulted in 20–50 nm particles of HAp. [Sanhofer 2015]
- Precipitation can also be performed in a flow reactor where CaOH and H_3PO_4 were mixed. Prepared particles were uniform and sized about 77 nm. [Castro 2016]
- Likewise, flow microchips with $Ca(OCH_3)_2$ and H_3PO_4 or more conventional $Ca(NO_3)_2$ and $(NH_4)_2HPO_4$ were used. The final product had a size of approx. 3 μm. [Nykl 2017]
- One more interesting method is synthesis directly in body fluids under physiological conditions (37 °C, pH = 7). This method led to HAp substituted with CO_2, which was very close to bone composition. [Ferraz 2004].

- **Electrodeposition** on a surface is used for titanium implant coating. In general, the titanium object used as a cathode is placed into an electrolyte solution containing Ca and P precursors in low concentrations.

As an example can serve the method published by Zhang et al., where electrolyte contained 0.042 M $Ca(NO_3)_2$ and 0.025 M $(NH_4)_2HPO_4$ at pH 4.5. The deposition was conducted at 120 V and the lowest possible current at 80 °C for 2 h [Zhang 2006]. In current classification electrodeposition can be also taken as a partial case of precipitation, however, used concentrations are significantly lower.

Synthesis in other solvents

- **Sol-gel methods** use sol appearance in the middle of synthesis, where reacting compounds are mixed already, but not reacted yet. Then the sol is aged and the final product is obtained. Literature declares mixing of Ca and P on a molecular level which improves the homogeneity of the final product as the main benefit of sol-gel methods. [Liu 2001] However, this statement is negotiable since compounds used in hydrothermal and precipitation methods are soluble in water and then thoroughly mixed. As an example, the sol-gel way can serve the preparation of HAp from Ca salts (typically nitrate) and triethyl phosphate in 2-methoxyethanol. The mixture reacted either at 80–90 °C for 16 hours [Hsieh 2001] or in ethanol at room temperature for 16 h and further treatment at 60 °C [Liu 2001]. Later the sol was aged for about a week. After ageing calcination followed at 600–800 °C. Furthermore, a shorter way also exists, where ageing is excluded, which significantly decreases preparation time [Ben-Arfa 2017]. Predominantly sol-gel methods are used for bigger-sized particle preparation.

Microwave (MW)-assisted synthesis covers a wide spectrum of preparation methods, where microwaves are used as heat treatment techniques. Usage of MW was described for wet precipitation, hydrothermal, solid-state, ultrasonic-assisted and reflux-assisted methods. In general heat treatment during synthesis influences the kinetics of the reaction and the morphology & size of the final product. [Hassan 2016]

EPR effect

Data on the enhanced permeability and retention effect of tumour tissue were first published in 1986 by Matsumura et al. and are still being studied. This effect occurs in solid cancers and leads to penetration and retention of particles or macromolecules in the tumour tissue. Basically, this is a passive transport with a rather high specificity, which allows it to deliver nanoparticles from 20 to 200 nm in size directly into the tumour. [Matsumura 1986, Vasey 1999]

The effect was first described during the study of protein transport mechanism into tumour tissue on alive mice. Studied proteins were sized from 12 to 160 kDa labelled with ^{51}Cr and included also albumin labelled with Evans Blue dye. It was found that the concentration of proteins finally was much higher in cancer than in healthy tissues including blood. [Matsumura 1986] Since the EPR effect was deeply studied on other proteins, for example, HPMA-based biopolymers [Lammers 2009, Ulbrich 2009], and nowadays several therapeutic drugs based on EPR are in practice [Maeda 2016], however, no EPR based radiopharm drug is available.

Enhanced permeability is the passive transport of the drug into the required tissue. This way can be used by any molecule, however, small ones are washed out. While small molecules are retained in the tissue for several minutes maximum, bigger nanoparticles, polymers and other macromolecules can be retained for a much longer time up to months. However, targeting the nanosized structures is not very fast and can last for several hours. [Thakor 2013, Maeda 2016]

The effect is caused by high porosity capillaries and poor lymphatic system in the tumour tissue (**Fig. 1**). Due to the fast growth of the tumour and all structures inside including blood vessels, capillary epithelium forms uneven with gaps sized approx. from 380 to 780 nm. Moreover, its physiological response differs from normal capillaries by producing more mediators. These two facts lead to enhanced permeability. On the other hand, the lymphatic system is not so important for nutrient transport, so its evolution is slowlier, which leads to an

undeveloped system and very slow drain and causes higher retention. [Thakor 2013]

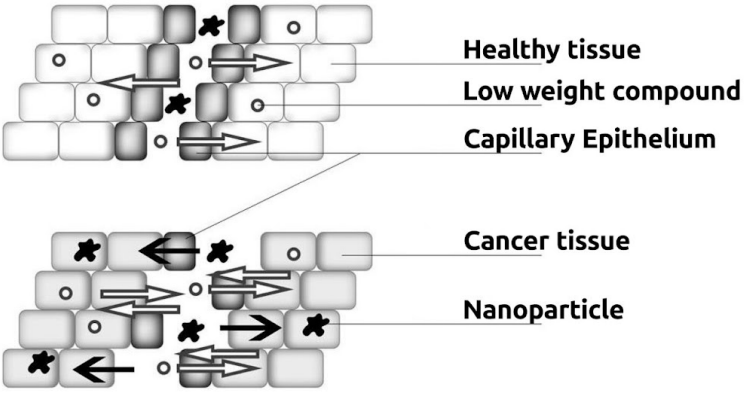

Fig. 1. Scheme of EPR effect.

The EPR effect occurs in many cancer types in varying degrees. Kidney or hepatic cancer usually shows a high EPR effect, while prostatic or pancreatic cancer shows a very poor effect due to lower blood supply. [Maeda 2016]

Nanoparticle radiolabelling

In general there are two main ways for nanoparticle labelling. The first one requires a special compound that bounds an RN and simultaneously is attached to the labelled NPs. This model is suitable for single decay radionuclides because decay energy is usually higher than chemical bond energy, so the atom is released after the decay. For multi-decay radionuclides such as ^{223}Ra, resorption of daughter nuclei is desirable.

The second way is direct labelling without any chelator. Radioisotope can be sorbed onto the nanoparticle surface or incorporated into its structure. However, these methods require appropriate chemical properties of both compounds. Direct labelling can be also performed via irradiation with neutrons or charged particles of ready-made NPs, nevertheless, the method requires either high purity precursors or further purification.

Radiolabelling of HAp

Hydroxyapatite as a radionuclide carrier has been studied for many years not just for medicinal applications, but also for radionuclide immobilisation (**Tab. 3**).

Based on published literature it can be concluded that the hydroxyapatite itself is remarkably suitable as a sorbent for a large variety of ions.

Tab. 3. Overview of ions tested with HAp.

Ion	Method	Result	Reference
^{111}Ag	Surface sorption	Radiochemical purity about 97 %, good in vitro stability for 7 days	Chattopad-hyay 2008
As^{5+}, Am^{3+} Pu^{6+}, Se^{6+} Tc^{7+}, U^{6+}	Surface sorption	Very high-sorption capacity for the Am, Pu, and U, and significant but less capacity for the oxyanions As and Se at neutral pH	Thomson 2003
Ce, Pr, Nd, Tb	Coprecipitation	Successfully doped, incorporation instead of Ca^{2+}, good cell viability	Kaur 2017
Co^{2+}	Surface sorption	Adsorption capacity 20.92 mg/g	Rigali 2016
$^{82}Sr/^{82}Rb$	Surface sorption	Model generator with synthetic HAp showed 99.9 % Sr retention on the column. Rb eluate yield was less than 30 %.	Haney 1986
^{169}Er	Surface sorption	Labelling yields more than 99 %, good in vitro stability for 30 days (99 %)	Chakraborty 2014
Eu^{3+}	Coprecipitation	Eu^{3+} has successfully doped the hexagonal lattice of hydroxylapatite	Andronescu 2019
^{18}F	Surface sorption	Dependence of uptake on F^- concentration from 19 to 84 %	Joyston-Bechal 1967
^{18}F	Surface sorption	Radiochemical purity more than 95 %, good in vitro stability for 120 min	Sandhöfer 2015
^{68}Ga	Surface sorption (^{68}Ga-NO2APBP)	Radiochemical purity more than 95 %, good in vitro stability for 120 min	Sandhöfer 2015
^{166}Ho	Surface sorption	Radiochemical purity more than 98 %, good in vitro stability for 72 h	Unni 2002
^{177}Lu	Surface sorption	Radiochemical purity about 99 %, good in vitro stability	Chakraborty 2006

Tab. 3. Overview of ions tested with HAp. Continuation.

Ion	Method	Result	Reference
^{99m}Tc	Reduction + surface sorption	Radiochemical purity more than 99 %, good in vitro stability for 24 h (>90 %)	Albernaz 2014
^{99m}Tc	Reduction + surface sorption + coprecipitation	Labelling yields more than 94 %, good in vitro stability for 31 h (>80 %)	Suchankova 2020 A
^{69m}Zn, ^{64,67}Cu	Coprecipitation + bifunctional chelates	Labelling yields were not determined	Orlova 2018
^{223}Ra	Surface sorption + coprecipitation	Radiochemical purity more than 95 %, good in vitro stability for 24 h (>85 %)	Kozempel 2015
^{223}Ra	Surface sorption + coprecipitation	Radiochemical purity more than 97 %	Vasiliev 2016
^{223}Ra	Surface sorption + coprecipitation	Labelling yields more than 94 %, good in vitro stability for 55 days	Suchankova 2020 A
^{153}Sm	Surface sorption	Radiochemical purity more than 80 %, good in vitro stability for 24 h	Calegaro 2013
Sr^{2+}	Surface sorption	19.5–94.7 % uptake (different soil samples)	Rigali 2016
TcO_4^-	Reduction + surface sorption	High efficacy at reducing, capturing and sequestering. Combined reduction and incorporation cause permanent sequestration of Tc into the apatite lattice	Rigali 2016
U, Th	Surface sorption	Complete immobilization within 1 hour (U,Th:HAp = 1:10)	Gauglitz 1992
UO_2^{2+}	Surface sorption	Uptake over 90 % from contaminated sediments	Rigali 2016
^{90}Y	Surface sorption	Radiochemical purity more than 95 %, good in vitro stability for 10 days	Vimalnath 2015

According to studied literature (**Tab. 3**), the number of ions with already proven retain ability on HAp is quite large. Since the last century synthetic and natural HAp attracted scientists' attention as the promising material for radionuclide

retention in radioactive waste repositories. Later with the development of radiotherapy, HAp nano and microparticles found their place in targeted therapy investigations. It was shown that surface sorption on HAp, when already prepared material was suspended in an aqueous solution containing studied ions, is still the easiest and most well-working method. It was found that sorption yields depended on HAp amounts, pH of the solution and temperature, however, all articles mentioned earlier described easily achievable experimental conditions.

Radionuclides

There is a wide range of approved and used RN all over the world, however, the list differs from country to country. The following table presents the list of chosen RN used all over the world (**Tab. 4**).

Tab. 4. List of chosen medicinal RN.

RN	Half-life	Main used irradiation type	Energy [keV]*	Usage (T/D)**
^{225}Ac	10.0 days	α	5935	T
^{211}At	7.2 hours	α	5982	T
^{18}F	109.8 min	β^+	633	D
^{68}Ga	67.6 min	β^+	1899	D
^{123}I	13.2 hours	γ	159	D
^{131}I	8.0 days	β^-	606	T + D
^{177}Lu	6.7 days	β^-	498	T + D
^{223}Ra	11.4 days	α	5716	T
^{153}Sm	46.3 hours	β^-	808	T + D
^{161}Tb	6.9 days	β^-	518	T + D
^{99m}Tc	6.0 hours	γ	140	D

* for β particle the maximum of β energy is mentioned; ** T - therapy, D - diagnostics.

For the current work already approved medicinal radionuclides, which are easily available and have well-known chemical behaviour, were chosen. The aim was to

show another possible application and to provide evidence of a rather easy approachable theranostic drug based on current technologies.

Among chosen RN belong three diagnostic: fluorine-18, gallium-68 and technetium-99m. These radionuclides cover the whole spectrum of applications, where ^{99m}Tc is used for SPECT, ^{18}F and ^{68}Ga for PET. Simultaneously, ^{68}Ga is a recently registered isotope, which can partially substitute widely spread ^{18}F due to generator production, while ^{18}F can be obtained on cyclotron only. However, due to the different chemistry of Ga and F, both radionuclides have their indications.

The fourth RN studied was ^{223}Ra, as a therapeutic one. It is already used all over the world only for prostate cancer treatment, so the possibility of diverse applications could be interesting not just for patients but also for the manufacturer. Among important radium benefits belong its possible in-house generator production and the fact that ^{223}Ra represents not just a single alpha-emitting radionuclide, but in vivo generator concept with four consequent alpha decays.

Labelling requirements differ for therapeutic and diagnostic radionuclides due to different half-lives. While therapeutic RN usually has quite a long half-life, so slow labelling kinetics is acceptable, the half-life of RN for diagnostics is significantly shorter, so the whole labelling process must be as fast as possible.

Fluorine-18

Fluorine-18 is one of the most often and widely used diagnostic PET radionuclides in nuclear medicine. The most popular drug containing fluorine is FDG or [^{18}F]-2-deoxy-2-fluoro-D-glucose. It is used to monitor glucose metabolism, which is more intense in a cancerous lesion, site of inflammation, and naturally in the brain (therefore FDG is not the best choice for brain problems diagnosis) [SPC FDG 2020]. Another very commonly used drug is [^{18}F]-NaF used to detect abnormal changes in osteogenic activity including cancer and bone injuries [SPC NaF 2017]. Furthermore, fluorinated amino acids like tyrosine are used to monitor their metabolism. Fluorine-18 is used in various radiopharmaceuticals for β-amyloid neuritic plaque density analysis [SPC Amyvid

2020, SPC Neuraceq 2020], prostate [SPC Axumin 2020, SPC Fluorocholine 2020] and other [SPC Fluorocholine 2020] cancer types detection. All mentioned applications are available in the Czech Republic, however, applications in other countries worldwide can be significantly wider or differ.

Physical and chemical properties of ^{18}F

Fluorine-18 with a half-life of 109.8 minutes decay to stable oxygen (^{18}O) by emitting 633 keV of positron radiation [LCN 2021] (**Fig. 2**). The mean positron range in soft tissue is about 0.27 mm before annihilation [Sanchez-Crespo 2013].

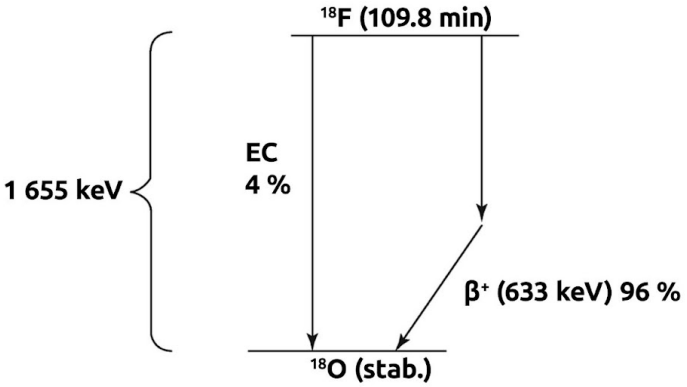

Fig. 2. Decay scheme of ^{18}F.

The chemistry of fluorine is the chemistry of halogens, so it undergoes nucleophilic substitution on benzene under the S_N2 mechanism. The reaction is catalysed, selective and finally very fast, which is very important for correct RF synthesis. [McMurry 2015]

Labelling of nanoparticles with ^{18}F

The usage of fluorine seems to be one of the easiest ways to radiolabel HAp due to its chemical properties. Fluoride can be incorporated into the structure instead of the OH^- group. Labelling of the prepared HAp has already been performed and yields were around 95 % for both unstabilized and citrate stabilized nanoparticles. Furthermore, the stability of the labelled particles in saline and PBS for 120 min was studied. About 95 % of the radioactivity remained bound to the nanoparticles. [Sandhofer 2015] However, fluorine is not

very popular for nanoparticle radiolabelling due to its short half-life and long NPs pharmacokinetics, but some other recent literature data are available.

Fluorine labelled Fe_3O_4@$Al(OH)_3$ NPs have shown very good labelling yields (over 98 %), but in-time stability was not sufficient even in saline (65 % of activity remains on NPs after 30 minutes). Foetal bovine serum stability experiments led to the release of 65 % of activity. Also, cell toxicity dependence on NPs concentration was investigated and the results showed a significant decrease in survival for concentrations of 100 μg/ml and more, which is a very high concentration for NPs. [González-Gómez 2019]

Irradiation of ^{18}O enriched TiO_2 NPs to create ^{18}F labelled titanium dioxide was performed by Pérez-Campaña et al. in 2014. Despite the method seems to be straightforward, the occurrence of ^{48}V, ^{47}V and ^{44g}Sc radioactive isotopes is unwanted as well as reactor use. [Pérez-Campaña 2014]

Gallium-68

Gallium-68 has appeared in nuclear medicine recently, but its popularity increases very fast due to generator production. Its development for nuclear medicine was initiated and supported already in the mid-2000s by the commercial availability of $^{68}Ge/^{68}Ga$ generators designed for clinical use.

In 2016 first DOTA-TOC (also known as edotreotide, **Fig. 3**) kit IASOtoc® (IASON GmbH, Graz, Austria) for ^{68}Ga labelling was approved. The compound named DOTA-TOC was already well known in nuclear medicine due to its well working chelating ligand DOTA (**Fig. 3**, light grey), which can complex 3–valent cations (^{90}Y and ^{111}In [Otte 1997], ^{177}Lu [Forrer 2005], ^{213}Bi and ^{225}Ac [Morgenstern 2018], ^{44}Sc and ^{152}Tb [Hennrich 2020]). However, from the medicinal point of view, the most important part is octreotide (**Fig. 3**, dark grey) which shows a high affinity to somatostatin receptors which increase in neuroendocrine tumours.

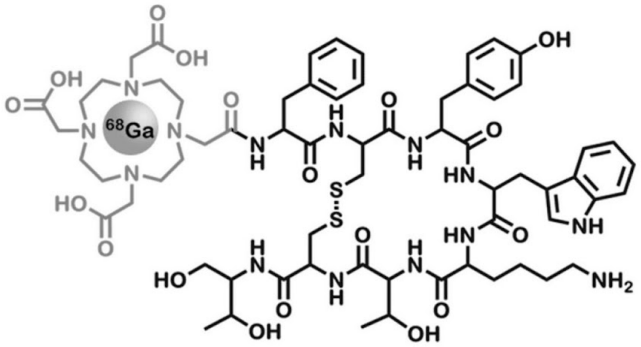

Fig. 3. Chemical structure of [^{68}Ga]-DOTATOC (DOTA(0)-Phe(1)-Tyr(3))octreotide) [Weber 2015].

Another way to use ^{68}Ga with DOTA is PSMA-11 or PSMA-617 labelling. Theranostic couple with [^{177}Lu]-DOTA-PSMA-617 showed similar biological behaviour and is already well suited for diagnostic and therapy of prostate cancer. [Scarpa 2017] Considering NPs a very interesting study showed the possibility to substitute ^{99m}Tc with ^{68}Ga for macroalbumon (MAA) labelling and obtained not only sufficient results of labelling yields but also patient imaging on PET [Maus 2011].

In 2017 gallium generator (GalliaPharm, Eckert & Ziegler Radiopharma GmbH, Germany) was approved in the Czech Republic [SPC GalliaPharm 2020]. Later DOTA-TOC kit (SomaKit TOC, Advanced Accelerator Applications, France) [SPC SomaKit 2020] got through European EMA approval and now is available in the Czech Republic. Another available kit for ^{68}Ga labelling is PSMA-11, however, it is not approved yet, but usage is possible under the Specific Therapeutic Programme [SPC 68Ga-PSMA 2020].

Physical and chemical properties of ^{68}Ga and its production

The half-life of ^{68}Ga is 67.7 minutes and it decays through positron emission (89 %) to the stable ^{68}Zn (**Fig. 4**) [LCN 2021]. The average positron energy is 836 keV, so its range is about 1.05 mm in soft tissue before the annihilation [Sanchez-Crespo 2013].

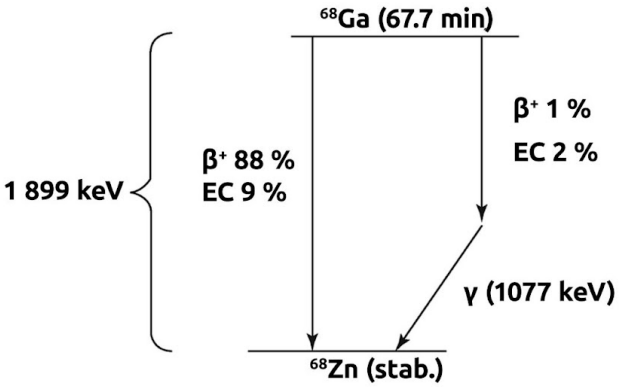

Fig. 4. Decay scheme of ^{68}Ga.

The most stable valence of Ga is 3+, however, it can also exist in 1+ and 2+ forms. In distilled water pure gallium dissolves and forms insoluble $Ga(OH)_3$, however, gallium hydroxide dissolves in weakly acidic solutions, such as 0.1 M HCl, or alkaline solutions with pH over 9.7 (**Fig. 5**) [Bradley 1990, Sheka 1963]. These chemical properties play a key role in ^{68}Ge/^{68}Ga generator construction.

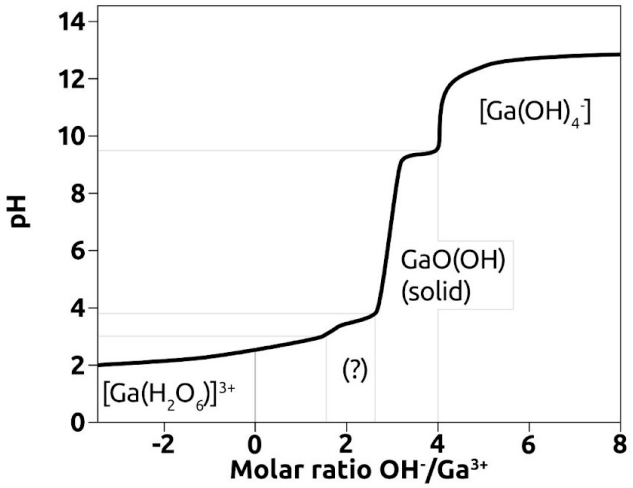

Fig. 5. Hydrolysis of 0.2 M $GaCl_3$ in water [Bradley 1990].

As mentioned earlier, ^{68}Ga is easily available in nuclear medicine due to generator production as well as ^{99m}Tc. It combines advantages of both ^{18}F, as PET radionuclide, and ^{99m}Tc, as a generator produces one. In available generators, the mother radionuclide ^{68}Ge is bound on titanium dioxide sorbent and ^{68}Ga is eluted with 0.1 M HCl. A higher concentration of HCl leads to the elution of Ge. According to generator construction, two elution volumes are possible: 5 ml

from GalliaPharm® (Eckert & Ziegler, Berlin, Germany) [SPC GalliaPharm 2020] and 1.5 ml from Galli Ad® (IRE ELit, Fleurus, Belgium) [SPC Galli Ad 2020].

The shelf-life of the GalliaPharm® generator is 12 months after the calibration date. The half-life of ^{68}Ge is 271 days, so activity decreases to the end of shelf-life by about 60 %. Due to the short half-life of ^{68}Ga, the generator can be eluted a few times per day. A maximum of ^{68}Ga activity is obtained 14 hours from previous elution, however, 3.5 hours after elution activity of ^{68}Ga reaches about 88 % of the maximum.

Besides all benefits, ^{68}Ga has some disadvantages. In comparison with ^{18}F, positron energy is higher, and the 1 mm range in soft tissue leads to a lower resolution. The possible maximum activity of ^{68}Ge loaded on the generator is limited. One of the critical generator quality parameters is the breakthrough of ^{68}Ge. Since the generator is eluted with HCl, labelling and patient applications require buffers for pH correction. And finally, the price of the generator is very high. [Hennrich 2020, Velikyan 2016]

Labelling of nanoparticles with ^{68}Ga

Labelling with ^{68}Ga, in general, is limited by its chemical properties, like hydrolysis at pH over 4. However, there are two ways to get through it. The first one is the application of compounds stable in low pH, so the pH during labelling does not increase over 4. As an example can serve the SomaKit TOC labelling procedure [SPC SomaKit 2020], where pH is controlled after labelling before patient application and must not exceed 3.9. Another way leads to two-step labelling for more sensitive compounds, where firstly Ga is complexed and stabilised at pH under 4, and then the compound is labelled under sufficient conditions.

Several publications describe the labelling of nanoparticles with ^{68}Ga. One of them studied CdTe/CdS quantum dots (QDs) functionalized with thioglycolic acid, which can form carboxylato-gallium (III) complexes from the (COO–) part and simultaneously stabilise the QDs surface. Labelling lasted 30 minutes and its yield was over 99 %. Incubation for 6 hours at 37 °C in human serum showed no

Ga release from nanoparticles. Labelled QDs were used for tumour imaging and showed excellent results. [Fazaeli 2020]

To label zirconia NPs with ^{68}Ga, DOTA was used. After 20 min labelling under 95 °C in HEPES with DOTA-ZrO_2-NPs labelling yields were over 90 % in HEPES and over 80 % in human serum for 180 minutes after labelling. Particle size stability after labelling was confirmed. [Polyak 2017]

Silica-coated iron oxide nanorods as potential PET/MR multimodal imaging agents after modification with both tBU-DO3A and PEG (in ratio 0:1, 1:1, 1:0) were labelled for 15 min at 90 °C. Achieved radiolabelling yields for all three modifications were about 100 %. The stability of the prepared samples was tested in EDTA (over 80 % of activity remained on the NPs) and human serum at 37 °C (over 95 % of activity remained on the NPs) for 3 hours. [Burke 2014]

Chelating agent DOTA was also used for gold nanoparticle labelling where labelling yields were over 80 % [Chilug 2020]. However, DOTA is used not only for nanoparticle labelling but in general for ^{68}Ga labelling, including DOTA-TOC, the main compound of SomaKit [SPC SomaKit 2020]. Also as chelating agents NO2AP-BP [Passah 2016, Sandhofer 2015], NOTA and TRAP [Adam 2014, Notni 2012], and TETA [Kilian 2014] appear in literature (**Fig. 6**).

It can be concluded that Ga labelling general approach using chelators leads to sufficient labelling yields of any compound.

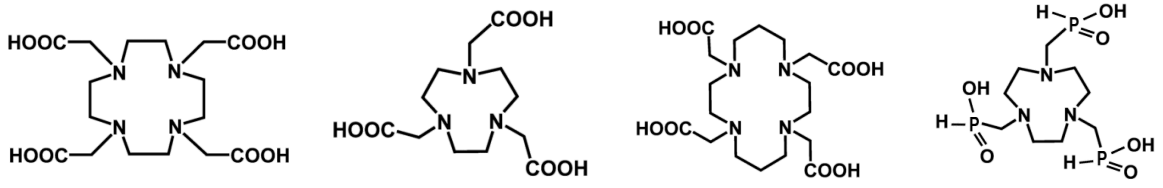

Fig. 6. Structures of DOTA, NOTA, TETA and TRAP ligands for ^{68}Ga complexation.

Technetium-99m

The first idea of ^{99m}Tc massive usage in medicine appeared in 1960, just after the first ^{99}Mo/^{99m}Tc generator was built (1957) [Molinski 1982]. This radionuclide is still the most widely used one in nuclear medicine. The quantity of technetium

radiopharmaceuticals is enormous and differs from country to country due to registration and legislative requirements. Technetium drugs can be divided into three groups: 1. technetium (VII) oxide (TcO_4^-) as a solution that does not require any preparation except elution, 2. cold kits, where eluate from the generator is added into the vial with lyophilizate (usually), and 3. hot kits, which are similar to cold kits, but are heated after eluate addition. All three pharmaceutical types are widely used for SPECT imaging.

Among the most frequently used technetium kits belong [^{99m}Tc]-HDP for bone imaging (cold kit), [^{99m}Tc]-sestamibi (hot kit) or [^{99m}Tc]-tetrofosmin (cold kit) for heart imaging. Other well-known ^{99m}Tc pharmaceuticals are listed in **Tab. 5**.

Tab. 5. Chosen ^{99m}Tc radiopharmaceuticals.

Oxidation state of Tc	Compound	Trade name (Manufacturer)	Organ/ tissue specificity
7+	Pertechnetate	Poltechnet (Polatom); Ultra Technekow FM (Curium)	Thyroid
5+	MAG_3 (betiatidum)	Technescan MAG3 (Curium)	Kidney
5+	HMPAO (exametazim)	Ceretec (GE Healthcare); Brain-Spect (Medi-Radiopharma)	Brain
5+	Tetrofosmin	MyoView (GE Healthcare)	Myocardium
4+	DTPA (acidum penteticum)	Technescan DTPA (Curium)	Kidney
4+	Phosphonates	Technescan HDP (Curium)	Bone
3+	DMSA (succimerum)	Technescan DMSA (Curium)	Kidney
1+	MIBI	Cardio-Spect (Medi-Radiopharma K)	Myocardium

Data are taken from SPC of mentioned radiopharmaceuticals, [FDA 2022, IAEA ^{99m}Tc Kit 2008, Kowalsky 2006].

Physical and chemical properties of ^{99m}Tc and its production

The half-life of ^{99m}Tc is 6.0 hours and it decays by an isomeric transition to the ground state ^{99g}Tc (**Fig. 7**). ^{99m}Tc emits gamma radiation with an energy of 140 keV (89 %) [LCN 2021]. Technetium-99m is usually obtained from ^{99}Mo/^{99m}Tc generators, where molybdenum (MnO_4^{2-}) is sorbed on aluminium oxide and technetium is eluted with water basically (in practice 0.9 % NaCl solution is used due to medicinal requirements) [Rathmann 2019].

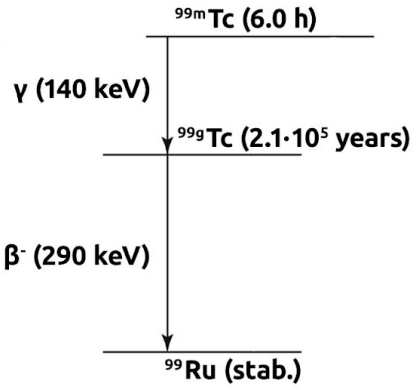

Fig. 7. Decay scheme of ^{99m}Tc.

There are two ^{99}Mo/^{99m}Tc generators available today on the Czech market: Poltechnet (Polatom, Poland) with declared activity 8–175 GBq and Ultra Technekow FM (GE Healthcare, USA) with declared activity 2–43 GBq.

The shelf-life of both the Ultra Technekow and Poltechnet generators is 21 days since the manufacture date [SPC Poltechnet 2021, SPC Ultra Technekow 2021]. Maximum activity of ^{99m}Tc is reached 22.9 hours from previous elution, and 80 % of maximum activity is reached in less than 10 hours from the previous elution. Seems that the Tc generator cannot be eluted two times per day, however in practice, the second elution is made 4–5 hours from the first one, when about 50 % of maximum activity is reached. A bigger delay is undesirable due to the decrease in activity obtained the next day.

The chemistry of Tc is similar to Rh. Pertechnetate (TcO_4^-) is very stable in aqueous solutions, however, compounds with Tc in oxidation states from -1 to +7 are known. Another compound stable in water is hydrolyzed reduction product TcO_2. As reducing agents, ascorbic acid and ferrous iron were used earlier, but

they often led to the incomplete reduction. Nowadays, sodium borohydride ($NaBH_4$) and sodium dithionite ($Na_2S_2O_4$) are used for reduction in alkaline pH, while stannous chloride ($SnCl_2$) is typically used in acidic pH. [Kowalsky 2006, Rathman 2019]

The stability of technetium complexes and compounds are controlled with pH, reducing agent, the complex itself, and other kit ingredients if added. Some complexes are formed with Tc in a specific oxidation state, like Tc^{1+} for sestaMIBI, other complexes can be formed with Tc in different oxidation states, like DMSA. It forms complex with Tc^{5+} at high pH and the drug is used for small tumour imaging (not allowed in the Czech Republic), also DMSA forms complex with Tc^{3+} at low pH for static kidney imaging. Finally, to stabilize complexes that are labile to oxidation ([^{99m}Tc]-DMSA, [^{99m}Tc]-HDP) antioxidants are added (inositol and gentisic acid respectively). [Kowalsky 2006, SPC HDP 2021, SPC DMSA 2021]

Labelling of nanoparticles with ^{99m}Tc

There are a number of conventional nanoparticles labelled with ^{99m}Tc, such as human albumin nanoparticles of different sizes (Macro-Albumon, Nanocoll etc) used for lung or lymphatic flow imaging. The albumin nanoparticles labelling procedure is very simple: sodium pertechnetate solution is added to a commercial kit containing $SnCl_2$. Incubation lasts 10–20 minutes at room temperature. Usual labelling yields are over 95 %. Stability of the [^{99m}Tc]-NPs is about 8 hours from the labelling. This mechanism and results show fast and easy procedures overall used in hospitals which can be repeated on other NPs.

Among NPs studied in the radiopharmacy group led by Jan Kozempel belong ferrum oxide NPs (SPIONs) and titanium dioxide NPs (TiO_2 NPs) already labelled with ^{99m}Tc. The radiochemical purity of [^{99m}Tc]-SPIONs was about 90 % and the labelling strategy was very similar to the albumin one [Sobkuliakova 2019]. These results are supported by Madru et. al. where labelling efficacy was 99 % after 6 hours. For more, [^{99m}Tc]-SPOINs showed 100 %ID/g accumulation in sentinel lymph nodes in vivo [Madru 2012].

For the TiO_2 NPs, two labelling strategies were chosen. The first one was surface radiolabelling where the particles were mixed with sodium pertechnetate (just

like albumin NPs labelling). The second one was coprecipitation, where nanoparticles were synthesised in the sodium pertechnetate solution. Labelling yields for both strategies of [^{99m}Tc]-TiO_2-NPs in physiological saline after an hour of incubation were over 95 %. Further stability experiments in biologically relevant media showed total released activity from 2 to 25 % during 31 hours. [Suchankova 2020 A]

Other frequently used NPs are gold ones (AuNPs). These AuNPs are usually functionalized with appropriate ligands, for better ^{99m}Tc labelling, and simultaneously targeting. [^{99m}Tc]-EDDA/HYNIC-GGC-AuNP-mannose nanoparticles built for mannose receptors in liver tissue showed radiochemical purity over 95 % and also specific accumulation in the liver (12 %ID/g) 1 hour after subcutaneous administration. [Ocampo-Garcia 2011 A] Based on these results, a prototype of the commercial kit was designed [Ocampo-Garcia 2011 B]. Another promising method is the stabilisation of AuNPs with polyethyleneimine with radiolabelling yields over 95 % [Zhao 2018].

HAp-NPs were also already labelled with ^{99m}Tc and achieved radiochemical purity was over 99 % after preparation and over 90 % within 24 hours. Biodistribution was also investigated in healthy mice and showed that the main activity was found in the kidneys. It is important to mention that the biodistribution of nanoparticles strongly depends on the size of the NPs, and this study does not provide any information considering the size. On the other hand, great labelling efficacy supports the idea of useful [^{99m}Tc]HAp-NPs. [Albernaz 2013]

Radium-223

Radium-223 has appeared in practical nuclear medicine quite recently, but the first notes about its older brother ^{226}Ra and its usage in medicine are dated from 1901 when it was used by dermatologists in Paris for cutaneous lupus treatment. The development of curietherapy led to the shielding of alpha and beta particles, so only gamma rays were used for treatment. [Lederman 1981] However, artificially produced gamma emitters, such as ^{60}Co, displaced ^{226}Ra in the 1930s [Harvie 1999]. Nowadays, radium is interested not as a gamma-ray source, but as an ionising particle source for targeted alpha therapy.

Bayer AG (Germany) is the only supplier of medicinal [^{223}Ra]Cl_2 so-called Xofigo®. It was registered in 2013 as a drug for bone metastases treatment. Its action is based on Ra to Ca similarity, so Ra^{2+} is firstly accumulated in fast-changing bone tissue. [SPC Xofigo 2020]

Physical and chemical properties of ^{223}Ra and its production

Radium-223 has an 11.4 day half-life. It is in the middle of the ^{235}U decay chain and ends with a stable ^{207}Pb [LCN 2021]. During ^{223}Ra decay 4 alpha and 2 beta particles are emitted (**Fig. 8**).

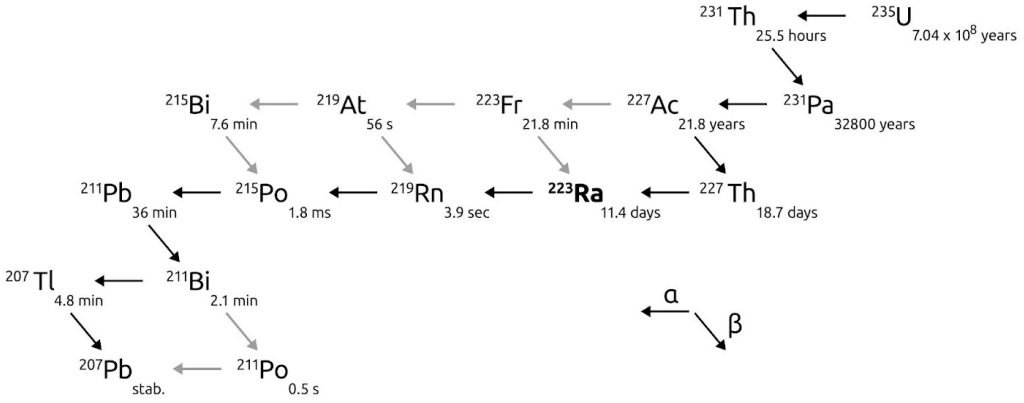

Fig. 8. ^{235}U decay scheme.

Radium-223 is produced on reactors mainly under the following reaction:

$$^{226}Ra(n,\gamma)^{227}Ac\ (21.8\ y,\ 98.6\ \%) \rightarrow {}^{227}Th\ (18.7\ d,\ 100\ \%) \rightarrow {}^{223}Ra\ (11.4\ d)$$

Actinium-227 also decays to ^{223}Fr with a probability of 1.4 %, however, Fr decays to ^{223}Ra with a probability of 99.99 %. This scheme allows the use of ^{227}Ac as a mother radionuclide in generators for radium production, however, due to its long half-life, it demands strong radiation protection and control of waste disposal. For more, each ^{223}Ra batch must be tightly controlled for ^{227}Ac impurities. [Weidner 2012]

The ^{227}Ac/^{223}Ra generator is being investigated and is not registered for medicinal usage yet. The generator is based on an anion exchanger eluted with a mixture of 0.8 M nitric acid and 80 % MeOH. Under this condition, Ac and Th remain on the column while Ra is eluted. However, due to the radiation damage

of the anion exchanger, ^{227}Ac leaking occurs in time. Another disadvantage of the current construction is the fact that the eluate requires further adjustment to be used in medicine: Ra must be transferred into a biologically acceptable medium, ideally saline. The most common way to transfer is evaporation with further dissolution, however, evaporation of active substances demands special equipment which is not ordinarily available in hospitals. [Guseva 2004, Kozempel 2014]

As far as radium belongs to the group II.A, its chemical properties are similar to Ba, Sr and Ca. It forms soluble in water chloride, bromide, nitrate and hydroxide salts. Among relevant properties are the fact that Ra can substitute Ca in the HAp structure, which leads to beneficial labelling of artificial HAp and also reliable bone-seeking. [Molinari 1990]

Labelling of nanoparticles with ^{223}Ra

In comparison with other mentioned radionuclides, ^{223}Ra is used for nanoparticle labelling more often. Not only inorganic NPs are being labelled with radium, but also liposomes that belong to organic NPs.

The labelling procedure for organic versus inorganic NPs is different. While inorganic particles are usually labelled via surface sorption and do not require gentle conditions, liposome labelling leads to the implementation of the radionuclide just inside the liposome. Moreover, liposomal labelling must be performed in strictly controlled conditions due to its sensitivity. For example, pegylated liposomal doxorubicin was labelled with ^{223}Ra in presence of sucrose with yield ranging from 51 to 67 %. Further study showed sufficient in vivo stability and promising biodistribution properties in mice. [Jonasdottir 2006]

Inorganic particle labelling occurs in literature more often in comparison with organic. Lanthanum (III) phosphate ($LaPO_4$) NPs coated with 2 shells and labelled with ^{223}Ra, ^{225}Ac, and ^{227}Th showed yields over 99 % for all three RN. Other nanoparticle labelling reported in the same work based on $GdVO_4$ NPs with Eu dopation showed partial retention of ^{223}Ra (~75 %), ^{225}Ac (75–95 %), and ^{227}Th (>96 %) [Toro-Gonzalez 2020]. Another study of $LaPO_4$ NPs showed up to 88 % ^{223}Ra retention during 35 days and 99 % for shell coated NPs [Rojas 2015].

Sorption of ^{223}Ra on nanodiamonds was also tested, however, it did not show sufficient retention under tested conditions [Garashchenko 2018]. Another interesting approach is NPs composed of poly(lactic-co-glycolic acid) as biodegradable and easy-to-functionalize material. Good encapsulation results were achieved with Ba labelling as a preliminary step for Ra labelling [Ambrogio 2020].

Nanozeolites conjugated with Substance P and labelled with ^{223}Ra have shown not just good retention (90–95 %), but also high affinity toward NK-1 receptors in glioma cells and cytotoxic effect. All experiments were conducted in vitro [Piotrowska 2017]. Other pegliated nanozeolites functionalized with anti-PSMA D2B antibody and labelled with ^{223}Ra also showed good yields and stability (over 95 % up to 12 days), affinity to the appropriate cells and cytotoxic activity, however, also it require further in vivo research [Czerwińska 2020].

Other inorganic nanoparticles investigated as ^{223}Ra vehicles for targeted α-therapy were barium ferrite NPs. These NPs were conjugated with trastuzumab, functionalized with 3-phosphonopropionic acid (CEPA), and labelled, so finally yield was over 98 % during 30 days. The obtained [^{223}Ra]-BaFe-CEPA-trastuzumab NPs exhibited high affinity, cell internalisation, and cytotoxicity towards the human ovarian adenocarcinoma SKOV-3 cells. [Gawęda 2020]

Aims of the Thesis

Based on literature research and conducted preliminary experiments HAp nanoparticles have shown themself as a prospective material for nanomedicine. Some work considering HAp nanoparticles was already performed by colleagues (Eva Malkova a Pavel Nykl), however, it was just the beginning. Their experiments just opened the research of HAp-NPs. This thesis greatly expands, structures, and summarises knowledge on HAp as a future nano-drug.

The main aims were the following:

- development of a usable labelling method for medicine practice with:
    - ^{18}F,
    - ^{68}Ga,
    - ^{99m}Tc,
    - ^{223}Ra;
- stability studies in biologically relevant media of the prepared HAp-NPs labelled with ^{68}Ga, ^{18}F, ^{99m}Tc, and ^{223}Ra.

These goals formulated shortly include not just labelling investigation, but also HAp-NPs preparation and purification, structure analysis, modelling of surface behaviour, in-depth research on pH influence and ageing.

Labelling method investigations were aimed at first on the possibility of labelling with both cations and anions, and then optimization for further use. Since the goal is the practical application of nanoparticles, the labelling techniques should be realisable under the usual working conditions of the personnel of the radiochemical laboratory of a general hospital.

Further stability studies are also extremely important to understand the behaviour of HAp-NPs in a biological environment and include investigation of the retained activity of labelled NPs in bovine serum, bovine plasma, albumin solutions, and saline.

Experiments & Results

Materials

All chemicals were of analytical grade and were used without further purification.

Merck, Germany: phosphoric acid, boric acid, acetic acid, nitric acid, sodium nitrate, calcium nitrate tetrahydrate, sodium chloride, sodium acetate

Lach-ner, Czech Republic: sodium hydroxide, ammonium hydroxide solution (28%), ammonium hydrogen phosphate.

The British drug houses Ltd, UK: tin(II) chloride.

Biowest, France: bovine blood serum, bovine blood plasma, human serum albumin lyophilised (pH 7).

Demineralized water of 18 $M\Omega \cdot cm^{-1}$ was obtained from Millipore, USA water purification system and was used for all experiments.

Radionuclides: fluorine-18 in the form of commercially available aqueous [^{18}F]NaF was obtained from ÚJF AV ČR, v. v. i. (Husinec - Řež, Czech Republic). Gallium-68 in the form of $GaCl_3$ in 0.1 M HCl was gained from the ^{68}Ge/^{68}Ga commercial generator (GalliaPharm, Eckert & Ziegler Radiopharma GmbH, Germany). Technetium-99m in the form of $NaTcO_4$ in saline was gained from ^{99}Mo/^{99m}Tc commercial generator DRYTEC™ (GE Healthcare LTD, Chicago, IL, USA). Radium-223 in the form of $Ra(NO_3)_2$ was obtained from the ^{227}Ac/^{227}Th/^{223}Ra generator prepared at the Department of Nuclear Chemistry according to Guseva et al. [Guseva 2014]. After the elution with 0.7 M HNO_3 in 80 % methanol, $Ra(NO_3)_2$ was dried and reconstituted in water.

Buffers: Required pH was reached by the addition of solution A to solution B under stirring and pH measurement.
Acetate buffer – solution A: 1 M sodium acetate; solution B: 1 M acetic acid.
Britton-Robinson buffer (BRB) – solution A: 1 M sodium hydroxide; solution B: 0.5 M of each phosphoric acid, formic acid, and boric acid.

Citrate buffer – solution A: 0.1 M citric acid; solution B: 0.1 M sodium citrate.
Phosphate buffer – solution A: 0.2 M monobasic sodium phosphate; solution B: 0.2 M dibasic sodium phosphate.

Experimental apparatus

Samples were mixed on a Stuart SSM3 rocker (Cole-Parmer Ltd., Vernon Hills, IL, USA) and centrifuged on VWR Micro Star 12 centrifuge (VWR International, Radnor, PA, USA). Radioactive experiments were performed under aseptic conditions in Vertical Laminar Flow Clean Bench Airflow 150 UV (Esi FLUFRANCE, France). The measurement of pH was performed on pH-metre Mettler-Toledo.

Gamma spectra were measured with a HPGe detector and analysed using the Maestro Software (ORTEC, Oak Ridge, TN, USA). Overall activities were measured with a well-type NaI(:Tl) crystal CII CRC-55tW (CAPINTEC, Ramsey, NJ, USA).

Fourier-transform infrared spectra were recorded on Nicolet iS50 FTIR (ThermoScientific, USA) in the middle infrared region 400–4000 cm^{-1} with a resolution of 2 cm^{-1} on a diamond crystal and compared to relevant records in HR Inorganics I. – Minerals database [HR IMD 2018].

Powder X-ray diffractograms (XRPD) were recorded using Rigaku MiniFlex 600 (Ni-filtered Cu-K_{α}1,2 radiation) equipped with NaI(:Tl) scintillation detector and compared to the relevant records in the ICDD PDF-2 database (version 2013) [ICDD 2013].

TEM analyses were conducted on a TEM microscope Tecnai G2 Spirit Twin 12; FEI Company, Czech Republic, at an accelerating voltage of 120 kV.

Potentiometric titrations were made on TIM845 Potentiometric Titrator (HACH, USA) equipped with Ag/AgCl electrode (HACH, USA).

Preparation

Hydroxyapatite NPs were prepared in bulk by adding the determined volume of 1.2 M $Ca(NO_3)_2$ into excess water, the pH was set to 11 with NH_4OH and maintained during the reaction. The equal volume of 0.7 M $(NH_4)_2HPO_4$ was added dropwise under stirring. The mixture was left overnight under stirring, washed with water (3 × 20 ml) and dried. The resulting powder was fine-grounded.

Hydroxyapatite formation undergo following reaction:

$10Ca(NO_3)_2 + 6(NH_4)_2HPO_4 + 2OH^- \rightarrow Ca_{10}(PO_4)_6(OH)_2 + 12NH_4NO_3 + 8NO_3^- + 6H^+$,

so high pH during the whole reaction is very important and its decrease leads to other phosphates formation.

Characterization

Characterization of produced nanoparticles via FTIR and XRPD was performed for each batch to prove its identity. Full characterization was performed for the first batch.

Confirmation of the material composition was made with FTIR and XRPD methods. ***Infrared spectra*** were recorded a few days after preparation (**Fig. 9**). These spectra showed the characteristic bands of PO_4^{3-} at 630–473 cm^{-1} and 1088–962 cm^{-1}. The small band at approx. 1400 cm^{-1} might be attributed to CO_3^{2-}. Bands at about 1630 cm^{-1} and 3000–3500 cm^{-1} correspond to deformation and stretching vibrations of OH^- respectively.

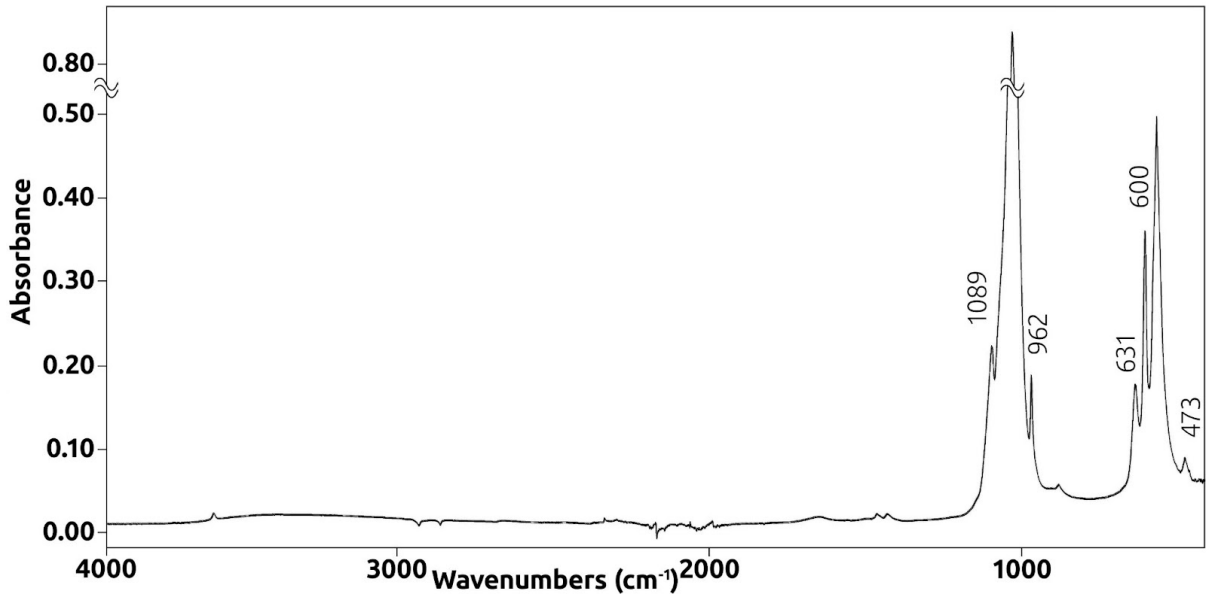

Fig. 9. FTIR spectrum of HAp.

Powder X-ray diffractograms (XRPD) have shown single-phase HAp in good agreement with the database record #01-071-5048 (**Fig. 10**). Unwashed nanoparticles showed the presence of NH_4NO_3 (**Fig. 11**) with very good crystallinity, so higher intensity on diffractograms.

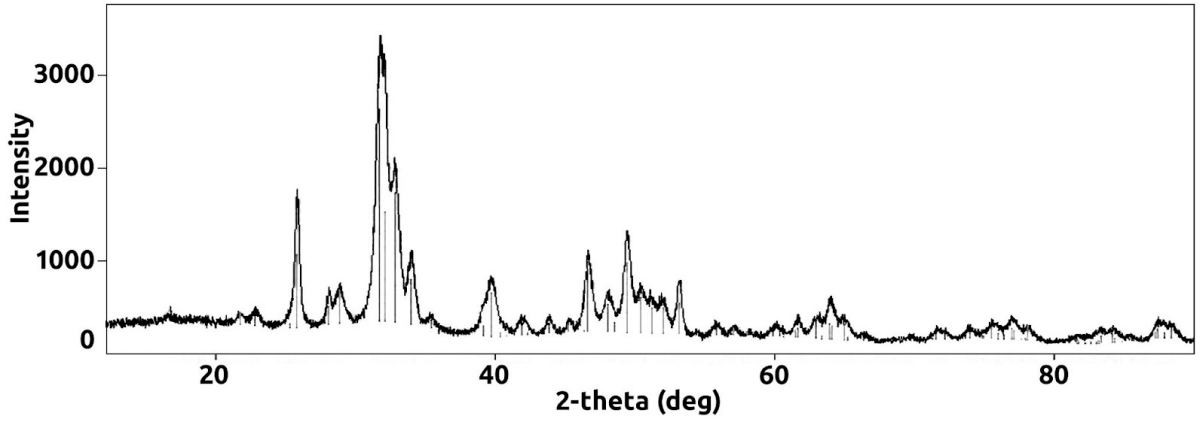

Fig. 10. XRPD diffractogram of HAp. The grey lines under the black curve represent database record #01-071-5048. The black curve is a recorded diffractogram.

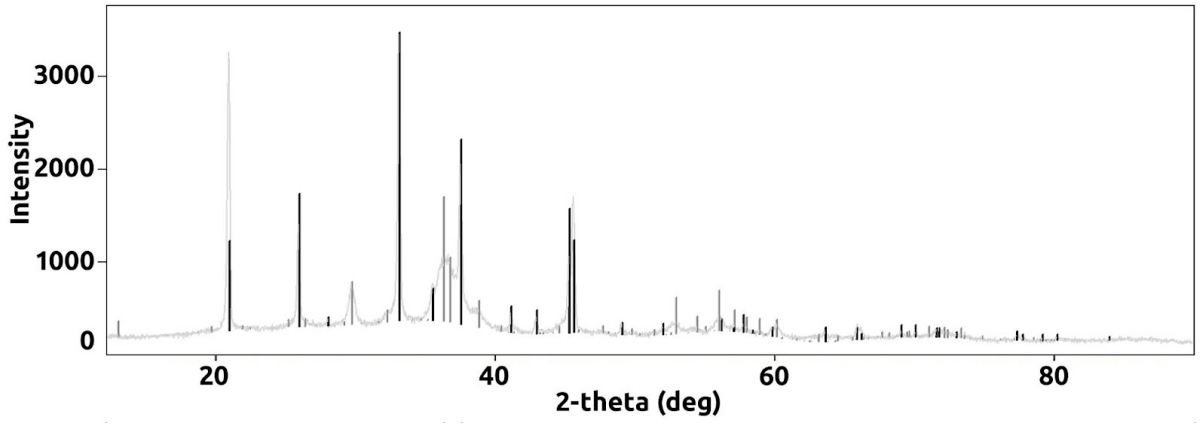

Fig. 11. XRPD diffractogram of HAp contaminated with NH_4NO_3. Black lines represent the database record of NH_4NO_3 (00-047-0867), the grey lines represent the database record of HAp, the light grey curve is recorded diffractogram.

The nano-sized structure was proven via ***TEM analyses***. The sample was dispersed in water on a supporting copper grid covered with an electron transparent carbon film. Particle morphology and crystalline structure study were performed with standard bright field imaging (TEM/BF), energy-dispersive analysis of X-rays (TEM/EDX) yielded the elemental composition, and selected area electron diffraction (TEM/SAED). HAp nanoparticles demonstrated narrow size distribution (**Fig. 12.**)

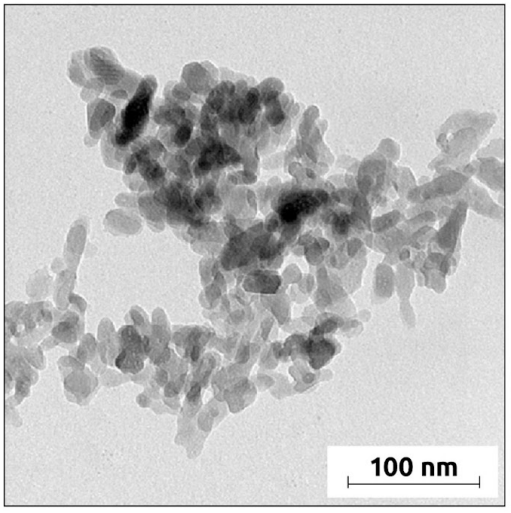

Fig. 12. TEM/BF micrograph showing the size and shape of HAp-NPs.

Crystalline structure comparison between measured TEM/SAED diffractograms and theoretically calculated XRD diffraction patterns were in good agreement.

HAp had the hexagonal structure confirmed with the record from Crystallography Open Database [COD 2018] COD #9001233 = HAp (**Fig. 13**).

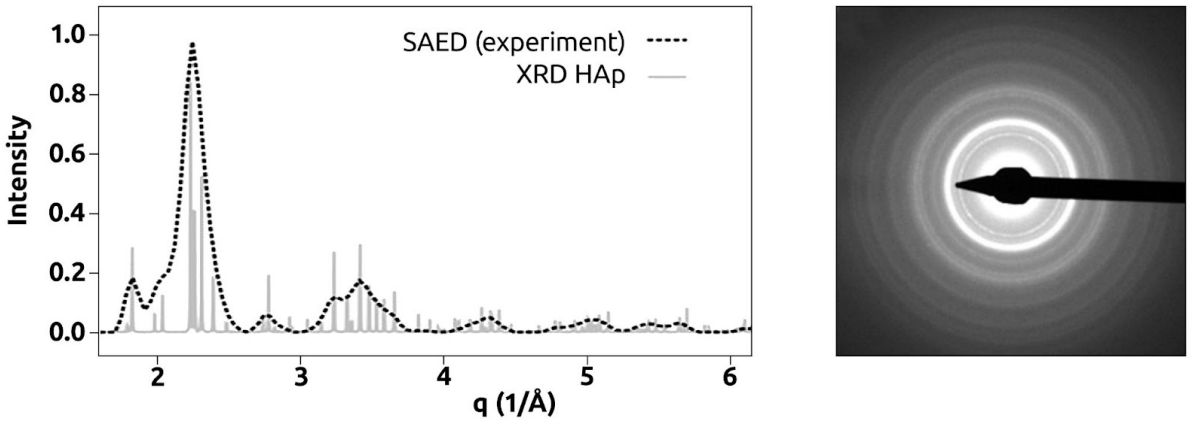

Fig. 13. Left - comparison of experimental and theoretically calculated patterns. Right - experimental TEM/SAED diffraction pattern.

Elemental composition investigated via TEM/EDX showed that prepared nanoparticles were free from impurities (**Fig. 14**). Well-seen peaks from carbon and copper ca1§me from the used supporting copper grid covered with a thin carbon layer.

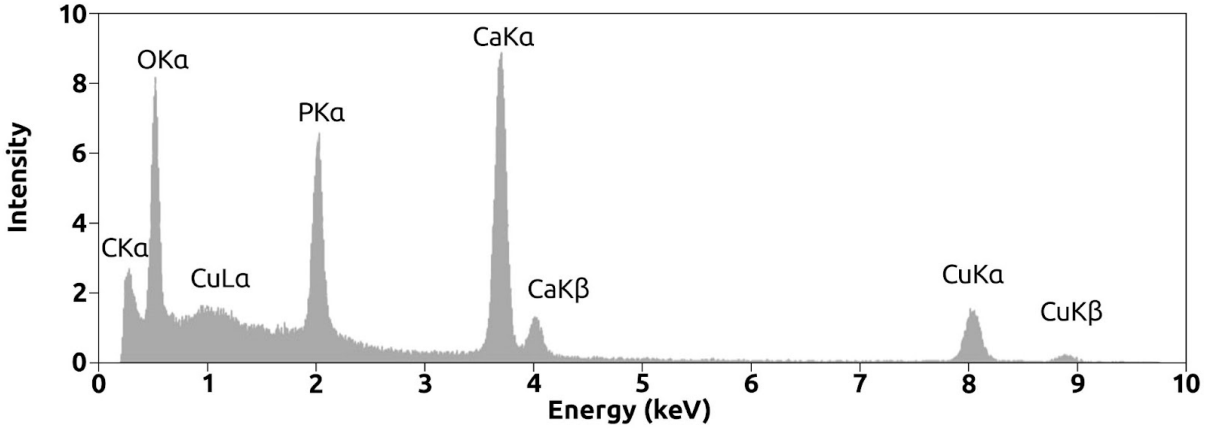

Fig. 14. TEM/EDX spectrum of HAp-NPs.

According to TEM/BF image results based on the Scherrer equation, nanoparticle size was calculated to be 21.7 ± 6.9 nm. Based on the results obtained from TEM analysis, the specific surface area was also calculated. Different calculation methods were applied, and the average result was found to be 93 ± 11 m^2/g.

Experimental results of the ***specific surface area*** calculated by selective sorption of nitrogen at the temperature of liquid nitrogen using a multi-point BET method were found to be 117 ± 8 m^2/g, so both numbers are in good agreement. Measurements and calculations are described in detail in the article published in 2019 [Kukleva 2019].

To determine the total concentrations of the edge sites and ion exchange groups, protonation and ion exchange constants (for Na^+/H^+ exchange) ***potentiometric titrations*** were performed. The HAp (150 mg) was dispersed in 50 ml of 0.1 M $NaNO_3$ at 23 ± 1 °C. Titration was performed with 0.1 M NaOH under N_2 bubbling for the alkaline part of the titration curve (3 times) and 0.1 M HNO_3 for the acidic one (3 times). The studied pH range was between 5 and 10. As a blank 50 mL of 0.1 M $NaNO_3$ without any solid phase added for both acidic and alkaline parts of the titration curve was used. Stability conditions were set to 20 mpH/min, and the addition of the titrant volume was by 0.05 ml. The results are provided and discussed in the Discussion chapter.

The usable pH range of HAp-NPs was studied via ***dissolving experiments***, where 5 mg of HAp was dispersed in 5 ml of Britton-Robinson buffer at pH from 2 to 8. The experiment lasted 1.5 hours, then the samples were centrifuged, washed with water 3 times, and dried on air for 3 days under the same conditions the bulk sample was stored. Test tubes were weighed before the HAp was added, then with HAp, and then after drying, so the weights of the HAp measured before and after the experiment were compared. Significant dissolution of HAp even at pH 4 was shown, while at pH 3 and lower the HAp has dissolved absolutely (**Fig. 15**). At pH 5 HAp-NPs dissolution can be taken as negligible, and at pH over 5 HAp did not dissolve in the studied solution.

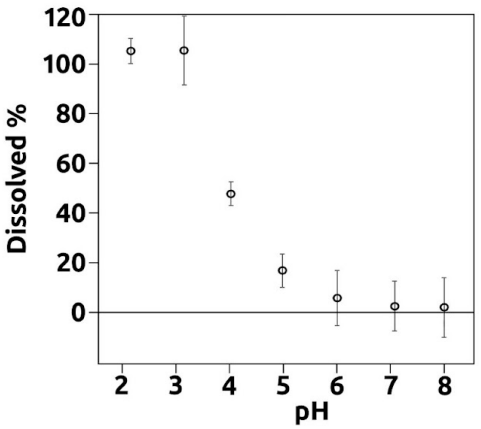

Fig. 15. Dissolution of HAp-NPs in Britton-Robinson buffer for 1.5 hours.

The ***ageing*** of HAp was also explored. The sample EM-3.1 prepared by Eva Málková in 2014 was characterised several times via FTIR and XRPD. Obtained results are compared with spectra and diffractograms recorded after preparation and described in the Discussion chapter.

Radiolabelling & Stability tests

In general, two radiolabelling strategies were tested: direct labelling of the NPs prepared earlier (ready-made NPs) and structure labelling, where NPs preparation was conducted in a radionuclide solution mixed with buffer/saline. However, strategies were modified according to radionuclide's different chemical properties. All labelling experiments were performed at least 3 times.

Labelling yields were determined based on the ratio of final activity after washing corrected on time to initial activity added into the sample (**Eq. 1, 2**). The activity of all separated solutions was also measured to ensure the accuracy of the experiments.

$$\text{Labelling yield [\%]} = \text{Final Activity}_{\text{corrected}} / \text{Initial Activity} \cdot 100\ \% \qquad \textbf{Eq. 1}$$

$$\text{Final Activity}_{\text{corrected}} = \text{Final Activity}_{\text{measured}} / e^{-\lambda t} \qquad \textbf{Eq. 2}$$

Here λ is the decay constant, t is the period between initial activity measurement and final activity measurement.

Stability tests were performed in vitro in relevant biological media: saline, albumin solution 1 % and 5 %, bovine serum and bovine plasma. Studied periods were different for all RN due to different half-lives. All stability tests were performed at least in triplets. Results were evaluated based on the ratio of released activity found in the separated solution to total sample activity at the same time (**Eq. 3**).

$$\text{Stability yield [\%]} = \text{Separated activity} / \text{Total Activity} \cdot 100\ \% \qquad \textbf{Eq. 3}$$

Fluorine-18

Labelling of ready-made HAp-NPs with ^{18}F was performed as follows: 5 mg of HAp-NPs were dispersed in 1 ml of saline in an eppendorf test tube, then approx. 10 MBq of ^{18}F was added to the particles. In 15 minutes the samples were centrifuged and labelling media was separated from the NPs. Then the samples were washed once with saline.

The chosen strategy has shown sufficient labelling yields of 92.8 ± 2.8 %.

Structure labelling with ^{18}F was also performed: 40 µl of 1.2 M $Ca(NO_3)_2$ was added into 1 ml of saline, and pH was adjusted to 11 with 0.1 M NaOH. Then approx. 10 MBq of ^{18}F was added and mixed. Afterwards, 40 µl of 0.7 M $(NH_4)_2HPO_4$ was added and mixed. In 15 minutes samples were centrifuged, washed and measured.

Labelling yields were about 95 %, however, further pilot stability experiments in saline have shown released activity of about 20 % during 30 min. Therefore, this labelling method was excluded from further experiments.

To determine optimal labelling time, ***kinetics experiment*** series was performed. Five samples with 5 mg of HAp-NPs were dispersed in 1 ml of saline. All samples were labelled with approx. 10 MBq of ^{18}F simultaneously. Then the labelling was ended with centrifugation and washing in 1, 2, 5, 10, and 15 min. Yields for each labelling period were calculated (**Fig. 16**)

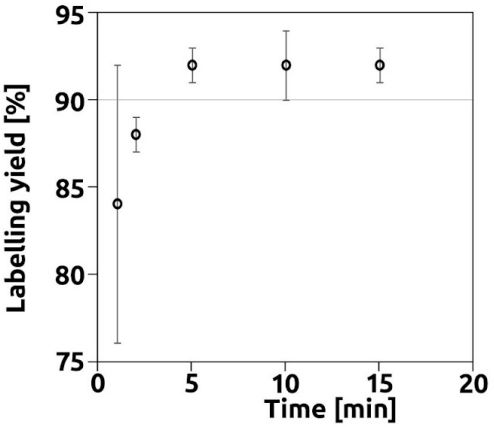

Fig. 16. Kinetics of HAp-NPs labelling with ^{18}F.

According to the obtained results, ***stability experiments*** were performed on ready-made NPs. Hydroxyapatite (5 mg) was labelled with ^{18}F (approx. 50–150 MBq) as described earlier, washed and then transferred into a fresh new media (0.5 ml). Behaviour in bovine serum, bovine plasma, 5 % albumin solution and saline was investigated. Media were changed to fresh every 1–2 hours. It was found that during 10 hours of remaining activity on the HAp-NPs was about 90 % in serum and plasma, which are the most relevant solutions in the meaning of future usage (**Fig. 17**). Results obtained in saline and 5 % albumin were comparable.

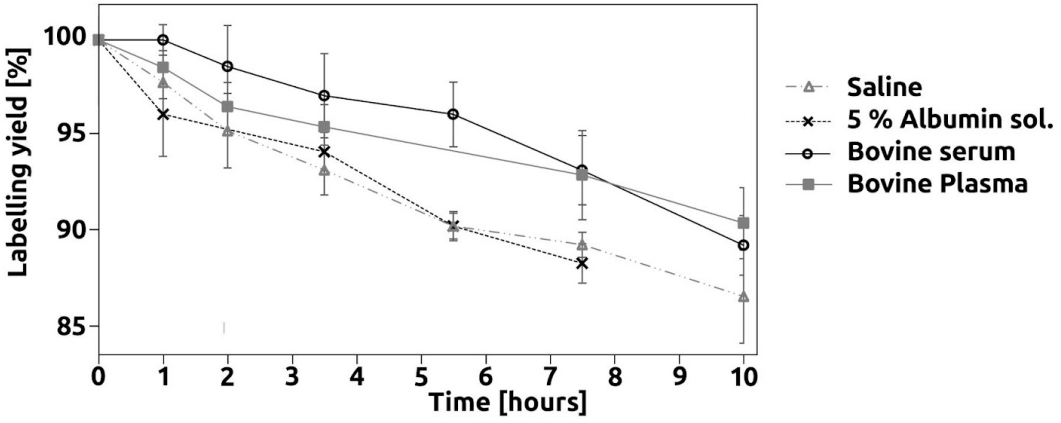

Fig. 17. [^{18}F]-HAp-NPs stability studies in saline, 5 % albumin solution, bovine serum and bovine plasma.

Gallium-68

Labelling of pristine ready-made HAp-NPs with ^{68}Ga was conducted in a variety of buffer solutions due to Ga hydrolysis in pH over 4 (**Fig. GA-3.**), therefore, labelling in saline under neutral pH was not possible. Four buffers were tested: citrate, Britton-Robinson, acetate and phosphate. These buffers were chosen to cover the whole pH range to find the best labelling conditions. The labelling procedure was following: 15–100 MBq of ^{68}Ga was added to 5 mg of HAp dispersed in 1 ml of buffer solution, let to react for 15 min, then centrifuged and washed with buffer 3 times.

It was found that citrate buffers cannot be used for HAp labelling (**Fig. 18**). For further experiments acetate and Britton-Robinson buffers at pH 5 were chosen.

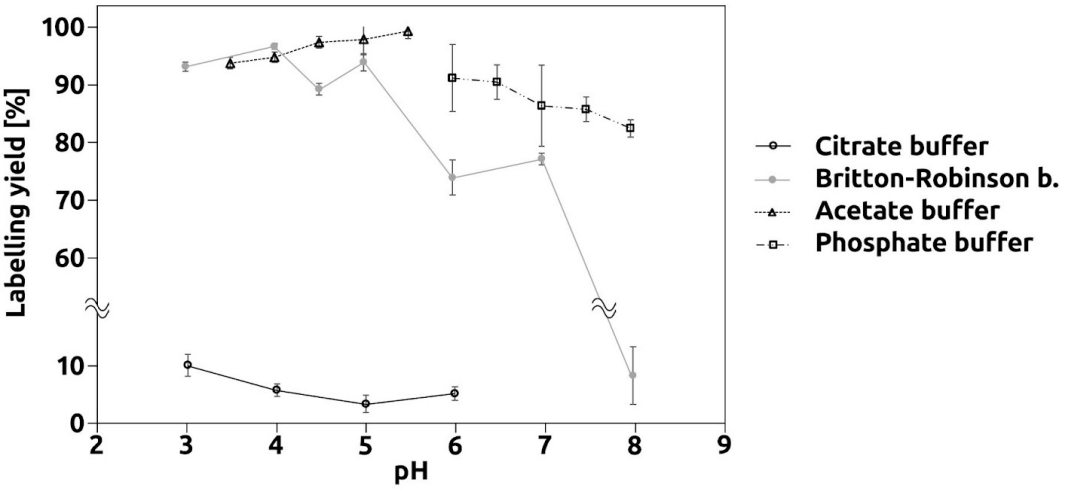

Fig. 18. Dependence of ^{68}Ga labelling yields on pH in different conditions for ready-made NPs.

Structure labelling with ^{68}Ga was also performed: 40 µl of 1.2 M $Ca(NO_3)_2$ was added into 2 ml of acetate buffer, and pH was adjusted to 11 with 0.1 M NaOH. Then 0.5 ml of ^{68}Ga was added and mixed. Afterwards 40 µl of 0.7 M $(NH_4)_2HPO_4$ was added and mixed. In 15 minutes samples were centrifuged, washed and measured.

Labelling yields were very poor (about 30 %), and this method was excluded from further experiments.

Labelling of chelating ligands with ^{68}Ga and attachment to HAp procedure was tested, where DOTA, NOTA, TETA, and TRAP (1 g/ml for all ligands) were first labelled with ^{68}Ga (10–50 MBq) at 95 °C for 30 minutes (according to the literature [SPC SomaKit 2021]), and then mixed with ready-made HAp-NPs in acetate buffer at pH 5–6. Nanoparticle labelling lasted 30 minutes at 95 °C. Yields were low (**Tab. 6**), so this labelling technique was rejected.

Tab. 6. Results of labelling of chelating ligands with ^{68}Ga and then HAp.

Sample	Yield
[^{68}Ga]-DOTA-HAp-NPs	3 ± 2 %
[^{68}Ga]-NOTA-HAp-NPs	1 ± 5 %
[^{68}Ga]-TETA-HAp-NPs	70 ± 3 %
[^{68}Ga]-TRAP-HAp-NPs	4 ± 2 %

Other labelling conditions for ready-made NPs labelling were also studied to increase labelling yields and stabilise labelled particles. ***Labelling in a presence of chelating ligands*** DOTA, NOTA, TETA, and TRAP (1 g/ml for all ligands) was provided. The procedure was similar to the earlier described pristine HAp labelling: 5 mg of HAp was dispersed in a mixture of 2 ml of buffer and 50 µl of ligand. The sample was heated to 95 °C, and then ^{68}Ga was added in the smallest possible volume (10–100 MBq). The mixture was let to react under heating and shaking for 15 minutes, then centrifuged and washed with saline 3 times. Here Britton-Robinson buffer was used due to its wide pH range. It was found that NOTA and TRAP are not suitable for Ga labelling under tested conditions. However, DOTA and TETA provided very promising results at pH 5 (**Fig. 19**). Further experiments were conducted with DOTA because of its better availability. Also, it was found that sufficient purification after labelling was reached with 1 time saline washing.

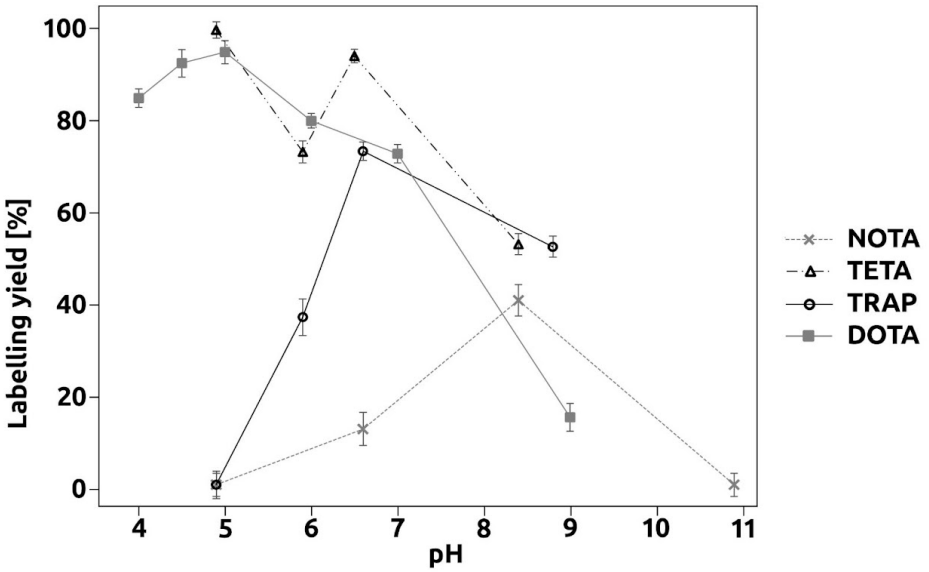

Fig. 19. Dependence of ^{68}Ga labelling yields on pH in Britton-Robinson buffer. HAp-NPs were labelled in the presence of chelating ligands NOTA, TETA, TRAP and DOTA.

Labelling kinetics was determined in the same manner as labelling in a presence of chelating ligands: 5 mg of HAp was dispersed in a mixture of 2 ml of Britton-Robinson buffer and 50 µl of ligand DOTA or without any ligand for pristine HAp labelling. The sample was heated to 95 °C, and then ^{68}Ga was added in the smallest possible volume (10–100 MBq). The mixture was let to react under heating and shaking for the required time, then centrifuged and washed with saline once. Uptake kinetics was very fast for both samples and showed a yield of about 95 % within 10 minutes (**Fig. 20**). A longer labelling period was not necessary, it did not lead to better labelling yields. Hydroxyapatite nanoparticles decorated with DOTA have shown better labelling yields with ^{68}Ga, therefore, this labelling procedure was chosen for further stability studies.

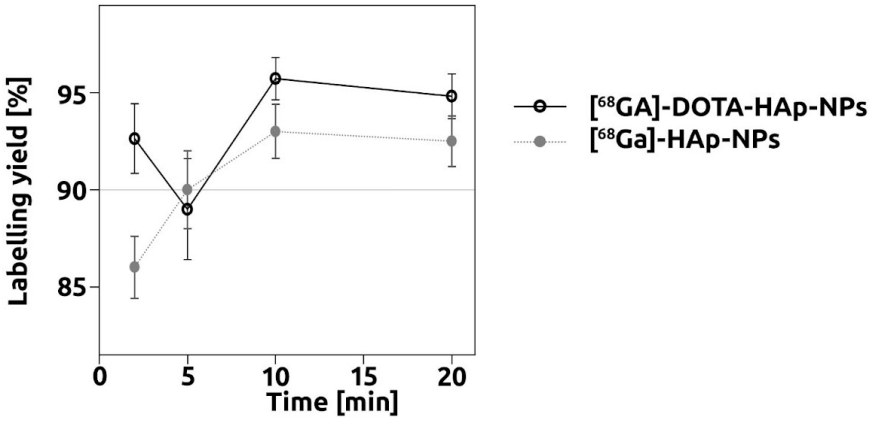

Fig. 20. Kinetics of HAp-NPs labelling with ^{68}Ga.

Stability experiments were performed on ready-made NPs. Hydroxyapatite (5 mg) was labelled with ^{68}Ga (approx. 100 MBq) in a presence of DOTA as described earlier, washed and then transferred into a fresh new media (1 ml). Behaviour in bovine serum, bovine plasma, 5 % albumin solution, and saline was investigated. The media was changed to fresh every 1–2 hours. It was found that during 4 hours remaining activity on the HAp-NPs was about 90 % in saline and 5 % albumin solution (**Fig. 21**). Unfortunately, labelled NPs in serum and plasma showed worth stability.

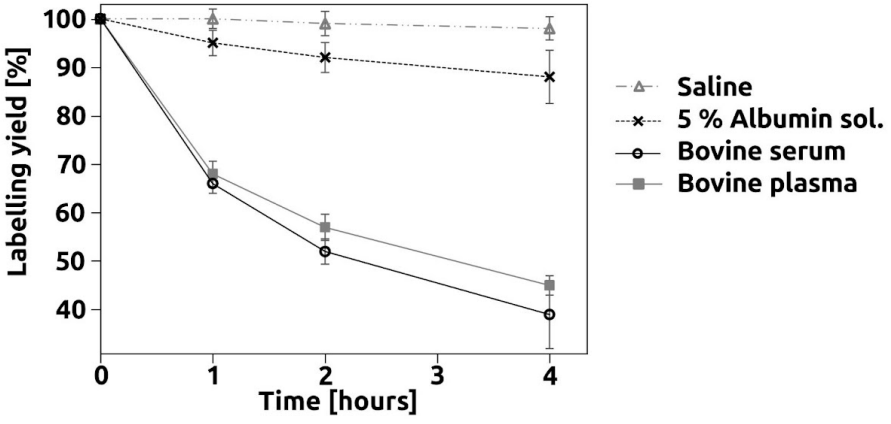

Fig. 21. [^{68}Ga]-DOTA-HAp-NPs stability studies in saline, 5 % albumin solution, bovine serum, and bovine plasma.

Technetium-99m

Labelling of ready-made HAp-NPs with ^{99m}Tc was performed similarly to ^{18}F labelling: 5 mg of HAp-NPs was dispersed in 0.5 ml of fresh stannous chloride solution (480 mg/l). Then 60–100 MBq of ^{99m}Tc in the eluted form was added. Samples were incubated for 1 hour, then centrifuged, and washed with saline 3 times.

Structure labelling with ^{99m}Tc was also conducted similar to ^{18}F labelling: 35 µl of 1.2 M $Ca(NO_3)_2$ was added into 0.5 ml of fresh stannous chloride solution (480 mg/l), pH was set to 11 with 1 M NH_4OH. Then 60–100 MBq of ^{99m}Tc in the eluted form was added and mixed. Afterwards, 35 µl of 0.7 M $(NH_4)_2HPO_4$ was added and mixed. After 1 hour the samples were centrifuged and washed 3 times with saline.

Both strategies have shown sufficient labelling yields of 95.9 ± 1.5 % and 94.6 ± 0.4 % for ready-made and structure labelling respectively.

Kinetics studies were conducted in order to determine optimal labelling time. The samples with 5 mg of HAp-NPs were dispersed in 1 ml of saline. Each sample was labelled with approx. 80 MBq of ^{99m}Tc according to the procedure described earlier. The labelling was ended with centrifugation and washing at a determined time after labelling initiation. Yields for each labelling period were calculated (**Fig. 22**) It was found that labelling yields over 90 % were reached within 15 minutes, however, 95 % labelling yields were obtained in 30 minutes.

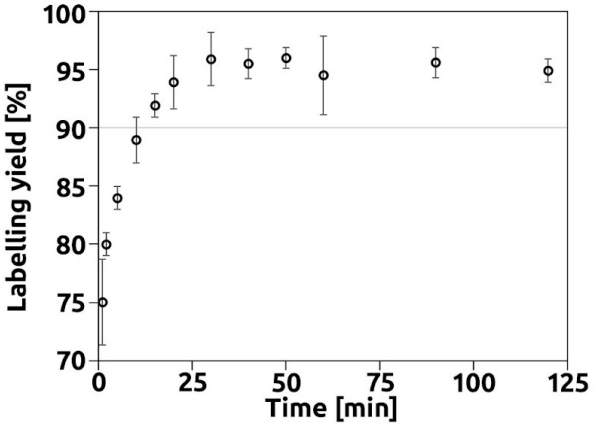

Fig. 22. Kinetics of HAp-NPs labelling with ^{99m}Tc.

Stability experiments were performed on both ready-made and structure labelled NPs. Both sample series were labelled as described earlier and washed with saline after labelling. Then the samples were transferred into a fresh new media (0.5 ml). Behaviour in bovine serum, bovine plasma, 1 & 5 % albumin solutions, and saline was investigated. The media was changed to fresh every 1–9 hours. The experiments showed that structure-labelled HAp-NPs seem to be more stable in biologically relevant media than ready-made-labelled NPs: stability within 32 hours was over 90 % for structure-labelled NPs in all media except plasma and over 80 % for ready-made labelling procedure. Both series showed similar stability in plasma over 60 % (**Fig. 23, 24**).

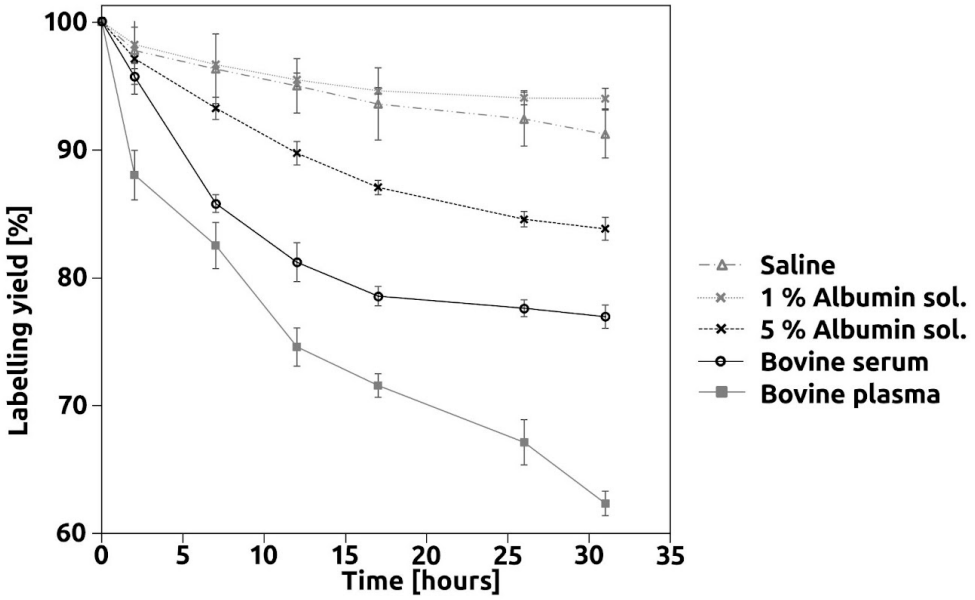

Fig. 23. Ready-made-labelled [^{99m}Tc]-HAp-NPs stability studies in saline, 1 % albumin solution, 5 % albumin solution, bovine serum and bovine plasma.

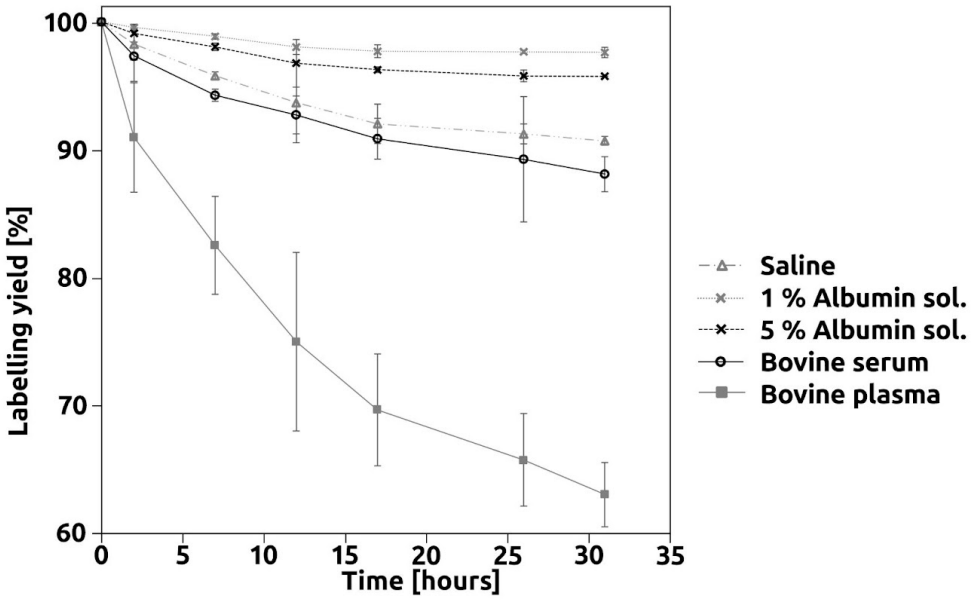

Fig. 24. Structure-labelled [^{99m}Tc]-HAp-NPs stability studies in saline, 1 % albumin solution, 5 % albumin solution, bovine serum and bovine plasma.

Radium-223

Labelling of ready-made HAp-NPs with ^{223}Ra was performed similarly to ^{18}F and to ^{99m}Tc labelling in order to obtain the comparable results: 5 mg of HAp-NPs were dispersed in 0.5 ml of saline. Then 1–10 kBq of ^{223}Ra in the $Ra(NO_3)_2$ form was added. Samples were incubated for 1 hour, then centrifuged, and washed with saline 3 times.

Structure labelling with ^{223}Ra was also conducted similar to ^{18}F and ^{99m}Tc labelling: 35 µl of 1.2 M $Ca(NO_3)_2$ was added into 0.5 ml of saline, pH was set to 11 with 1 M NH_4OH. Then 1–10 kBq of ^{223}Ra was added and mixed. As the last step, 35 µl of 0.7 M $(NH_4)_2HPO_4$ was added and mixed. After 1 hour the samples were centrifuged and washed 3 times with saline.

Both strategies have shown sufficient labelling yields of 94.2 ± 0.5 % and 97.0 ± 0.5 % for ready-made and structure labelling respectively.

pH dependence of ^{223}Ra labelling yields in Britton-Robinson buffer solution was already determined by Pavel Nykl in 2017 [Nykl 2017]. The results were summarised, analysed and published [Suchankova 2020 B]. ***Labelling kinetics*** was determined earlier by colleagues also [Nykl 2017]. The results were used for modelling and were already published in 2020 by Suchankova et al. [Suchankova 2020 C]. Both experimental results, as well as modelling evaluation, are observed in the Discussion chapter.

Stability studies were conducted in several biologically relevant media: saline, bovine serum, bovine plasma, and 1 % & 5 % albumin solutions. As far as labelling yields were sufficient for both labelling strategies, both ready-made and structure labelled NPs were tested. Both sample series were labelled as described earlier and washed with saline after labelling. Then the samples were transferred into a fresh new media (0.5 ml), which were changed to fresh one every 1–9 hours for a total of 59 hours for a short-term stability study. A long-term stability study was also conducted. The media were exchanged every 11 days, so stability experiments lasted 55 days in total.

It was found that structure-labelled HAp-NPs showed in general worth stability in various media in comparison with ready-made-labelled NPs (**Fig. 25–28**). All

sample series showed good stability in bovine serum (over 80 % activity remind on NPs for short-term and over 90 % for long-term experiments), and moderate values for other media.

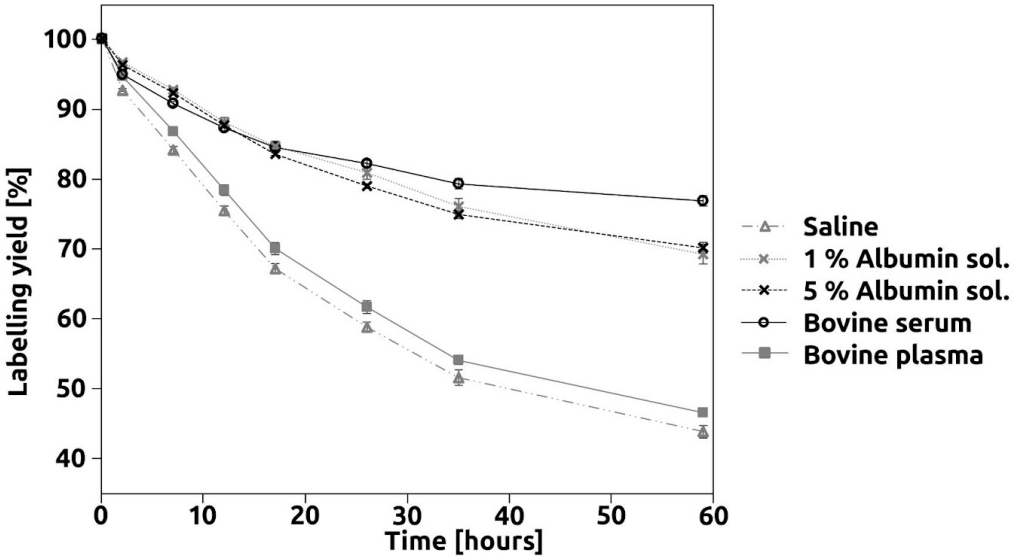

Fig. 25. Short-term ready-made-labelled [^{223}Ra]-HAp-NPs stability studies in saline, 1 % albumin solution, 5 % albumin solution, bovine serum and bovine plasma.

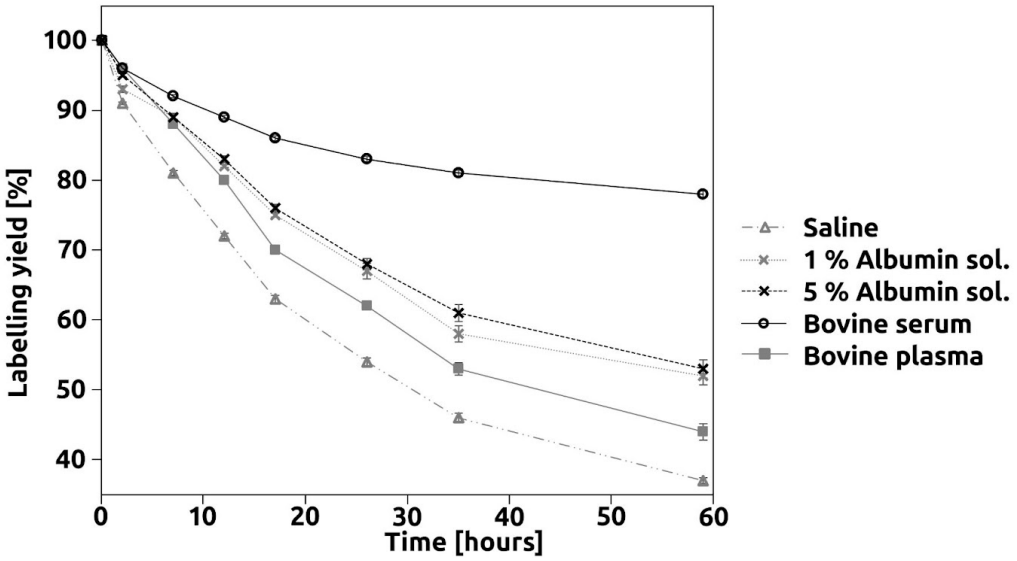

Fig. 26. Short-term structure-labelled [^{223}Ra]-HAp-NPs stability studies in saline, 1 % albumin solution, 5 % albumin solution, bovine serum and bovine plasma.

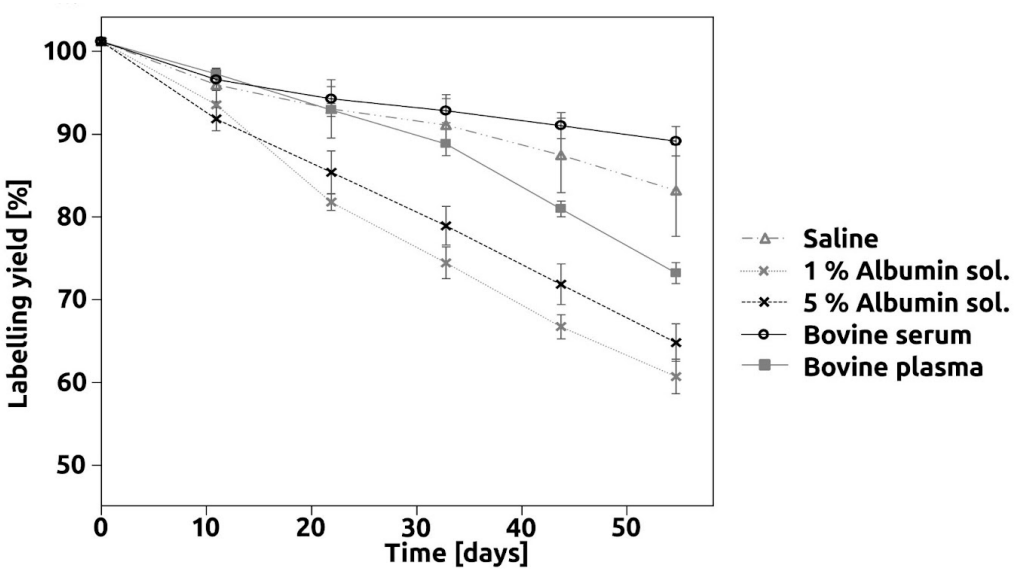

Fig. 27. Long-term ready-made-labelled [^{223}Ra]-HAp-NPs stability studies in saline, 1 % albumin solution, 5 % albumin solution, bovine serum and bovine plasma.

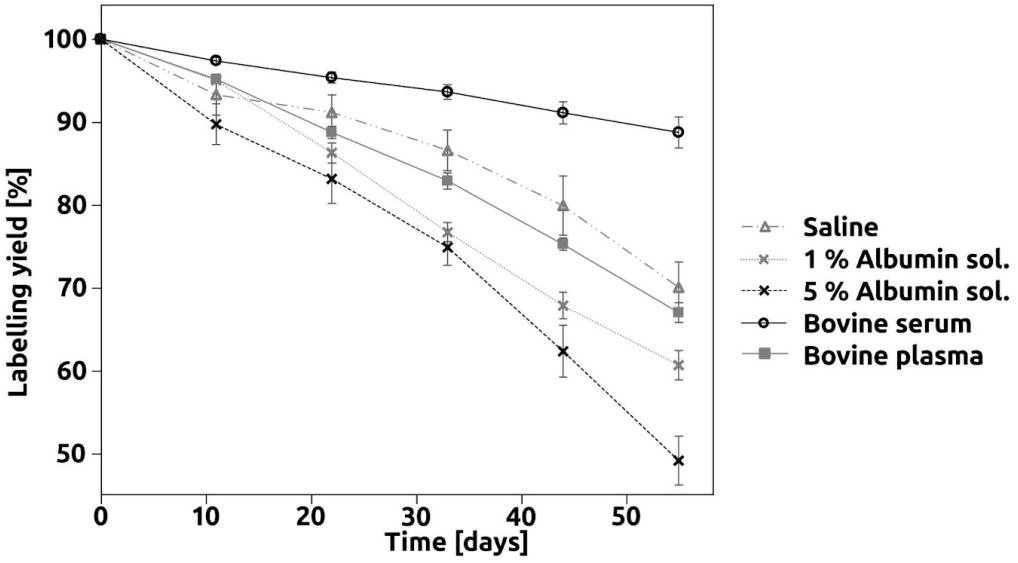

Fig. 28. Long-term structure-labelled [^{223}Ra]-HAp-NPs stability studies in saline, 1 % albumin solution, 5 % albumin solution, bovine serum and bovine plasma.

Discussion

This work deals with HAp-NPs as a material for radionuclide sorption that can be used in medicine. There are a few parameters important for the current aim: biocompatibility, biodegradability, low toxicity, high sorption capacity with different ions, radiation stability of the NPs, and stability of labelled NPs without leakage. However, the mentioned parameters are also important for environmental usages, such as water and soil decontamination, or a variety of applications in radioactive waste depository construction. Therefore, current work can be taken not just as strictly medicine-bound investigation, but also as wide-spectrum research applicable in different branches.

The research covers material preparation, its labelling and in vitro stability with chosen radionuclides. Studied methods can be easily expanded on bulk production and require ordinary equipment available in the standard radiochemical laboratories, like shaker and centrifuge.

Preparation & Characterisation

Hydroxyapatite nanoparticle preparation method resulted in pure material with high reproducibility. All impurities that appeared during the formation were washed easily because of their high solubility in water.

Further HAp characterisation was already published [Kukleva 2019]. Based on experimentally obtained dependencies (**Fig. 29**) in-depth surface characterisation of edge and layer sites was performed. As the main parameters concentration of edge sites (ΣPOH), ion exchange groups (layer sites) (ΣX), protonation (K_1, K_2), and ion exchange (KNa^+/H^+) constants were calculated. Calculations were based on three models usually used for protonation and sorption processes ongoing on edge sites: Constant Capacitance Model (CCM), Diffusion Double Layer Model (DLM), and non-electrostatic Chemical Equilibrium Model (CEM). Layer site processes could be described by the Ion Exchange Model (IExM). Combining these models six possible routes were analysed, however, only two of them (CEM + IExM & DLM + IExM) were in good agreement with experimental data. The agreement was figured out according to appropriate

values of the WSOS/DF value (weighted sum of squares of differences divided by the degrees of freedom) that should be in the interval 0.1 < WSOS/DS < 20. A detailed description of calculations and modelling was described in [Kukleva 2019].

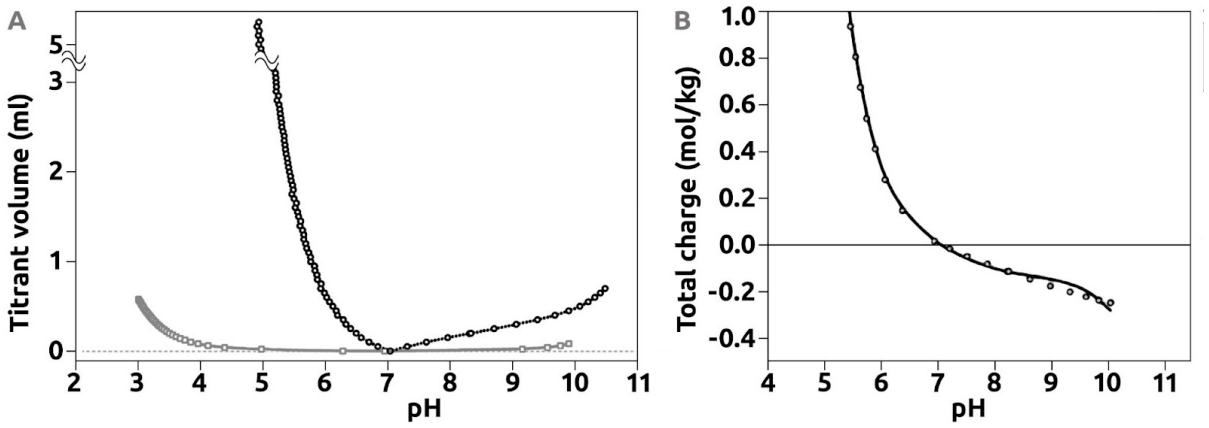

Fig. 29. A - Experimental dependences of added volume of titrant on pH. The black curve is the sample with HAp-NPs, and the grey curve is a blank sample of 0.1 M $NaNO_3$. **B** - Experimental data (circles) and calculated titration curve (line) with CEM + IExM model.

Concerning chosen models, CEM + IExM & DLM + IExM, total concentrations of the edge sites and ion exchange groups, protonation and ion exchange constants (for Na^+/H^+ exchange) were calculated (**Tab. 7**).

Tab. 7. The total HAp-NPs concentration of edge sites (ΣPOH) and ion exchange groups (layer sites) (ΣX), protonation (K_1, K_2), and ion exchange ($K_{Na+/H+}$) constants based on the titration curve evaluation (the table was taken from [Kukleva 2019]).

Model	ΣPOH [mol/kg]	ΣX [mol/kg]	K_1 [10^{11} l/mol]	K_2 [10^6 l/mol]	$K_{Na+/H+}$ [10^6 –]
CEM + IExM	5.10 ± 1.20	0.15 ± 0.01	5.12 ± 1.10	0.12 ± 0.03	3.01 ± 0.33
DLM + IExM	13.90 ± 4.35	0.20 ± 0.10	1.83 ± 0.68	18.00 ± 5.07	0.11 ± 0.33

According to all obtained experimental data the best way to describe ongoing processes is to apply the CEM + IExM model (**Fig. 29-B**). Evaluation of the titration curve was based on reactions playing roles on edge and layer sites:

$$\equiv PO^- + H^+ \leftrightarrow \equiv POH \quad \text{(edge site)},$$

$$\equiv POH + H^+ \leftrightarrow \equiv POH_2^+ \quad \text{(edge site)},$$

$$\equiv XNa + H^+ \leftrightarrow \equiv XH + Na^+ \quad \text{(layer site)}.$$

Molar fractions of each species were calculated as a function of pH based on the CEM + IExM model combination (**Fig. 30**). The value of the pH seems to be extremely important for the expected sorption of cations on PO and X or surface complexation ongoing on the PO group.

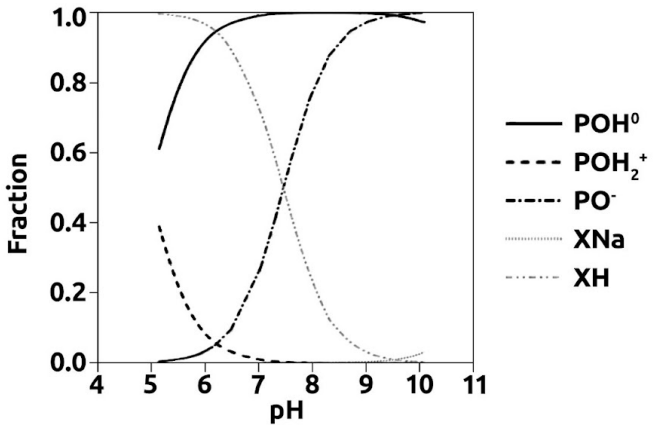

Fig. 30. Molar fractions of individual forms of surface sites for nHAp (CEM + IExM).

Those calculations showed the behaviour of hydroxyapatite NPs, which was important to understanding the RN sorption mechanism. These results allow us to predict and analyze the kinetics and sorption dependencies of a variety of RN including ^{223}Ra and its decay products.

Results obtained by modelling are in good agreement with dissolving experiments, which specify HAp-NPs applicability pH range over 5. In comparison with TiO_2, whose usable pH range is wider (2–11), HAp surface site density is greater, which can be regarded as its advantage. Simultaneously, the modelling has shown that HAp-NPs deprotonated edge sites (≡PO–) are virtually able to sorb only cationic species. Other species' edge site uptake (anionic, molecular) can undergo surface complexation mechanism. However, this side of the research was not studied.

The ageing of HAp was also investigated. The sample marked EM-3.1 prepared in 2014 was used. Infra-red spectra recorded in recent years did not show any

structure changes (**Fig. 31**). Disappearing of bands at 3500–2900 cm^{-1} and 1650 cm^{-1} and shape changes of the background at approx. 800–400 cm^{-1} were caused by the drying of the sample. The absorbance intensity decrease seen at the end of 2021 was caused by a shorter recording time. Diffractograms of the sample confirmed the lack of structural changes during 5 years (**Fig. 32**). These results show HAp stability, even if it was stored at room temperature without any sealing.

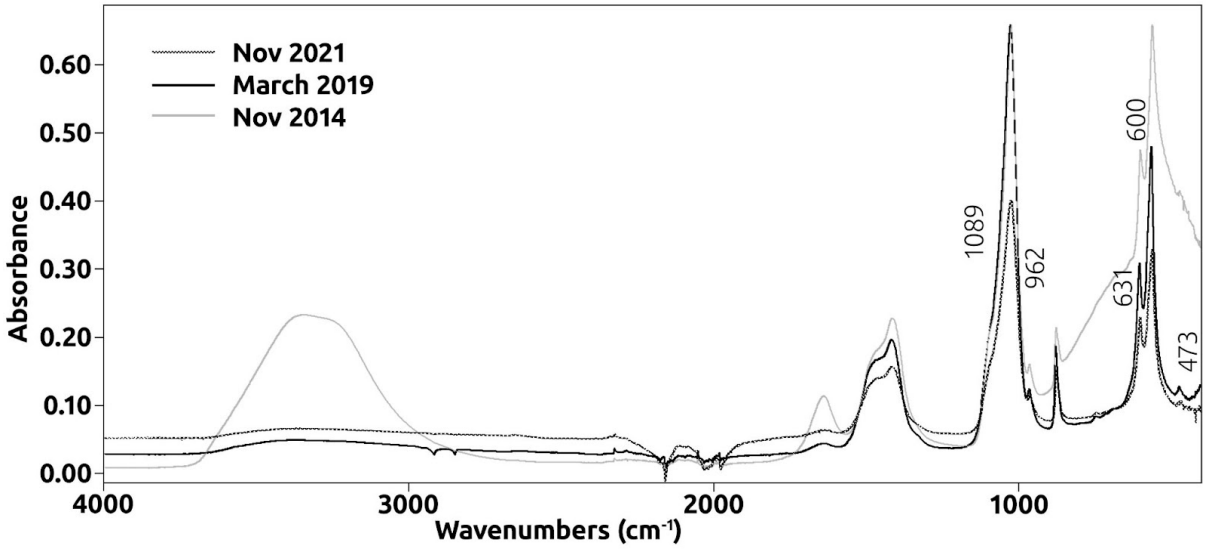

Fig. 31. FTIR spectra of the EM-3.1 sample recorded in different periods.

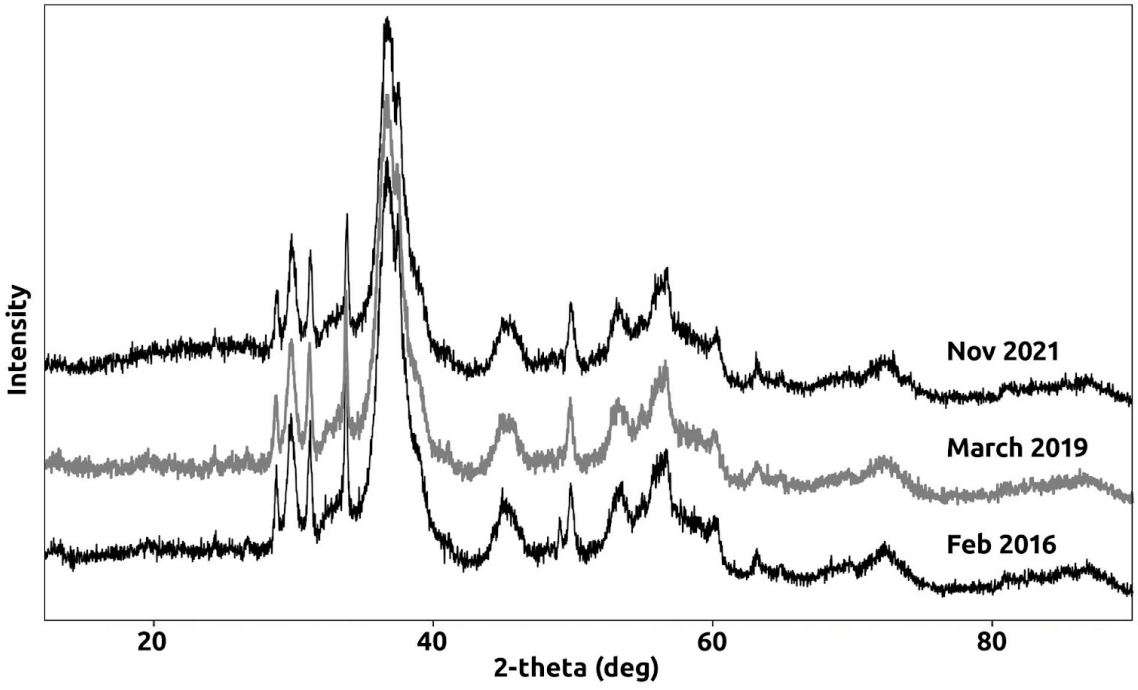

Fig. 32. Diffractograms of the EM-3.1 sample recorded in different periods.

Another important point for HAp application is its usable pH range. Dissolving experiments have shown that HAp-NPs cannot be used at pH under 4, however, starting from pH 5 and higher its dissolution can be taken as negligible (**Fig. 15**). These usage confines correspond with medicinal restrictions, where injected drugs must have an adequate pH range in order not to harm a patient.

Labelling & Stability

The main idea of the two labelling methods was to find out a better labelling way. Labelling of ready-made HAp-NPs is an easy method applicable for kit radiopharmaceuticals. Structure labelling's main idea was to implement radionuclides directly into the structure to increase stability. Both methods can be also easily used for individually prepared radiopharmaceuticals in hospitals or for further NPs modifications.

Labelling

In ready-made and structure labelling methods the same HAp preparation procedure was used, therefore it was assumed that precipitation of HAp during structure labelling lead to the same HAp as ready-made NPs. It was proven by FTIR analysis of structure-labelled [^{99m}Tc]-HAp-NPs 10 days after labelling when technetium activity decreased to undetectable. Achieved labelling results are presented in **Tab. 8**.

Tab. 8. Overview of HAp-NPs labelling yields.

RN	Method	Yield
^{18}F	ready-made	92.8 ± 2.8 %
	structure	95 ± 6.9 %
^{68}Ga	ready-made + DOTA	95.6 ± 1.2 %
	structure	Approx. 30 %
^{99m}Tc	ready-made	95.9 ± 1.5 %
	structure	94.6 ± 0.4 %
^{223}Ra	ready-made	94.2 ± 0.5 %
	structure	97.0 ± 0.5 %

It was found that all studied radionuclides can be used for HAp-NPs labelling with yields of about 95 %. In other words, hydroxyapatite is a good sorbent for any type of ions, so can be used not for medicine only, but also in other branches. Obtained data are in good agreement with the literature observed in the State-of-the-art chapter, where HAp behaviour with a variety of ions was overviewed.

Structure-labelled [^{18}F]-HAp-NPs were excluded due to very poor pilot stability experiments (retained activity was under 30 %). However, it was expected to form a stable product called fluorapatite, which is spread in nature in a mixture with HAp. However, the expectations were not proven. Probably fluorapatite formation requires conditions distinguished from HAp formation studied in the current work. The chemistry of this process was not studied.

Structure labelling with ^{68}Ga also yielded very poorly (about 30 %), and this method was excluded from further experiments. It was probably caused by inaccurate HAp formation conditions, such as pH. As far as Ga is eluted in 0.1 M HCl and used without further purification, pH maintenance is complicated. Simultaneously, preparation of HAp requires a pH over 11, which is not acceptable for Ga. Therefore, probably there were two influencing moments. The first was the formation of anion $Ga(OH)_4^-$, which probably did not sorb on NPs and did not incorporate into the structure. However, it was expected. The second point was pH decreasing because of 0.1 M HCl addition. Small buffer volume was important for a similar experimental setup but was not enough to buffer approx. 0.1–0.3 ml of diluted HCl. Experimental pH was set up before the Ga addition, and pH decrease was taken into account, however, it was unpredictable in some cases. Simultaneously, other pH conditions lead to other phosphate formation, but this question was not studied in the current work.

Not just structure labelling with ^{68}Ga brought some confusion, but the labelling of ready-made NPs also. First of all, labelling in saline was not possible due to pH changes after ^{68}Ga addition, as far as it was eluted in 0.1 M HCl. The idea of citrate buffer as media for labelling came from the paper chromatography method of [^{68}Ga]-DOTA-TOC analysis [SomaKit SPC]. The citrate buffer is used for quantitative free-^{68}Ga separation. It was found that citrate buffer could not be used for labelling due to the formation of a strong complex of $GaCit_3$. However,

obtained results even with preliminary DOTA labelling showed that the formed gallium-citrate complex was quite strong and prevented not just from [^{68}Ga]-HAp-NPs formation, but also from [^{68}Ga]-DOTA formation. Therefore, other buffers were tested.

Britton-Robinson buffer was chosen due to its wide pH range, but it required time-consuming and demanding preparation. Acetate and phosphate buffers are two-compound buffers which means faster and easier preparation, however, the pH range of these buffers does not cover the required range (pH 3.5–5.5 for acetate and pH 6–8 for phosphate buffer).

Usage of phosphate buffer here was not necessary because of Ga behaviour limitations, however, it was done to cover the widest pH range possible. Surprisingly, labelling yields of pristine HAp were ranging from 80 to 90 % at pH 6–8, while yields in Britton-Robinson buffer under the same pH were significantly lower (**Fig. 18**). Probably, the high yields in the phosphate environment were caused by gallium phosphate ($GaPO_4$) formation and its further sorption on HAp-NPs.

pH dependence

Study of labelling yield dependence on pH was performed for ^{68}Ga and ^{223}Ra only. Both ^{18}F and ^{99m}Tc labelling was conducted in saline and yielded about 95 %, so optimization of labelling conditions was not necessary. Furthermore, pH maintenance requires a buffer as labelling media, which, contrary to saline, complicates the sample preparation procedure and also increases the cost. Therefore buffer labelling is undesirable if possible.

Labelling with ^{68}Ga was not possible in saline due to Ga behaviour. Pilot experiments in saline showed yields under 30 %, which has just proved the need for a buffer for pH adjustment. A wide pH range was tested in different buffers: from 3 to 8 in citrate, phosphate, acetate and Britton-Robinson buffers. It was already mentioned that Ga at pH over 4 forms solid compound GaO(OH) and at pH over approx. 9 forms anion $Ga(OH)_4^-$. It was found that Ga in solid form was absorbed by HAp. However, it is important to mention that Ga concentration was 9.77×10^{-14} mol/ml (for 10 MBq), which is very low. The behaviour of Ga in low

concentrations was not analysed, however, it is well known, that the behaviour of very low concentrated ions in solutions differs from those in an adequate concentration.

Labelling in phosphate buffers showed very interesting results (**Fig. 18**). Even at pH 8 yield was over 80 %, while in BRB yield decreased to 10 % under the same pH. Probably it was caused by phosphate presence in a certain concentration in phosphate buffer (0.2 M). Simultaneously, BRB also contained phosphoric acid (0.5 M), and at pH 8 should behave similarly to phosphate buffer. But evidently, other compounds influenced the course of the experiment.

Detailed research was also conducted on ^{223}Ra at the pH range from 4.5 to 12 by Pavel Nykl [Nykl 2017, Suchankova 2020 B]. The experiments were conducted in the following manner: 2 mg of HAp were dispersed in 1 ml of BRB, and then 1.4–2.4 kBq of ^{223}Ra was added. The pH of the Ra solution was adjusted to not exceed buffer capacity. Samples were incubated for 24 hours, centrifuged and washed with saline. Sorption of ^{223}Ra on test tube walls was also analysed in the same manner without NPs addition.

According to experimental results, Ra speciation diagrams were calculated based on available data of stability constants for Ra^{2+} primary, but also Ba^{2+}, Sr^{2+} and Ca^{2+}. Based on already determined concentrations of edge-sites and layer-sites of HAp-NPs, the modelling was performed. The model was based on the chemical equilibrium model (CEM). [Suchankova 2020 B]

Speciation diagram calculations were not easy due to the very complex buffer on the one hand, where 3 anions were presented, and the lack of stability constants for Ra on the other hand. Unavailable data for Ra were substituted with those for Ba, Sr and Ca. All the experiments were conducted under free air conditions, so the presence of air CO_2 was also taken into account. [Suchankova 2020 B]

It was found that the surface complexation model type of CEM was the right choice. The modelling showed that both layer and edge-sites were included in Ra uptake (**Fig. 33**), therefore the labelling process is better described with sorption than co-precipitation. It was found that major reactions ongoing on

layer-sites were with Ra^{2+} and $RaH_2PO_4^+$, and on the edge-sites with $RaPO_4^-$, $RaHPO_4$ and $RaCO_3$. Layer-site reactions were determined as follows:

$$2XH + Ra^{2+} \leftrightarrow X_2Ra + 2H^+,$$
$$XH + RaH_2PO_4^+ \leftrightarrow XRaH_2PO_4 + H^+.$$

The edge-site reaction can be described in general, where X is the earlier mentioned species with the chemical equation $PO^- + X^+ \leftrightarrow POX$. [Suchankova 2020 B]

It was found that deprotonated species PO^- were not available in the case of HAp-NPs at pH 6 and lower, which played a key role in edge-site reactions.

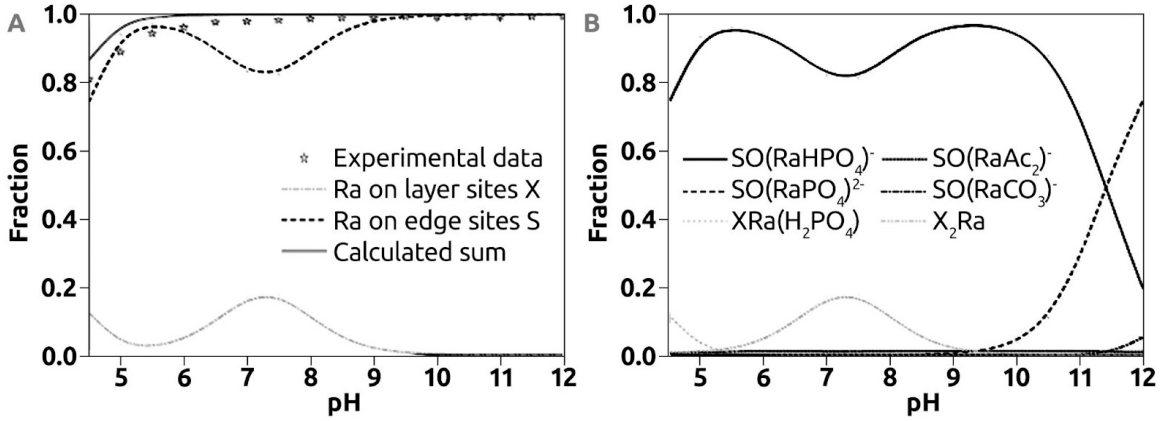

Fig. 33. Sorption on HAp: **A** - ^{223}Ra uptake vs. pH; **B** - uptake of given species vs. pH [Suchankova 2020 B].

Kinetics

Among important labelling parameters belongs labelling time. Labelling time could be understood as the period required by the system to reach an equilibrium state between the concentration of ions in solid and liquid phases. However, for the current work, it was determined as the time elapsed before labelling yield reached 95 % (if possible).

Labelling kinetics of all four studied RN were determined (**Fig. 34**). Kinetics data of ^{223}Ra labelling was taken from the previously published source [Nykl 2017] and are presented here to compare with other RN. It is interesting to mention that kinetics corresponds with RN half-life. The radionuclide ^{223}Ra with the longest half-life required about 2 hours to reach equilibrium, while the equilibrium of the shortest-half-life ^{18}F was reached within 5 minutes. Short

half-life RN kinetics is fast, so activity decrease during labelling is acceptable. In the case of long-lived RN, the labelling rate lasted 1–2 hours, but it is also acceptable for medicinal applications.

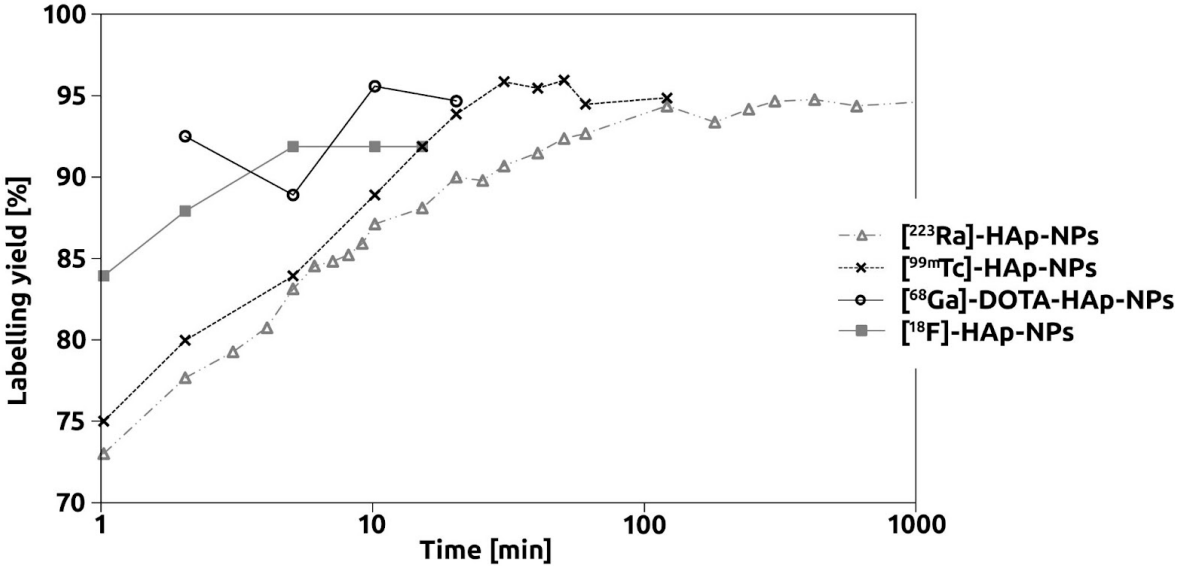

Fig. 34. Comparison between dependances of labelling yield on time for studied radionuclides. X-axes are in logarithmic scale. [^{223}Ra]-HAp-NPs data were taken from [Nykl 2017]. The data are presented without error bars for better visualisation.

Kinetics of ^{223}Ra labelling was studied in-depth. Modelling variations were based on different rate-controlling processes: mass transfer (DM), film diffusion (FD), diffusion in inert layer (ID), diffusion in reacted layer (RLD), a chemical reaction (CR), and gel diffusion (GD). The procedure described in detail was already published [Suchankova 2020 C]. The only relevant results are presented here.

Mathematically two of the six studied models were found as suitable for further modelling: ID and RLD. However, from the physical and chemical viewpoints, the diffusion through reacted layer (RLD) model seems to better correspond with the studied systems than the diffusion through the inert one (ID). Therefore, the RLD model was used for further research (**Fig. 35**).

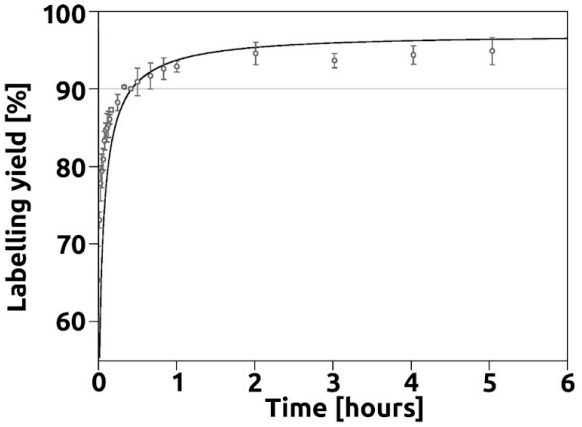

Fig. 35. Ready-made-labelled [^{223}Ra]-HAp-NPs sorption kinetics. Points represent experimental data, solid lines are calculated fit. [Suchankova 2020 C].

The aim of the modelling was to determine the values of the overall mass transfer coefficient, *K*, diffusion coefficient, *D*, and sorption half-life, $t_{1/2}$. The overall mass transfer coefficient is a key parameter in predicting the rate of any two-phase system and is determined by the equation published in [Suchankova 2020 C]. The diffusion coefficient (D) can be determined in the following way: "The diffusion coefficient is the amount of a particular substance that diffuses across a unit area in 1 s under the influence of a gradient of one unit." [Wilson 2000] Sorption half-life was determined as the period required for the labelling yield to increase by 50 % from its maximal experimental level. The results are summarised in **Tab. 9.** The significant measurement uncertainty was probably caused by fast sorption kinetics and very low Ra concentration, therefore, small inaccuracy in sampling could lead to high enough mistakes. However, radium sorption kinetics can be interpreted as fast and these results can be easily applied to any radium isotope.

Tab. 9. The values of the overall mass transfer coefficient, *K*, diffusion coefficient, *D*, and sorption half-life, $t_{1/2}$ calculated via the RLD model [Suchankova 2020 C].

$K \pm \sigma$ [cm^3/(g·min)]	$D \pm \sigma$ [cm^2/min]	$t_{1/2} \pm \sigma$ [min]
0.50 ± 0.27	$(2.50 \pm 1.80) \cdot 10^{-12}$	0.75 ± 0.18

Stability

The aim of the stability experiments was to find out the behaviour of the labelled nanoparticles in different media. According to the fact that the thesis is focused on medicine, biologically relevant media such as saline, bovine plasma, bovine serum and water albumin solutions (1 & 5 %) were chosen. These media cover a wide range of biosystems.

Saline is the main water solution used in medicine for storage and administration of pharmaceuticals, for hydration and in some cases as blood substitution. In current work behaviour of labelled NPs in saline was understood not just as a blank experiment, but also as a storage condition investigation of already labelled products before administration.

Albumin solutions, bovine serum and bovine plasma represented blood flow and tissue behaviour. Albumin is known as a stabilising agent, simultaneously it is the blood protein with the highest concentration. The serum is the liquid that remains after the blood has clotted. Plasma is the liquid that remains when clotting is prevented with the addition of an anticoagulant [Cellero 2022] and consists mainly of water, proteins (albumins, globulins, fibrinogen etc), ions, saccharides and sodium citrate as a stabilising agent in a commercially available material.

The following figures present obtained data on the same scale and without error bars for better visualisation. For all experiments, errors did not exceed 5 %.

Overview of stability experimental results is summarised in **Tab. 10**.

Tab. 10. Overview of HAp-NPs stability studies.

RN	Method	Stability time	Retained activity
^{18}F	ready-made	10 hours	Over 85 % (S,A_5,BS,BP)
	structure	30 min	Approx. 20 %
^{68}Ga	ready-made + DOTA	4 hours	Over 90 % (S,A_5) Approx. 40 % (BS,BP)
	structure	– – –	– – –
^{99m}Tc	ready-made	32 hours	Over 80 % (S,A_5,A_1,BS) Approx. 60 % (BP)
	structure	32 hours	Over 90 % (S,A_5,A_1,BS) Approx. 60 % (BP)
^{223}Ra	ready-made	55 days	90–60 %
	structure	55 days	90–50 %

S - saline, A_5 - 5 % albumin solution, A_1 - 1 % albumin solution, BS - bovine serum, BP - bovine plasma

Stability in saline

Saline experiments have shown that activity that remained on the particles was high in the case of ^{68}Ga and both ^{99m}Tc sample series (**Fig. 36**). However, the release of ^{223}Ra within 59 hours was significant, so storage of radium-labelled particles in saline is not a good decision. Ready-made-labelled NPs with both ^{99m}Tc and ^{223}Ra showed better stability than structure labelled. However, in the case of ^{99m}Tc, the difference was negligible. In the case of ^{223}Ra difference between ready-made and structure labelled NPs was noticeable, but anyway both stability results were deficient. Retain of ^{18}F was moderate. In general, it could be concluded that short-time storage (up to 10 hours) of labelled NPs in saline is safe for any RN and labelling route.

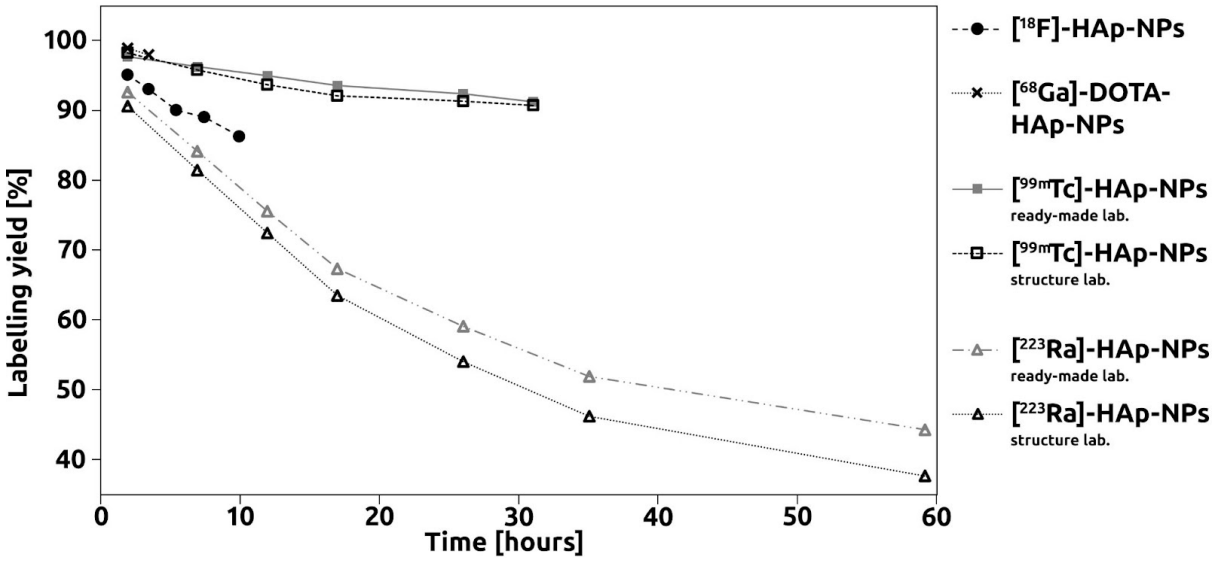

Fig. 36. Stability of labelled HAp-NPs in saline.

Stability in bovine plasma

Bovine plasma test series have shown very similar results for almost all samples except ^{68}Ga labelled (**Fig. 37**). The difference between saline and plasma series was probably caused by the decline of resorption, which was observed in saline. Plasma proteins and other molecules evidently can catch released RN and prevent them from resorption on NPs. It is important to notice that the labelling strategy here did not play any role, so the easier ready-made method seems to be preferable. One of the factors that can affect retained activity negatively is citrate presence. Its direct impact was studied for ^{68}Ga and ^{223}Ra only, but this compound is known as a good complexant, which can affect the results. Bovine plasma without citrate is not commercially available.

Nanoparticles labelled with ^{68}Ga have shown very low retain activity. The complex of [^{68}Ga]-DOTA is known to be stable in biological liquids, however, the durability of [^{68}Ga]-DOTA-HAp-NPs formation was under research. Evidently, the bond between [^{68}Ga]-DOTA and HAp-NPs was not strong enough. Simultaneously, citrate presence in plasma must be taken into account. According to the results found in citrate buffer, it could intensively affect not just resorption but also washing out of the RN.

Shortened stability tests were conducted on [^{223}Ra]-HAp-NPs samples in order to understand citrate influence. Samples' behaviour was studied in 1 % sodium citrate solution, but such a massive activity release was not observed. Nonetheless, plasma citrate concentration data were not available, so the influence of citrate as a complexing agent can not be excluded.

One more notice must be mentioned. Short-term plasma, serum and albumin stabilities were performed without any preservative addition. The microbiology of the samples was not studied. All the work was performed under somehow aseptic conditions, however, it was never verified. Therefore, the appearance of microorganisms in the samples was possible. The influence of microorganisms' presence on the stability of studied NPs could be an interesting topic for further research. Here it is assumed that frequent media changes and ionised irradiation prevent any culture appearance.

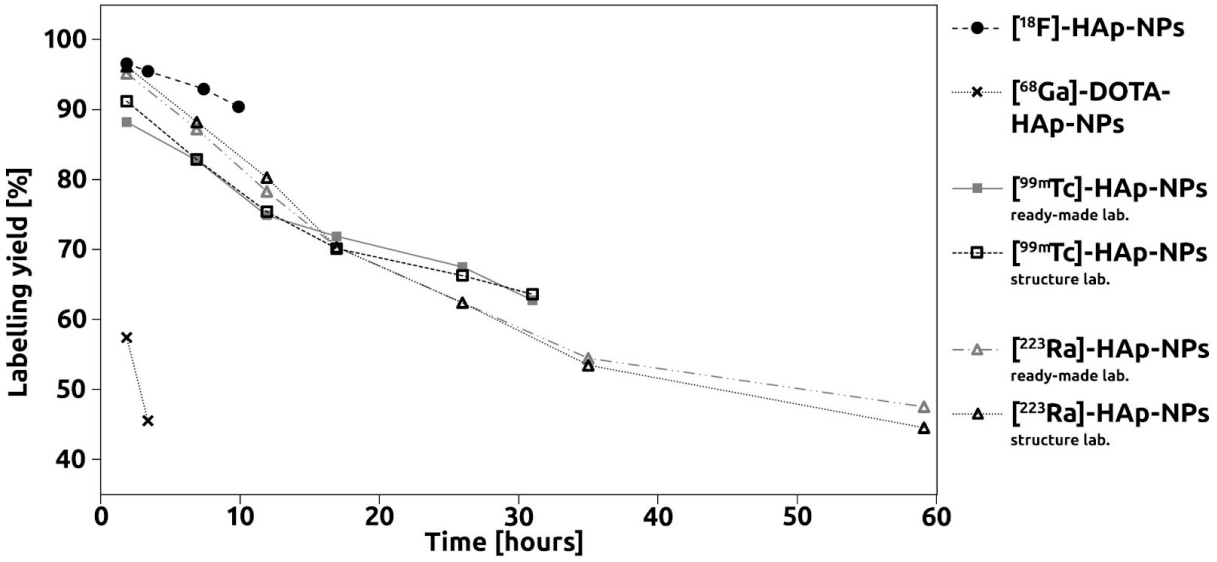

Fig. 37. Stability of labelled HAp-NPs in bovine plasma.

Stability in bovine serum

Results obtained in bovine serum are very different from those in plasma (**Fig. 38**). The retained activity was found to be over approx. 80 % for almost all sample series except ^{68}Ga labelled. Better stability in comparison with plasma for ^{18}F, ^{99m}Tc and ^{223}Ra samples was probably caused by the difference between serum and plasma. Simultaneously, serum did not contain citrate, however, it might have affected ^{68}Ga labelling results. But it did not (in comparison with plasma). So, probably, citrate is not the main compound influencing the amount of retained activity. Since biological liquids are produced from real animals, behaviour from batch to batch can be different. This difference could also have an influence on stability results.

Here, the difference between structure and ready-made-labelled NPs with ^{99m}Tc and ^{223}Ra is noticeable. It seems that structure-labelled NPs showed better stability than ready-made-labelled NPs. However, the difference between Ra-labelled is negligible here contrary to the serious difference in the case of ^{99m}Tc.

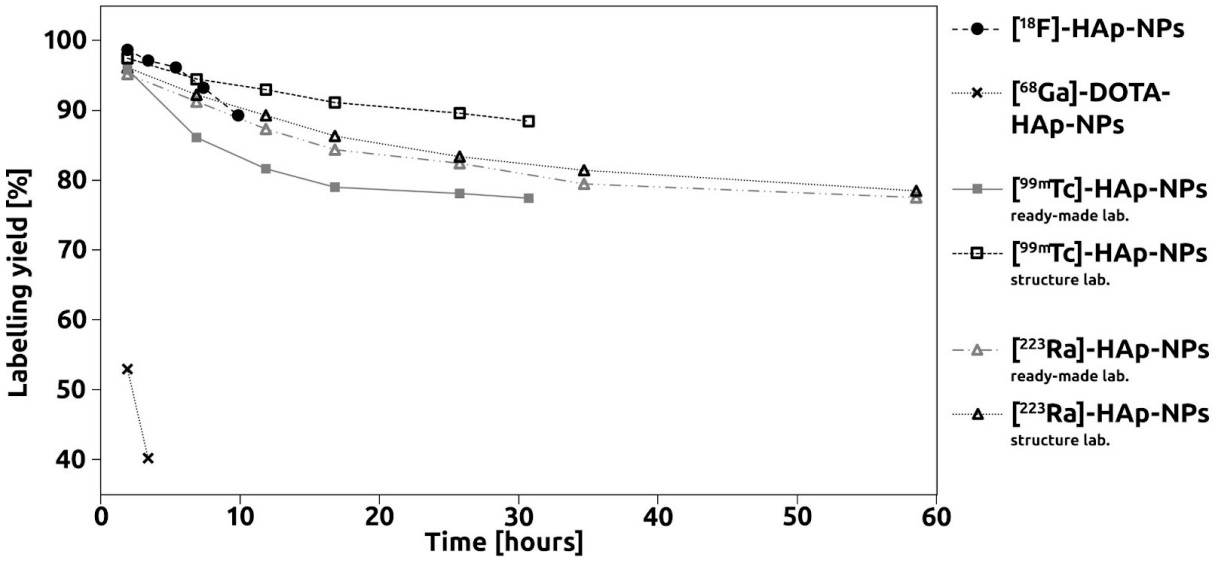

Fig. 38. Stability of labelled HAp-NPs in bovine serum.

Short-term stability of [^{223}Ra]-HAp-NPs were partially already performed by Eva Málková [Malkova 2016]. She has tested [^{223}Ra]-HAp and [^{223}Ra]-HPMA-HAp stability in saline, plasma and serum. Also, quantity dependence on labelling

yields and stability was analysed. Her results have shown a similar trend, where maximum released activity was found in plasma & released activity percentage strongly depended on the amount of HAp-NPs, where 1 mg did not have enough capacity.

These results were verified and extended. Stability studies were not just updated by 1 & 5 % albumin solution, but also prolonged from 131 hours (5.5 days) to 55 days to show long-term trends for the long-live radionuclide. Results obtained in the current study were in good comparison with the result found earlier.

Stability in albumin

Since albumin is the main component of blood, it was decided to test its effect on the stability of labelled NPs separately for ^{99m}Tc and ^{223}Ra. The concentration of 5 % was chosen due to the upper border of the reference human level in serum, which is determined at 46 g/l [IKEM 2022]. The lower concentration of 1 % was chosen as an additional option. It was not surprising that both concentration stability results were similar (**Fig. 39, 40**). At the first glance, the behaviour of [^{223}Ra]-HAp-NPs was almost the same in both solutions, while NPs labelled with ^{99m}Tc showed slightly different results. Nonetheless, I believe the difference in stability between 1 % and 5 % albumin was negligible and was mainly caused by experimental uncertainty. It is interesting to notice that ^{99m}Tc stability for both experimental series in 1 % albumin solution was higher than in saline, probably due to the albumin stabilising effect.

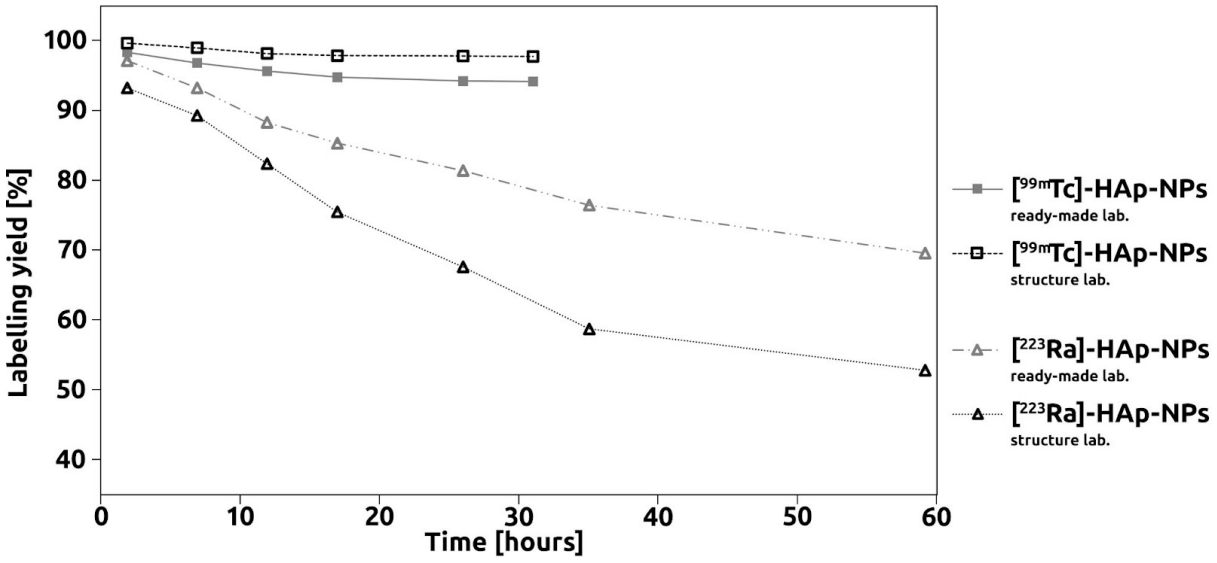

Fig. 39. Stability of labelled HAp-NPs in 1 % albumin.

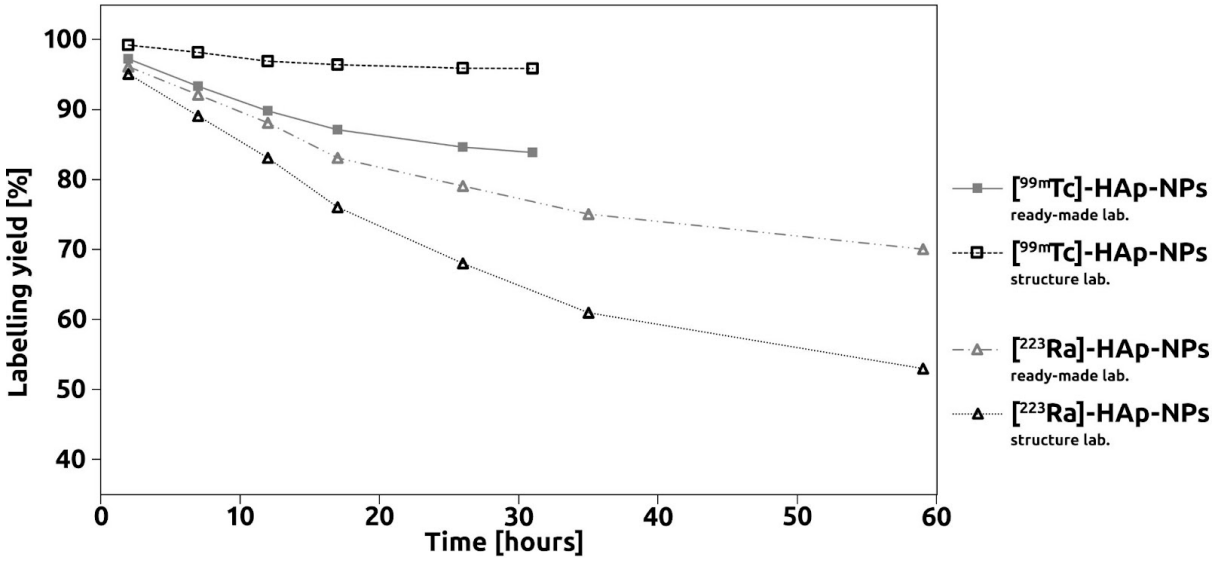

Fig. 40. Stability of labelled HAp-NPs in 5 % albumin.

Long-term stability studies were performed for ^{223}Ra only due to its long half-life. The results were very similar to the short-term study of HAp-NPs labelled with Ra, which can be caused by distribution coefficients and fast kinetics.

Comparing all presented stability results of [^{99m}Tc]-HAp-NPs, structure-labelled NPs have shown the results either the same or better than ready-made-labelled.

Probably Tc ion can be incorporated into the HAp structure, which leads to better activity retention despite worth labelling yield.

The stability study of [^{223}Ra]-HAp-NPs has shown the opposite result. Structure-labelled HAp-NPs performed with either worth or the same retained activity as ready-made-labelled. It was assumed that Ra can substitute Ca in HAp crystal lattice, and it was partially proved by labelling results. Nonetheless, stability experiments have shown that substitution is neither stable nor happened. Lower retained activity may also indicate a breach in HAp structure caused by the preparation method due to the size of the Ra ion.

Literature comparison

It seems that the usability of already labelled [^{18}F]-HAp-NPs and [^{68}Ga]-HAp-NPs in medicine is quite contradictory, because of the slow distribution of NPs in the body and simultaneously short half-life of these two RN. It means that by the time the nanoparticle achieves a target tissue, the activity carried by the nanoparticle could become inadequate to provide imaging. This issue can be circumvented by labelling after distribution: first, non-labelled NPs should be targeted to the tissue, and then labelled in vivo. Of course, this possibility must be studied in detail before being applied.

The mentioned idea of labelling after distribution is already supported by recent articles. One study evaluated ^{18}F as a HAp seeking agent in rats for a reloadable carrier system, so systemically administered drugs could bind to the HAp due to a high chemical affinity [Raina 2019]. Such an interesting approach corresponds with the described investigation and my results can be utilised for further research. Another report showed the possibility of imaging with ^{18}F or ^{99m}Tc via tumour extracellular HAp as an imaging biomarker [Tantawy 2021]. A study from 2012 evaluated the biodistribution of [^{18}F]-HAp in rabbits [Zheng 2012]. All these researches show the possibility of HAp-NPs application even with RN with short half-lives. However, they do not go in-depth with labelling and stability study.

Simultaneously another research published in 2015 investigated feasibility to label HAp (pristine and citrate-modified) with ^{18}F and ^{68}Ga [Sandhöfer 2015] for further i.v. application and imaging. Obtained results are in very good

agreement with the results found in current work, including HAp characterisation parameters: adsorption kinetics for both radionuclides was very fast, as well as labelling yield were over 95 %. Retained activity in saline and PBS for 120 min was also over 95 %. Moreover, in vivo administered labelled NPs in mice showed possibility of imaging for both ^{18}F and ^{68}Ga labelled NPs.

Obtained results for ^{99m}Tc are in good agreement with literature data. Hydroxyapatite labelled with ^{99m}Tc was studied by Albernaz et al. in 2014. They have reached 99.3 % labelling yield via a very similar to the ready-made labelling method and then tested stability for 24 hours in the reaction solution. The retained activity was 92 %. [Albernaz 2014] Another study has shown in vivo bone uptake of [^{99m}Tc]-HAp-NPs in healthy mice [Maia 2016].

Hydroxyapatite labelling with ^{223}Ra made by Vasiliev [Vasiliev 2017] has shown that not just nanoparticles can absorb the radionuclide fast and easily, but also spherical microparticles. Washing out investigation in saline is comparable with stability study. Obtained results showed desorption of up to 22 %, which is equal to 78 % of retained activity in approx. 7 days. All published findings are in good agreement with data published in current work.

Conclusions

Hydroxyapatite as a useful material for medicinal approach is being used already for a number of applications. However, new possibilities of such a suitable substance are always welcome. Due to HAp's beneficial properties such as biocompatibility, low toxicity, high sorption capacity, and biodegradability, it becomes an interesting material for radionuclide sorption research.

This research is important not just for the medicine approach mainly discussed in this paper, but also for any type of RN sorption study including waste management. All the results can be utilised in practice for understanding ongoing processes during RN sorption. Despite the fact that only Ra sorption was studied in detail, similar labelling yields of all RN could mean similar ongoing processes.

This thesis shows the in-depth investigation of HAp-NPs labelling with ^{18}F, ^{68}Ga, ^{99m}Tc, and ^{223}Ra and further evaluation of labelled NPs' stability in biologically relevant media. The results are expanded by the detailed exploration of HAp's surface properties.

This work aimed to develop a usable labelling method for medicine practice. Complicated and unpredictable methods like structure Ga labelling were excluded without further investigation. On the one hand, theoretical science requires analysis of such complex tasks in-depth. On the other hand, wasting time with an unimaginable approach for applied science is not acceptable.

The usable labelling methods with all four studied RN were developed with desirable yields. The experimental set up for all experiments was the easiest possible. All experiments were performed under free air and at room temperature in order to simulate real conditions seamlessly implemented in practice.

Agreement of found data with already published not just support the idea of HAp-NPs as radiopharmaceutical for diagnostics and therapy, but also show the feasibility of this idea on in vivo results.

Labelling stability studies have shown that even if labelling methods seem to have an impact on retain activity level, it must be concluded that changes were not consistent. Therefore, I would say that changes are mostly caused by manual and/or measurement errors, rather than labelling methods. Despite the fact that measurements, dosing and weighing were carried out with a high accuracy, a human factor cannot be excluded.

Despite all possible inaccuracies and deviations, the general trend is extremely clear. Hydroxyapatite can become the carrier for both diagnostic and therapeutic radionuclides. Possibility of labelling with only one radionuclide was already proven. However, due to the high sorption capacity, one nanoparticle could be labelled with two radionuclides simultaneously, one for therapeutic effect, and the second one for distribution monitoring. Furthermore, since HAp can be reloaded, diagnostic imaging could be initiated a few days after therapy began, or repeated when needed.

Anyway, obtained results have shown good sorption properties of HAp prepared from easily available initial compounds under ordinary conditions. Even if some stability results in biologically relevant media were unsatisfactory, and use in medicine could be discussed, other approaches such as waste management and environment decontamination are still the great option. Therefore, usage of cheap and easy-to-prepare artificial HAp of high purity and defined properties is possible in a wide spectra of branches.

References

Abbas, K., Cydzik, I., Del Torchio, R., et al. (2009). Radiolabelling of TiO2 nanoparticles for radiotracer studies. Journal of Nanoparticle Research, 12(7), 2435–2443. doi:10.1007/s11051-009-9806-8

Adam, J., Kadeřávek, J., Kužel, F., et al. (2014). Současné trendy ve využívání PET radiofarmak k onkologické diagnostice. Klinická Onkologie. (27), S129-S136.

Albernaz, M., Ospina, de S., Rossi, C.A., et al. (2014). Radiolabelled nanohydroxyapatite with 99mTc: perspectives to nanoradiopharmaceuticals construction. Artificial Cells, Nanomedicine, and Biotechnology, 42(2), 88–91. doi:10.3109/21691401.2013.785954

Allen, T.M., Cullis, P.R. (2013). Liposomal drug delivery systems: from concept to clinical applications. Advanced Drug Delivery Review. 65(1), 36– 48. doi:10.1016/j.addr.2012.09.037

Amartey, J.K. (2016). FDA Update: 68Ge /68Ga Generators and 68Ga radiolabeled Approved Kit. [cit. 9.2.2017]. Available online at
http://www.fda.gov/downloads/Drugs/ScienceResearch/ResearchAreas/Oncology/UCM512685.pdf

Ambrogio, M. W., Toro-González, M., Keever, T. J., McKnight, T. E., & Davern, S. M. (2020). Poly(lactic-co-glycolic acid) Nanoparticles as Delivery Systems for the Improved Administration of Radiotherapeutic Anticancer Agents. ACS Applied Nano Materials. doi:10.1021/acsanm.0c02350

Andronescu, E., Predoi, D., Neacsu, I. A., et al. (2019). Photoluminescent Hydroxylapatite: Eu3+ Doping Effect on Biological Behaviour. Nanomaterials. 9(9), 1187. doi:10.3390/nano9091187

Anjaneyulu, U., Swaroop , V.K., Vijayalakshmi, U. (2016). Preparation and characterization of novel Ag doped hydroxyapatite–Fe3O4 –chitosan hybrid composites and in vitro biological evaluations for orthopaedic applications. RSC Advanced. 6(13), 10997-11007. doi: 10.1039/C5RA21479C

Apalight flyer (2020) [cit. 2020-05-09]. Available online: http://kalichem.it/allegati/apalight_ok.pdf

Banerjee, I., De, K., Chattopadhyay, S., et al. (2014). An easy and effective method for radiolabelling of solid lipid nanoparticles. Journal Radioanalytical and Nuclear Chemistry. 302(2), 837-843. doi: 10.1007/s10967-014-3258-z

Bankura, K.P., Maity, D., Mollick, M.M.R., et al. (2012). Synthesis, characterization and antimicrobial activity of dextran stabilized silver nanoparticles in aqueous medium. Carbohyd Polym. 89, 1159–1165. doi: 10.1016/j.carbpol.2012.03.089

Bayda, S., Adeel, M., Tuccinardi, T., et al. (2019). The History of Nanoscience and Nanotechnology: From Chemical–Physical Applications to Nanomedicine. Molecules, 25(1), 112. doi:10.3390/molecules25010112

Ben-Arfa, B.A.E., Salvado, I.M.M., Ferreira, J.M.F., et al. (2017). Novel route for rapid sol-gel synthesis of hydroxyapatite, avoiding ageing and using fast drying with a 50-fold to 200-fold reduction in process time. Materials Science and Engineering: C. 70(1), 796-804. doi: 10.1016/j.msec.2016.09.054.

Bobo, D., Robinson, K.J., Islam, J., et al. (2016). Nanoparticle-Based Medicines: A Review of FDA-Approved Materials and Clinical Trials to Date. Pharmaceutical Research. 33(10), 2373-2387. doi: 10.1007/s11095-016-1958-5

Bochkarev, A.A., Polyakova, I.V. (2012). Emission of Ag2 Dimers From a Substrate During Vacuum Deposition of the Mixture of Silver and Water Vapor. Thermophysics and Aeromechanics, 19 (3), 435-447.

Bogatu, C., Perniu, D., Sau, C., et al. (2017). Ultrasound assisted sol-gel TiO 2 powders and thin films for photocatalytic removal of toxic pollutants. Ceramics International, 43(11), 7963–7969. doi:10.1016/j.ceramint.2017.03.054

Boisselier, E., Astruc, D., Islam, J., et al. (2009). Gold nanoparticles in nanomedicine: preparations, imaging, diagnostics, therapies and toxicity. Chem Soc Rev, 38(6), 1759-. doi: 10.1039/b806051g

Bradley, S.M., Kydd, R.A., Yamdagni R. (1990). Comparison of the hydrolyses of gallium(III) and aluminium(III) solutions by nuclear magnetic resonance spectroscopy. J Chem Soc., Dalton Trans, 2653-2656, doi: 10.1039/DT9900002653

BSE (1969) Bolšaya Sovětskaya Enciklopediya, 3 vydání, Moskva, část 1.

Burke, B. P., Baghdadi, N., Clemente, G. S., et al. (2014). Final step gallium-68 radiolabelling of silica-coated iron oxide nanorods as potential PET/MR multimodal imaging agents. Faraday Discuss. doi:10.1039/c4fd00137k

Calegaro, J. U. M., Machado, J., Furtado, R. G., et al. (2013). The use of 185 MBq and 740 MBq of 153-samarium hydroxyapatite for knee synovectomy in haemophilia. Haemophilia, 20(3), 421–425. doi:10.1111/hae.12319

Castro, F., Ribeiro, V.P., Ferreira, A., et al. (2016). Continuous-flow precipitation as a route to prepare highly controlled nanohydroxyapatite: in vitro mineralization and biological evaluation: preparations, imaging, diagnostics, therapies and toxicity. Materials Research Express, 3(7), 075404-. doi: 10.1088/2053-1591/3/7/075404.

Cędrowska, E., Pruszynski, M., Majkowska-Pilip, A., et al. (2018). Functionalized TiO2 nanoparticles labelled with 225Ac for targeted alpha radionuclide therapy. Journal of Nanoparticle Research, 20(3). doi:10.1007/s11051-018-4181-y

Cellero - Serum vs. Plasma: What's the Difference? [cit 8.4.2022] Available online at https://cellero.com/blog/ask-scientist-whats-difference-serum-plasma/#:~:text=Serum%20is%20the%20liquid%20that,the%20addition%20of%20an%20anticoagulant

Chakraborty, S., Das, T., Banerjee, S., Sarma, H. D., & Venkatesh, M. (2006). Preparation and preliminary biological evaluation of 177Lu-labelled hydroxyapatite as a promising agent for radiation synovectomy of small joints. Nuclear Medicine Communications, 27(8), 661–668. doi:10.1097/00006231-200608000-00008

Chakraborty, S., Das, T., Chirayil, V., Lohar, S. P., & Sarma, H. D. (2014). Erbium-169 labeled hydroxyapatite particulates for use in radiation synovectomy of digital joints – a preliminary investigation. Radiochimica Acta, 102(5). doi:10.1515/ract-2013-2166

Chakraborty, S., Vimalnath, K.V., Rajeswari, A., et al. (2014). Preparation, evaluation, and first clinical use of 177Lu-labeled hydroxyapatite (HA) particles in the treatment of rheumatoid arthritis: utility of cold kits for

convenient dose formulation at hospital radiopharmacy. J Labelled Compd Rad, Vol. 57, 7, 453–462. doi: 10.1002/jlcr.3202.

Chattopadhyay, S., Vimalnath, K. V., Saha, S., Korde, A., Sarma, H. D., Pal, S., & Das, M. K. (2008). Preparation and evaluation of a new radiopharmaceutical for radiosynovectomy, 111Ag-labelled hydroxyapatite (HA) particles. Applied Radiation and Isotopes, 66(3), 334–339. doi:10.1016/j.apradiso.2007.09.003

Chilug, L. E., Niculae, D., Leonte, R. A., Nan, A., Turcu, R., Mustaciosu, C., at al. (2020). Preclinical Evaluation of NHS-Activated Gold Nanoparticles Functionalized with Bombesin or Neurotensin-Like Peptides for Targeting Colon and Prostate Tumours. Molecules, 25(15), 3363. doi:10.3390/molecules25153363

COD - Crystallography Open Database—an open-access collection of crystal structures, http://www.crystallography.net/cod/search.html, accessed May 2018.

Coelho, C. C., Grenho, L., Gomes, P. S., et al. (2019). Nano-hydroxyapatite in oral care cosmetics: characterization and cytotoxicity assessment. Scientific Reports, 9(1). doi:10.1038/s41598-019-47491-z

Corami, A., Mignardi, S., Ferrini, V. (2007). Copper and zinc decontamination from single- and binary-metal solutions using hydroxyapatite. Journal of Hazardous Materials, 146(1-2), 164–170. doi:10.1016/j.jhazmat.2006.12

Czerwińska, M., Fracasso, G., Pruszyński, M., et al (2020). Design and Evaluation of 223Ra-Labeled and Anti-PSMA Targeted NaA Nanozeolites for Prostate Cancer Therapy–Part I. Materials, 13(17):3875. https://doi.org/10.3390/ma13173875

Daniel, M.C., Astruc, D. (2004). Gold Nanoparticles: Assembly, Supramolecular Chemistry, Quantum-Size-Related Properties, and Applications toward Biology, Catalysis, and Nanotechnology. Chem Rev, 104, 293–346.

Dědourková, T., Zelenka, J., Zelenková, M., et al. (2012). Synthesis of Sphere-like Nanoparticles of Hydroxyapatite. Procedia Engineering, 42, 1816–1821. doi:10.1016/j.proeng.2012.07.576

Devaraj, N.K., Keliher, E.J., Thurber, G.M., et al. (2009). 18F Labeled Nanoparticles for in Vivo PET-CT Imaging. Bioconjugate Chem , 20(2), 397-401.

Duan, D., Liu, H., Xu, Y., et al. (2018). Activating TiO2 Nanoparticles: Gallium-68 Serves as a High-Yield Photon Emitter for Cerenkov-Induced Photodynamic Therapy. ACS Applied Materials & Interfaces, 10(6), 5278–5286. doi:10.1021/acsami.7b17902

Fazaeli, Y., Zare, H., Karimi, S., et al. (2020). 68Ga CdTe/CdS fluorescent quantum dots for detection of tumors: investigation on the effect of nanoparticle size on stability and in vivo pharmacokinetics. Radiochimica Acta, 0(0). doi:10.1515/ract-2019-3184

FDA - FDA-approved radiopharmaceuticals. [cit 10.2.2022] Available online at https://www.cardinalhealth.com/content/dam/corp/web/documents/fact-sheet/cardinal-health-fda-approved-radiopharmaceuticals.pdf

Ferraz, M. P., Mateus, A. Y., Sousa, J. C., et al. (2007). Nanohydroxyapatite microspheres as delivery system for antibiotics: Release kinetics, antimicrobial activity, and interaction with osteoblasts. Journal of Biomedical Materials Research Part A, 81A(4), 994–1004. doi:10.1002/jbm.a.31151

Ferraz, M.P., Monteiro, F.J., Manuel, C.M. (2004). Hydroxyapatite nanoparticles: A review of preparation methodologies. J Appl Biomater Biomech, 2(2), 74-80. doi:10.1177/228080000400200202

Fitzsimmons, J., Atcher, R. (2007). Synthesis and evaluation of a water-soluble polymer to reduce Ac-225 daughter migration. J Label Compd Radiopharm, 50, 147–153. doi: 10.1002/jlcr.1143

Flores, C.Y., Miñán, A.G., Grillo, C.A., et al. (2013). Citrate-Capped Silver Nanoparticles Showing Good Bactericidal Effect against Both Planktonic and Sessile Bacteria and a Low Cytotoxicity to Osteoblastic Cells. ACS Appl Mater Interfaces, 5 (8), 3149–3159.

Forrer, F., Uusijärvi, H., Storch, D., et al. (2005). Treatment with 177Lu-DOTATOC of Patients with Relapse of Neuroendocrine Tumors After Treatment with 90Y-DOTATOC. J Nucl Med August 1, 46(8), 1310-1316

Fu, Q., Zhou, N., Huang, W., et al. (2004). Preparation and characterization of a novel bioactive bone cement: Glass based nanoscale hydroxyapatite bone cement. Journal Of Materials Science: Materials In Medicine, 15, 1333– 1338.

Gao, M., Sun, L., Wang, Z., et al. (2013). Controlled synthesis of Ag nanoparticles with different morphologies and their antibacterial properties. Materials Science and Engineering: C, 33(1), 397-404. doi: 10.1016/j.msec.2012.09.005.

Garashchenko, B. L., Dogadkin, N. N., Borisova, N. E., & Yakovlev, R. Y. (2018). Sorption of 223Ra and 211Pb on modified nanodiamonds for potential application in radiotherapy. Journal of Radioanalytical and Nuclear Chemistry. doi:10.1007/s10967-018-6330-2

Gauglitz, R., Holterdorf, M., Franke, W., & Marx, G. (1992). Immobilization of Heavy Metals by Hydroxylapatite. Radiochimica Acta, 58-59(2). doi:10.1524/ract.1992.5859.2.253

Gawęda, W., Pruszyński, M., Cędrowska, E., et al (2020). Trastuzumab Modified Barium Ferrite Magnetic Nanoparticles Labeled with Radium-223: A New Potential Radiobioconjugate for Alpha Radioimmunotherapy. Nanomaterials, 10(10):2067. https://doi.org/10.3390/nano10102067

González-Gómez, M. A., Belderbos, S., Yañez-Vilar, S., Piñeiro, Y., Cleeren, F., Bormans, G., … Rivas, J. (2019). Development of Superparamagnetic Nanoparticles Coated with Polyacrylic Acid and Aluminum Hydroxide as an Efficient Contrast Agent for Multimodal Imaging. Nanomaterials, 9(11), 1626. doi:10.3390/nano9111626

Guseva, L.I., Tikhomirova, G.S., Dogadkin, N.N. (2004). Anion-Exchange Separation of Radium from Alkaline-Earth Metals and Actinides in Aqueous-Methanol Solutions of HNO3. 227Ac/223Ra Generator. Radiochemistry, Vol. 46, No. 1, 58-62.

Handley-Sidhu, S., Mullan, T.K., Grail, Q., et al. (2016) , Sci. Rep., 2016, 6.

Haney, P.S., Gennaro, G.P. (1986). Hydroxylapatite-based 82Sr/82Rb generator. Sixth international symposium on radiopharmaceutical chemistry. Abstracts. Part IV. (1986). Journal of Labelled Compounds and Radiopharmaceuticals, 23(10-12), 1381–1382. doi:10.1002/jlcr.2580231005

Harvie, D. I. (1999). The radium century. Endeavour, 23(3), 100–105. doi:10.1016/s0160-9327(99)01201-6

Hassan, M. N., Mahmoud, M. M., El-Fattah, A. A., & Kandil, S. (2016). Microwave-assisted preparation of Nano-hydroxyapatite for bone substitutes. Ceramics International, 42(3), 3725–3744. doi:10.1016/j.ceramint.2015.11.044

Hennrich, U., & Benešová, M. (2020). [68Ga]Ga-DOTA-TOC: The First FDA-Approved 68Ga-Radiopharmaceutical for PET Imaging. Pharmaceuticals, 13(3), 38. doi:10.3390/ph13030038

Henriksen, G., Schoultz, B.W., Michaelsen, T.E., et al. (2004). Sterically stabilized liposomes as a carrier for α-emitting radium and actinium radionuclides. Nucl Med Biol, 31, 441–449. doi: 10.1016/j.nucmedbio.2003.11.004.

Hildebrand, H.; Schymura, S.; Holzwarth, U.; et al. (2015). Strategies for radiolabeling of commercial TiO2 nanopowder as a tool for sensitive nanoparticle detection in complex matrices. J Nanopart Res, Vol. 17, 278-289, ISSN 1572-896X.

HR IMD - HR Inorganics I. – Minerals database – FTIR, Thermo Scientific OMNIC, USA. Accessed May 2018.

Hrubý, M., Kučka, J., Kozempel, J., Lebeda, O. (2006). Cílené polymerní nosiče léčiv v terapii nádorových onemocnění. Chem. Listy, 100, 10–16.

Hsieh, M.F., Perng, L.H., Chin, T.S., Perng, H.G. (2001) Phase purity of sol-gel-derived hydroxyapatite ceramic. Biomaterials, 22, 2601-2607.

IAEA ^{99m}Tc KIT (2008). Technetium-99m radiopharmaceuticals: manufacture of kits. Vienna: International Atomic Energy Agency. ISSN 0074–1914, ISBN 978–92–0–100408–6

ICDD PDF-2 database, Version 2013, ISDD, USA.

Ichedef, C., Simonelli, F., Holzwarth, U., et al. (2013). Radiochemical synthesis of 105gAg-labelled silver nanoparticles. J Nanopart Res, 15:2073. doi: 10.1007/s11051-013-2073-8.

Ikeda, Y., Nagasaki, Y. (2011). PEGylation Technology in Nanomedicine. In: Polymers in Nanomedicine, Vol. 247 of the series Advances in Polymer Science. 115-140.

IKEM - Albumin v séru [cit 9.4.2022] Available online at
https://www2.ikem.cz/plm_lp/_LP_00507-L0000006.htm

Janiszewska, Ł.; Koźmiński, P.; Pruszyński, M.; et al. (2015). Gold Nanoparticle-Substance P(5-11) Conjugate as a Carrier for 211At in Alpha Particle Therapy. Abstrakt – 9th Symposium on Targeted Alpha Therapy, Varšava, Polsko.

Johnson's web site. [cit 3.3.2022] Available online at
https://www.johnsonsbaby.com/baby-products/johnsons-baby-powder-aloe-vitamin-e#ingredients

Jonasdottir, T.J., Fisher, D.R., Borrebæk3, J., et al. (2006). First In Vivo Evaluation of Liposome-encapsulated 223Ra as a Potential Alpha-particle-emitting Cancer Therapeutic Agent. Anticancer Research, 26: 2841-2848.

Joyston-Bechal, S., Duckworth, R., & Braden, M. (1967). The role of iso-ionic exchange in the uptake of 18F labelled fluoride by hydroxyapatite and enamel. Archives of Oral Biology, 12(10), 1097–1105. doi:10.1016/0003-9969(67)90057-x

Kalilight 2020 [cit 3.3.2022] Available online at
http://kalichem.it/allegati/A%20-%20KALILIGHT%20brochure.pdf

Kalita, S. J., Bhardwaj, A., & Bhatt, H. A. (2007). Nanocrystalline calcium phosphate ceramics in biomedical engineering. Materials Science and Engineering: C, 27(3), 441–449. doi:10.1016/j.msec.2006.05.018

Kaur, K., Singh, K. J., Anand, V., Islam, N., Bhatia, G., Kalia, N., & Singh, J. (2017). Lanthanide (=Ce, Pr, Nd and Tb) ions substitution at calcium sites of hydroxyl apatite nanoparticles as fluorescent bio probes: Experimental and density functional theory study. Ceramics International, 43(13), 10097–10108. doi:10.1016/j.ceramint.2017.05.029

Kilian, K. (2014). 68Ga-DOTA and analogs: Current status and future perspectives. Reports of Practical Oncology, 19, S13-S21. doi: 10.1016/j.rpor.2014.04.016.

Kim, H.L., Jung, G.Y., Yoon, Y.H., et al. (2015) Preparation and characterization of nano-sized hydroxyapatite/alginate/chitosan composite scaffolds for bone tissue engineering. Materials Science and Engineering: C, 54, 20-25. doi: 10.1016/j.msec.2015.04.033.

Kowalsky, R.J. (2006). Technetium Radiopharmaceutical Chemistry. University of New Mexico Health Sciences Center Pharmacy Continuing Education Albuquerque, New Mexico, 12(3).

Kozempel, J., Kománková, L., Šebesta, F., et al. (2014) Effect of mobile phase salinity on the Ac-227/Ra-223 generator. In: BOOKLET OF ABSTRACTS 17th Radiochemical Conference, 344.

Kozempel, J., Vlk, M., Málková, E., et al. (2015) Prospective carriers of 223Ra for targeted alpha particle therapy. J Radioanal Nucl Chem, 304(1), 443-447, doi: 10.1007/s10967-014-3615-y.

Kučka, J., Hrubý, M., Koňák, Č., et al. (2006) Astatination of nanoparticles containing silver as possible carriers of 211At. Appl Rad Isot, Vol. 64, 201-206, ISSN 0969-8043.

Kukleva, E., Suchánková, P., Štamberg, K., Vlk, M., Šlouf, M., & Kozempel, J. (2019). Surface protolytic property characterization of hydroxyapatite and titanium dioxide nanoparticles. RSC Advances, 9(38), 21989–21995. doi:10.1039/c9ra03698a

Lammers, T., Ulbrich, K., Ferreira, J.M.F., et al. (2010). HPMA copolymers: 30years of advances. Adv Drug Deliver Rev, 62(2), 119-121. doi: 10.1016/j.addr.2009.12.004.

LCN - Live Chart of Nuclides [online]. Austria: IAEA. 2021. [cit 6.7.2021] Available online at https://www-nds.iaea.org/relnsd/vcharthtml/VChartHTML.html

Lederman, M. (1981). The early history of radiotherapy: 1895–1939. International Journal of Radiation Oncology*Biology*Physics, 7(5), 639–648. doi:10.1016/0360-3016(81)90379-5

LeGeros, R.Z., Ito, A., Ishikawa, K., et al. (2009). Fundamentals of Hydroxyapatite and Related Calcium Phosphates. Advanced Biomaterials, 19. doi: 10.1002/9780470891315.ch2.

Liu, D.-M., Troczynski, T., & Tseng, W. J. (2001). Water-based sol–gel synthesis of hydroxyapatite: process development. Biomaterials, 22(13), 1721–1730. doi:10.1016/s0142-9612(00)00332-x

Liu, J., Ye, X., Wang, H., Zhu, M., Wang, B., & Yan, H. (2003). The influence of pH and temperature on the morphology of hydroxyapatite synthesized by hydrothermal method. Ceramics International, 29(6), 629–633. doi:10.1016/s0272-8842(02)00210-9

Madru, R., Kjellman, P., Olsson, F., Wingardh, K., Ingvar, C., Stahlberg, F., … Strand, S.-E. (2012). 99mTc-Labeled Superparamagnetic Iron Oxide Nanoparticles for Multimodality SPECT/MRI of Sentinel Lymph Nodes. Journal of Nuclear Medicine, 53(3), 459–463. doi:10.2967/jnumed.111.092437

Maeda, H., Nakamura, H., Fang, J., et al. (2013). The EPR effect for macromolecular drug delivery to solid tumors: Improvement of tumor uptake, lowering of systemic toxicity, and distinct tumor imaging in vivo. Adv Drug Deliv Rev, Vol. 65, 1, 71-79. doi: 10.1016/j.addr.2012.10.002.

Maeda, H., Tsukigawa, K., Fang. J. (2016). A Retrospective 30 Years After Discovery of the Enhanced Permeability and Retention Effect of Solid Tumors: Next-Generation Chemotherapeutics and Photodynamic Therapy—Problems, Solutions, and Prospects. Microcirculation, 23, 173–182.

Maia, A. L. C., Cavalcante, C. H., Souza, M. G. F. de, Ferreira, C. de A., Rubello, D., Chondrogiannis, S., … Soares, D. C. F. (2016). Hydroxyapatite nanoparticles. Nuclear Medicine Communications, 37(7), 775–782. doi:10.1097/mnm.0000000000000510

Málková, E. (2016) Příprava a studium nanonosičů pro nukleární medicínu. Praha 2016. Diplomová práce, FJFI ČVUT.

Matsumura, Y., Maeda, H. (1986). A New Concept for Macromolecular Therapeutics in Cancer Chemotherapy: Mechanism of Tumoritropic Accumulation of Proteins and the Antitumor Agent Smancs. Cancer Research, 46, 6387-6392.

Maus, S., Buchholz, H.-G., Ament, S., Brochhausen, C., Bausbacher, N., & Schreckenberger, M. (2011). Labelling of commercially available human serum albumin kits with 68Ga as surrogates for 99mTc-MAA microspheres. Applied Radiation and Isotopes, 69(1), 171–175. doi:10.1016/j.apradiso.2010.09.008

Mclaughlin, M.F., Woodward, J., Boll, R.A., et al. (2013). Gold Coated Lanthanide Phosphate Nanoparticles for Targeted Alpha Generator Radiotherapy. Plos One, Vol. 8, 1. doi: 10.1371/journal.pone.0054531.

McMurry, J. (2015) Organická chemie. Translated Budka, J., Cibulka, R., at al. Brno: Vysoké učení technické v Brně, VUTIUM. ISBN 978-80-214-4769-1.

Meisenheimer, M., Saenko, Y., Eppard, E. (2019). Gallium-68: Radiolabeling of Radiopharmaceuticals for PET Imaging - A Lot to Consider. Medical Isotopes. doi: 10.5772/intechopen.90615

Mendoza-Sánchez, A.N., Ferro-Flores, G., Ocampo-García, et al. (2010). Lys3-bombesin conjugated to 99mTc-labelled gold nanoparticles for in vivo gastrin releasing peptide-receptor imaging. J Biomed Nanotechnol, Vol. 6, No. 4, 375-384.

Mičolová, P., Sakmár, M., Málková, E., et al. (2016). Oxid titaničitý, perspektivní nosič teranostických radionuklidů, příprava, značení, stabilita in vitro. In: Nukleární medicína. Praha: Česká lékařská společnost Jana Evangelisty Purkyně, pp. 13-14. ISSN 1805-1146.

Mokhodoeva, O., Vlk, M., Málková, E., et al. (2016). Study of 223Ra uptake mechanism by Fe3O4 nanoparticles: towards new prospective theranostic SPIONs. J Nanopart Res, Vol. 18, 10. doi: 10.1007/s11051-016-3615-7.

Molinari, J., Snodgrass, W.J. (1990). THE CHEMISTRY AND RADIOCHEMISTRY OF RADIUM AND THE OTHER ELEMENTS OF THE URANIUM AND THORIUM NATURAL DECAY SERIES... p.11-56 https://inis.iaea.org/collection/NCLCollectionStore/_Public/21/039/21039568.pdf#page=21

Molinski, V. J. (1982). A review of 99mTc generator technology. The International Journal of Applied Radiation and Isotopes, 33(10), 811–819. doi:10.1016/0020-708x(82)90122-3

Morgenstern, A., Apostolidis, C., Kratochwil, C., Sathekge, M., Krolicki, L., & Bruchertseifer, F. (2018). An Overview of Targeted Alpha Therapy with 225Actinium and 213Bismuth. Current Radiopharmaceuticals, 11. doi:10.2174/1874471011666180502104524

Ng, K.T.Q., Olariu, C.I., Yaffee, M., et al. (2014). Indium-111 labeled gold nanoparticles for in-vivo molecular targeting. Biomaterials, Vol. 35, 7050-7057.

Notni, J., Pohle, K., Wester, H.J. (2012). Comparative gallium-68 labeling of TRAP-, NOTA-, and DOTA-peptides: practical consequences for the future of gallium-68-PET. EJNMMI Research, 2:28. doi: 10.1186/2191-219X-2-28.

Nykl, P. (2017). Studium záchytu a transportu značených nanočástic v rostlinách. Dipolomova prace, CVUT, FJFI.

Ocampo-García, B. E., Ramírez, F. de M., Ferro-Flores, G., et al. (2011 A). 99mTc-labelled gold nanoparticles capped with HYNIC-peptide/mannose for sentinel lymph node detection. Nuclear Medicine and Biology, 38(1), 1–11. doi:10.1016/j.nucmedbio.2010.07.007

Ocampo-García, B., Ferro-Flores, G., Morales-Avila, E., & Ramírez, F. de M. (2011 B). Kit for preparation of multimeric receptor-specific 99mTc-radiopharmaceuticals based on gold nanoparticles. Nuclear Medicine Communications, 32(11), 1095–1104. doi:10.1097/mnm.0b013e32834acf33

Orlova, M.A., Nikolaev, A.L., Trofimova, T.P., Orlov, A.P., Severin, A.V., & Kalmykov, S.N. (2018). Hydroxyapatite And Porphyrin-Fullerene Nanoparticles For Diagnostic And Therapeutic Delivery Of Paramagnetic Ions And Radionuclides. Bulletin Of Rsmu, 6. doi:10.24075/brsmu.2018.075

Othmani, M., et al. (2016). Synthesis and characterization of hydroxyapatite-based nanocomposites by the functionalization of hydroxyapatite nanoparticles with phosphonic acids. Colloid Surface A, 508, 336-344.

Otte, A., Jermann, E., Behe, M., Goetze, M., et al. (1997). DOTATOC: A powerful new tool for receptor-mediated radionuclide therapy. European Journal of Nuclear Medicine, 24(7), 792–795. doi:10.1007/bf00879669

Owusu Asimeng, B., Walter Afeke, D., & Kwason Tiburu, E. (2020). Biomaterial for Bone and Dental Implants: Synthesis of B-Type Carbonated Hydroxyapatite from Biogenic Source. Biomaterials. doi:10.5772/intechopen.92256

Passah, A., Tripathi, M., Ballal, S., et al. (2017). Evaluation of bone-seeking novel radiotracer 68Ga-NO2AP-Bisphosphonate for the detection of skeletal metastases in carcinoma breast: towards new prospective theranostic SPIONs. Eur J Nucl Med Mol Imaging, 44(1):41-49. Epub 2016. doi: 10.1007/s00259-016-3469-3.

Pérez-Campaña, C., Sansaloni, F., Gómez-Vallejo, V., et al (2014). Production of 18F-Labeled Titanium Dioxide Nanoparticles by Proton Irradiation for Biodistribution and Biological Fate Studies in Rats. Particle & Particle Systems Characterization, 31(1), 134–142. doi:10.1002/ppsc.201300302

Piotrowska, A., Męczyńska-Wielgosz, S., Majkowska-Pilip, A., et al (2017). Nanozeolite bioconjugates labeled with 223Ra for targeted alpha therapy. Nuclear Medicine and Biology, 47(), 10–18. doi:10.1016/j.nucmedbio.2016.11.005

Polyak, A., Naszalyi Nagy, L., Mihaly, J., Görres, S., et al. (2017). Preparation and 68Ga-radiolabeling of porous zirconia nanoparticle platform for PET/CT-imaging guided drug delivery. Journal of Pharmaceutical and Biomedical Analysis, 137, 146–150. doi:10.1016/j.jpba.2017.01.028

Radiesse. Dermal Fillers from Radiesse. [cit. 7.2.2017]. Available online at http://www.radiesse.com/

Raina, D. B., Liu, Y., Isaksson, H., Tägil, M., & Lidgren, L. (2019). Synthetic hydroxyapatite: a recruiting platform for biologically active molecules. Acta Orthopaedica, 1–9. doi:10.1080/17453674.2019.1686865

Rajeswari, A., Vimalnath, K. V., Sarma, H. D., et al. (2016). Hydroxyapatite (HA) microparticles labeled with 32P – A promising option in the radiation synovectomy for inflamed joints. Applied Radiation and Isotopes, 116, 85–91. doi:10.1016/j.apradiso.2016.07.022

Rathmann, S. M., Ahmad, Z., Slikboer, S., Bilton, H. A., Snider, D. P., & Valliant, J. F. (2019). The Radiopharmaceutical Chemistry of Technetium-99m. Radiopharmaceutical Chemistry, 311–333. doi:10.1007/978-3-319-98947-1_18

Rigali, M. J., Brady, P. V., & Moore, R. C. (2016). Radionuclide removal by apatite. American Mineralogist, 101(12), 2611–2619. doi:10.2138/am-2016-5769

Rivera-Muñoz, E.M. (2011) Hydroxyapatite-Based Materials: Synthesis and Characterization, Biomedical Engineering - Frontiers and Challenges. In: InTech. [cit. 10.2.2017]. Available online at http://www.intechopen.com/books/biomedical-engineering-frontiers-and-challenges/hydroxyapatitebased-materials-synthesis-and-characterization

Rojas, J. V., Woodward, J. D., Chen, N., Rondinone, A. J., Castano, C. H., & Mirzadeh, S. (2015). Synthesis and characterization of lanthanum phosphate nanoparticles as carriers for 223 Ra and 225 Ra for targeted alpha therapy. Nuclear Medicine and Biology, 42(7), 614–620. doi:10.1016/j.nucmedbio.2015.03.007

Ruparelia, J.P., Chatterjee, A.K., Duttagupta, S.P., et al. (2007). Strain specificity in antimicrobial activity of silver and copper nanoparticles. Acta Biomaterialia, 4(3), 707-716. doi: 10.1016/j.actbio.2007.11.006.

Rusu, V., Ng, C., Wilke, M., et al. (2005). Size-controlled hydroxyapatite nanoparticles as self-organized organic-inorganic composite materials. Biomaterials, 26(26), 5414-5426. doi: 10.1016/j.biomaterials.2005.01.051.

Sanchez-Crespo, A. (2013). Comparison of Gallium-68 and Fluorine-18 imaging characteristics in positron emission tomography. Applied Radiation and Isotopes, 76, 55–62. doi:10.1016/j.apradiso.2012.06.034

Sandhöfer, B., Meckel, M., Delgado-López, J. M., Patrício, T., Tampieri, A., Rösch, F., & Iafisco, M. (2015). Synthesis and Preliminary in Vivo Evaluation of Well-Dispersed Biomimetic Nanocrystalline Apatites Labeled with Positron Emission Tomographic Imaging Agents. ACS Applied Materials & Interfaces, 7(19), 10623–10633. doi:10.1021/acsami.5b02624

Sangi web site. [cit 3.3.2022] Available online at https://www.sangi-co.com/en/company/apataite-company/index.html

Saxena, V., Shukla, I., & Pandey, L. M. (2019). Hydroxyapatite: an inorganic ceramic for biomedical applications. Materials for Biomedical Engineering, 205–249. doi:10.1016/b978-0-12-816909-4.00008-7

Scarpa, L., Buxbaum, S., Kendler, D., Fink, K., Bektic, J., Gruber, L., … Virgolini, I. (2017). The 68Ga/177Lu theragnostic concept in PSMA targeting of castration-resistant prostate cancer: correlation of SUVmax values and absorbed dose estimates. European Journal of Nuclear Medicine and Molecular Imaging, 44(5), 788–800. doi:10.1007/s00259-016-3609-9

Sheka, I.A., Chaus, I.S., Mityureva, T.T. (1963). Галлий. Гостехиздат, Kyiv, USSR.

Smith, L., Kuncic, Z., Ostrikov, K., et al. (2012). Nanoparticles in Cancer Imaging and Therapy. J Nanomater, doi: 10.1155/2012/891318

Sobkuliaková, Z., Valová, V., Kukleva, E., et al. (2019). Štúdium nosičov značených 99mTc pre viacfázovú angiogénnu diagnostikuю In: Zborník recenzovaných príspevkov. Vydavateľstvo UK. ISBN 978-80-223-4711-2

Song, J., Saiz, E., Bertozzi, C.R., Tomsia, A.P. (2008). Flexible Hydrogel-based Functional Materials. USA. US 2008/0275171 A1. Patent.

Sonmez, E., Cacciatore, I., Bakan, F., et al. (2016). Toxicity assessment of hydroxyapatite nanoparticles in rat liver cell model in vitro: 30years of advances. Human and Experimental Toxicology, 35(10), 1073-1083. doi: 10.1177/0960327115619770.

SPC 68GA-PSMA-11. [cit. 10.5.2021]. Available online at https://www.sukl.cz/modules/medication/search.php

SPC Amyvid. [cit. 10.5.2021]. Available online at https://www.sukl.cz/modules/medication/search.php

SPC Axumin. [cit. 10.5.2021]. Available online at https://www.sukl.cz/modules/medication/search.php

SPC DMSA. [cit. 10.5.2021]. Available online at https://www.sukl.cz/modules/medication/search.php

SPC Fluorocholine. [cit. 10.5.2021]. Available online at https://www.sukl.cz/modules/medication/search.php

SPC Galli Ad. [cit. 10.5.2021]. Available online at https://www.sukl.cz/modules/medication/search.php

SPC GalliaPharm. [cit. 10.5.2021]. Available online at https://www.sukl.cz/modules/medication/search.php

SPC HDP. [cit. 10.5.2021]. Available online at https://www.sukl.cz/modules/medication/search.php

SPC NaF. [cit. 10.5.2021]. Available online at https://www.sukl.cz/modules/medication/search.php

SPC Neuraceq. [cit. 10.5.2021]. Available online at https://www.sukl.cz/modules/medication/search.php

SPC Ontak. [cit. 10.5.2021]. Available online at https://www.accessdata.fda.gov/drugsatfda_docs/label/2008/103767s5094lbl.pdf

SPC Poltechnet. [cit. 10.5.2021]. Available online at https://www.sukl.cz/modules/medication/search.php

SPC Ultra Technekow. [cit. 10.5.2021]. Available online at https://www.sukl.cz/modules/medication/search.php

SPC Xofigo. [cit. 10.5.2021]. Available online at https://www.ema.europa.eu/en/documents/product-information/xofigo-epar-product-information_cs.pdf

Stojanović, Z.S., Ignjatović, N., Wu, V., et al. (2016). Hydrothermally processed 1D hydroxyapatite: Mechanism of formation and biocompatibility studies. Materials Science and Engineering: C, 68(10), 746-757. doi: 10.1016/j.msec.2016.06.047.

Suchánková, P., Kukleva, E., Nykl, E. et al. (2020 A). Hydroxyapatite and Titanium Dioxide Nanoparticles: Radiolabelling and In Vitro Stability of Prospective Theranostic Nanocarriers for 223Ra and 99mTc. Nanomaterials, 10(9), 1632. doi:10.3390/nano10091632

Suchankova, P., Kukleva, E., Stamberg, K. et al (2020 B). Study of 223Ra uptake mechanism on hydroxyapatite and titanium dioxide nanoparticles as a function of pH. RSC Adv., 10, 3659-3666. doi: 10.1039/C9RA08953E

Suchankova, p., Kukleva, E., Stamberg, K. et al. (2020 C). Determination, Modeling and Evaluation of Kinetics of 223Ra Sorption on Hydroxyapatite and Titanium Dioxide Nanoparticles. Materials 2020, 13(8), 1915. doi: 10.3390/ma13081915

Taniguchi, N. (1974). On the Basic Concept of 'Nano-Technology, Proc. Intl. Conf. Prod. Eng. Tokyo, Part II, Japan Society of Precision Engineering.

Tantawy, M.N. et al. (2021) Detection and treatment of Ovarian cancer by targeting tumor extracellular hydroxyapatite: a new paradigm. Report [cit 10.4.2022] Available online at https://apps.dtic.mil/sti/pdfs/AD1146192.pdf

Teixeira, C.M.A., Piccirillo, C., Tobaldi, D.M. et al. (2017). Effect of preparation and processing conditions on UV absorbing properties of hydroxyapatite-Fe2O3 sunscreen: Mechanism of formation and biocompatibility studies. Materials Science and Engineering: C, 71(10), 141-149. doi: 10.1016/j.msec.2016.09.065.

Thakor, A.S., Gambhir, S.S. (2013). Nanooncology: The Future of Cancer Diagnosis and Therapy. CA CANCER J CLIN, 63, 395–418.

Thomson, B. M., Smith, C. L., Busch, R. D., Siegel, M. D., & Baldwin, C. (2003). Removal of Metals and Radionuclides Using Apatite and Other Natural Sorbents. Journal of Environmental Engineering, 129(6), 492–499. doi:10.1061/(asce)0733-9372(2003)129:6(492)

Toro-González, M., Dame, A. N., Foster, C. M., Millet, L. J., Woodward, J. D., Rojas, J. V., … Davern, S. M. (2020). Quantitative encapsulation and retention of 227Th and decay daughters in core–shell lanthanum phosphate nanoparticles. Nanoscale, 12(17), 9744–9755. doi:10.1039/d0nr01172j

Turturro, F. (2014). Denileukin diftitox: a biotherapeutic paradigm shift in the treatment of lymphoid-derived disorders. Expert Rev Anticancer Ther, 7(1), 11-17. doi: 10.1586/14737140.7.1.11.

Ulbrich, K., Šubr, V., Tobaldi, D.M. et al. (2010). Structural and chemical aspects of HPMA copolymers as drug carriers: Mechanism of formation and biocompatibility studies. Adv Drug Deliver Rev, 62(2), 150-166. doi: 10.1016/j.addr.2009.10.007.

Unni, P. ., Chaudhari, P. ., Venkatesh, M., Ramamoorthy, N., & Pillai, M. R. . (2002). Preparation and bioevaluation of 166 Ho labelled hydroxyapatite (HA) particles for radiosynovectomy. Nuclear Medicine and Biology, 29(2), 199–209. doi:10.1016/s0969-8051(01)00303-1

Vasey, P.A., Kaye, S.B., Morrison, R. (1999). Phase I Clinical and Pharmacokinetic Study of PK1 [N-(2-Hydroxypropyl)methacrylamide Copolymer Doxorubicin]: First Member of a New Class of Chemotherapeutic Agents—Drug-Polymer Conjugates. Clinical Cancer Research, Vol. 5, 83–94.

Vasiliev, A.N., Severin, A., Lapshina, E. et al. (2017). Hydroxyapatite particles as carriers for 223Ra. J Radioanal Nucl Chem 311, 1503–1509. https://doi.org/10.1007/s10967-016-5007-y

Velikyan, I. (2014) Prospective of 68 Ga-Radiopharmaceutical Development. Theranostics, 4(1), 47-80. doi: 10.7150/thno.7447.

Vimalnath, K. V., Chakraborty, S., Rajeswari, A., Sarma, H. D., Nuwad, J., Pandey, U., … Dash, A. (2015). Radiochemistry, pre-clinical studies and first clinical investigation of 90 Y-labeled hydroxyapatite (HA) particles prepared utilizing 90 Y produced by (n,γ) route. Nuclear Medicine and Biology, 42(5), 455–464. doi:10.1016/j.nucmedbio.2015.01.006

Vimalnath, K.V., Chakraborty, S., Rajeswari, A., et al (2015). Nucl. Med. Biol., 2015, 42 , 455 —464 CrossRef CAS .

Weber, J., Haberkorn, U., & Mier, W. (2015). Cancer Stratification by Molecular Imaging. International Journal of Molecular Sciences, 16(3), 4918–4946. doi:10.3390/ijms16034918

Weidner, J. W., Mashnik, S. G., John, K. D., Ballard, B., Birnbaum, E. R., Bitteker, L. J., … Nortier, F. M. (2012). 225Ac and 223Ra production via 800MeV proton irradiation of natural thorium targets. Applied Radiation and Isotopes, 70(11), 2590–2595. doi:10.1016/j.apradiso.2012.07.003

Wijesinghe, W.P.S.L., Mantilaka, M.M.M.G.P.G., Premalal, E.V.A., et al. (2014). Facile synthesis of both needle-like and spherical hydroxyapatite nanoparticles: Effect of synthetic temperature and calcination on morphology, crystallite size and crystallinity. Materials Science and Engineering: C, 42, 83-90. doi: 10.1016/j.msec.2014.05.032.

Wilson, I. (2000). Encyclopedia of Separation Science, 1st Edition - August 23. Appendix 12a. ISBN: 9780080917795

Woodward, J., Kennel, S.J., Stuckey, A., et al. (2011). LaPO4 Nanoparticles Doped with Actinium-225 that Partially Sequester Daughter Radionuclides. Bioconjugate Chem, 22, 766–776. doi: 10.1021/bc100574f.

Zhang, Y., Tao, J., Pang, Y., et al. (2006). Electrochemical deposition of hydroxyapatite coatings on titanium. Transactions of Nonferrous Metals Society of China, 16(3), 633-637. doi: 10.1016/S1003-6326(06)60112-X.

Zhao, L., Wen, S., Zhu, M., Li, D., Xing, Y., Shen, M., … Zhao, J. (2018). 99mTc-labelled multifunctional polyethylenimine-entrapped gold nanoparticles for dual mode SPECT and CT imaging. Artificial Cells, Nanomedicine, and Biotechnology, 1–11. doi:10.1080/21691401.2018.1430696

Zheng, J., & Zhou, W. (2012). In Vivo Imaging of Nano-hydroxyapatite Biodistribution Using Positron Emission Tomography Imaging. Chemistry Letters, 41(12), 1606–1607. doi:10.1246/cl.2012.1606

Zhu, A., Lu, J., Zhou, Y., Dai, S. (2010). Spherical N-carboxyethylchitosan/hydroxyapatite nanoparticles prepared by ionic diffusion process in a controlled manner. J Mater Sci: Mater Med, 21, 3095–3101. doi: 10.1007/s10856-010-4157-7

Zitzmann-Kolbe, S., Hammer, S., Hennekes, H., et al. (2019). Targeted Alpha Therapy with PSMA-TTC: Preclinical Activity at Different Dosing Schedules and Total Antibody Doses in Prostate Cancer Xenograft Models. Journal of Medical Imaging and Radiation Sciences, 50(1), S4. doi:10.1016/j.jmir.2019.03.013

Zuo, G., Wei, X., Sun, H., et al. (2017). Morphology controlled synthesis of nano-hydroxyapatite using polyethylene glycol as a template. J Alloy Compd, 692(1), 693-697. doi: 10.1016/j.jallcom.2016.09.117.

Publication List

Published articles:

- Kukleva, E., Suchánková, P., Štamberg, K., Vlk, M., Šlouf, M., Kozempel, J. (2019). Surface protolytic property characterization of hydroxyapatite and titanium dioxide nanoparticles. RSC Advances. 21989-21995. ISSN 2046-2069.
- Kukleva, E., Kozempel, J., Vlk, M., Mičolová, P., Vopálka, D. (2015). Preparation of 227Ac/223Ra by neutron irradiation of 226Ra. Journal of Radioanalytical and Nuclear Chemistry, 304(1), 263-266. ISSN 0236-5731.
- Manaenkov, A., Steinerova, M., Kukleva, E. (2021). Effect of Kaolin Addition into Metakaolin Geopolymer Composite. Journal of Materials in Civil Engineering (ASCE). 33(1), ISSN 0899-1561.
- Suchánková, P., Kukleva, E., Nykl, E., Nykl, P., Sakmár, M., Vlk, M., Kozempel, J. (2020). Hydroxyapatite and Titanium Dioxide Nanoparticles: Radiolabelling and In Vitro Stability of Prospective Theranostic Nanocarriers for 223Ra and 99mTc. Nanomaterials. 10(9), ISSN 2079-4991.
- Suchánková, P., Kukleva, E., Štamberg, K., Nykl, P., Sakmár, M., Vlk, M., Kozempel, J. (2020). Determination, Modelling and Evaluation of Kinetics of 223Ra Sorption on Hydroxyapatite and Titanium Dioxide Nanoparticles. Materials. 13(8), ISSN 1996-1944.
- Suchánková, P., Kukleva, E., Štamberg, K., Nykl, P., Vlk, M., Kozempel, J. (2020). Study of 223Ra uptake mechanism on hydroxyapatite and titanium dioxide nanoparticles as a function of pH. RSC Advances. 10(7), 3659-3666. ISSN 2046-2069.
- Mokhodoeva, O., Vlk, M., Málková, E., Kukleva, E., Mičolová, P., Štamberg, K., Šlouf, M., Dzhenloda, R et al. (2016). Study of 223Ra uptake mechanism by Fe3O4 nanoparticles: towards new prospective theranostic SPIONs. Journal of Nanoparticle Research. ISSN 1388-0764.

- Bajzíková, A., Kozempel, J., Vlk, M., Kukleva, E., Mičolová, P. (2016). Kontrola kvality eluátu 223Ra. Nukleární medicína. 5(2), 22-26. ISSN 1805-1146.

Patents:

- Kozempel, J., Vlk, M., Suchánková, P., Kukleva, E., Fialová, K., Kománková, L., Bajziková, A., Svoboda, K. et al. (2020). Method for isolation Ac from mixture of Radium, Actinium and Thorium. European Patent Office. Patent EP3430177.
- Kozempel, J., Vlk, M., Mičolová, P., Kukleva, E., Jandová, L., Merhautová, H., Ficenzová, K. (2018). Kombinace pro radionuklidovou terapii pro použití jako léčivo. Czechia. Patent CZ 307369.
- Kozempel, J., Vlk, M., Mičolová, P., Kukleva, E., Fialová, K., Kománková, L., Bajzíková, A., Podlaha, J. et al. (2017). Způsob izolace Ac ze směsi radia, aktinia a thoria. Czechia. Patent CZ 306722.
- Kozempel, J.; Vlk, M.; Mičolová, P.; Kukleva, E.; Jandová, L.; Merhautová, H.; Ficenzová, K. Sada pro radionuklidovou terapii a její použití, 2016 - Patentová přihláška

Functional Samples:

- Suchánková, P., Červenák, J., Skálová, M., Palušák, M., Kukleva, E., Kozempel, J. (2022). Preparát radionuklidově čistého Tb-161. Functional Sample
- Adámek, K., Šebesta, F., Vlk, M., Fialová, K., Kozempel, J., Kukleva, E. (2018). Sorbent pro radionuklidový generátor 68Ge/68Ga. Functional Sample
- Kukleva, E., Kozempel, J., Vlk, M., Sakmár, M., Fialová, K., Lobaz, V., Hrubý, M. (2017). [99mTc]HAp-PEG. Functional Sample
- Kukleva, E., Sakmár, M., Kozempel, J., Vlk, M., Suchánková, P., Lobaz, V., Hrubý, M. (2017). [99mTc]HAp-PEOX. Functional Sample

- Kukleva, E., Kozempel, J., Vlk, M. (2017). [18F]F-nHAp. Functional Sample
- Vlk, M., Bajzíková, A., Kukleva, E., Mičolová, P., Kozempel, J., Náhunek, M. (2015). HPLC kolona s makroporézním sorbentem. Functional Sample

Conferences:

2021

- Skálová, M., Palušák, M., Kukleva, J., Fialová, K., Kozempel, J., Suchánková, P. (2021). Separace terbia, gadolinia a dysprosia pro účely přípravy radiofarmak značených 161Tb. Zborník recenzovaných príspevkov. Univerzita Komenského v Bratislave, 738-743. ISBN 978-80-223-5132-4.

2020

- Janská, T., Kukleva, E. (2020). Účinnost značení nanočástic hydroxyapatitu a oxidu titaničitého Ga-68 v závislosti na pH. Nukleární medicína molekulární výzkum, diagnostika a terapie. Praha: Česká lékařská společnost J. E. Purkyně. vol. 4. ISSN 1805-1146.
- Bátorová, K., Kukleva, E., Kozempel, J. (2020). Stanovenie rádionuklidovej čistoty vybraných medicinálnych nuklidov pomocou extrakčnej chromatografie na papieri. Nukleární medicína molekulární výzkum, diagnostika a terapie. Praha: Česká lékařská společnost J. E. Purkyně. vol. 4. ISSN 1805-1146.

2019

- Kozempel, J., Kukleva, E., Suchánková, P., Vlk, M., Jandová, L., Merhautová, J., Ficenzová, K. (2019). Tuning of the Radium biodistribution by Dietary Supplements in a CD1 Mice Model. 11th International Symposium on Targeted-Alpha-Therapy. Toronto: THE JOURNAL OF MEDICAL IMAGING ANDRADIATION SCIENCES.
- Sakmár, M., Kukleva, E., Suchánková, P., Vlk, M., Nykl, E., Nykl, P., Kozempel, J. (2019). VÝSKUM A VÝVOJ HYDROXYAPATITU AKO NOSIČA RÁDIOFARMAK PRE NUKLEÁRNU MEDICÍNU. XLI. pracovní dny

Radiofarmaceutické sekce České společnosti nukleární medicíny ČLS JEP. Prague: ČLS JEP.

- Kukleva, E., Suchánková, P. (2019). NOVÁ RYCHLÁ METODA KONTROLY KVALITY SESTAMIBI ANEB ČISTOTA MIBI ZA 10 MINUT BEZ CHLOROFORMU. XLI. pracovní dny Radiofarmaceutické sekce České společnosti nukleární medicíny ČLS JEP. Prague: ČLS JEP.

- Sobkuliaková, Z., Valová, V., Kukleva, E., Sakmár, M., Lobaz, V., Hrubý, M., Vlk, M., Kozempel, J. et al. (2019). Štúdium nosičov značených 99mTc pre viacfázovú angiogénnu diagnostiku. Zborník recenzovaných príspevkov. Vydavateľstvo UK. ISBN 978-80-223-4711-2.

- Sakmár, M., Suchánková, P., Kukleva, E., Lobaz, V., Nový, Z., Vlk, M., Hrubý, M., Petřík, M. et al. (2019). Modifikácia nanočastíc HAp s využitím fosfónových ligandov. Zborník recenzovaných príspevkov. Vydavateľstvo UK. ISBN 978-80-223-4711-2.

- Valová, V., Sobkuliaková, Z., Kukleva, E., Lobaz, V., Šlouf, M., Hrubý, M., Vlk, M., Kozempel, J. (2019). Zobrazovací magnetické sondy značené Ga-68. Zborník recenzovaných príspevkov. Vydavateľstvo UK, 984-988. ISBN 978-80-223-4711-2.

2018

- Sakmár, M., Suchánková, P., Kukleva, E., Kozempel, J., Vlk, M. (2018). Surface modification of 99mTC-HAp-NPs. Czech Chemical Society Symposium Series 16 (2). Praha: Česká společnost chemická, 16. vol. 2. ISSN 2336-7202.

- Valová, V., Sobkuliaková, Z., Kukleva, E., Mokhodoeva, O., Vlk, M., Kozempel, J. (2018). Magnetické nanočástice značené 68Ga a 18F. 55. Dny Nukleární Medicíny. Praha: Česká lékařská společnost J. E. Purkyně. ISSN 1805-1146.

- Kukleva, E., Čepa, A. (2018). Farmaka pro cílenou alfa terapii-klinické zkoušky. 55. Dny Nukleární Medicíny. Praha: Česká lékařská společnost J. E. Purkyně. ISSN 1805-1146.

- Valová, V., Sobkuliaková, Z., Kukleva, E., Sakmár, M., Mokhodoeva, O., Vlk, M., Kozempel, J. (2018). THERANOSTIC SUPERPARAMAGNETIC IRON OXIDE NANOVECTORS. Symposium Scientific Programme and Collection of Abstracts. Praha: Česká společnost chemická. ISBN 978-80-86238-89-0.
- Sakmár, M., Vlk, M., Suchánková, P., Kukleva, E., Kozempel, J., Hrubý, M., Lobaz, A. (2018). In vitro and in vivo studies of 223Ra labelled HAp nanoparticles modificated with phosphonic acids. Symposium Scientific Programme and Collection of Abstracts. Praha: Česká společnost chemická. ISBN 978-80-86238-89-0.
- Kukleva, E., Vlk, M., Kozempel, J. (2018). HYDROXYAPATITE NANOPARTICLES LABELLED WITH 18F. Czech Chemical Society, Symposium Series 2. Praha: Česká společnost chemická. ISSN 2336-7202.
- Kukleva, E., Vlk, M., Kozempel, J., Suchánková, P. (2018). DOTA DECORATED HYDROXYAPATITE NANOPARTICLES LABELLED WITH 68Ga. Symposium Scientific Programme and Collection of Abstracts. Praha: Česká společnost chemická. ISBN 978-80-86238-89-0.
- Kozempel, J., Vlk, M., Kukleva, E., Sakmár, M., Suchánková, P. (2018). HYDROXYAPATITE NANOPARTICLES AS THERANOSTIC VECTORS FOR RADIOPHARMACY. Symposium Scientific Programme and Collection of Abstracts. Praha: Česká společnost chemická. ISBN 978-80-86238-89-0.
- Sobkuliaková, Z., Valová, V., Kukleva, E., Sakmár, M., Mokhodoeva, O., Vlk, M., Kozempel, J. (2018). LABELLED SUPERPARAMAGNETIC IRON OXIDE NANOPARTICLES. Czech Chemical Society, Symposium Series 2. Praha: Česká společnost chemická. ISSN 2336-7202.

2017

- Kukleva, E., Vlk, M., Kozempel, J. (2017). Alfa a beta zářiče v terapii. Kutnohorský experiment - Studentská konference radiologické fyziky. Praha: ČVUT, Fakulta jaderná a fyzikálně inženýrská, KDAIZ.
- Kozempel, J., Vlk, M., Suchánková, P., Kukleva, E., Nykl, P., Sakmár, M. (2017). Nanonosiče 223Ra pro cílenou alfa-částicovou terapii. 54. Dny

Nukleární Medicíny. Praha: Česká lékařská společnost J. E. Purkyně. ISSN 1805-1146.

- Kukleva, E., Mičolová, P., Nykl, P., Sakmár, M., Vlk, M., Kozempel, J., Nespesna, L. (2017). Hydroxyapatite nanoparticles labelled with medicinal radionuclides. The 22nd International Symposium on Radiopharmaceutical Sciences. New York: J. Wiley. vol. 60. ISSN 0362-4803.
- Mičolová, P., Kukleva, E., Nykl, P., Sakmár, M., Vlk, M., Nespesna, L., Kozempel, J. (2017). Titanium Dioxide - perspective nanocarrier material for medicinal nuclides delivery systems. The 22nd International Symposium on Radiopharmaceutical Sciences. New York: J. Wiley. vol. 60. ISSN 0362-4803.
- Kozempel, J., Vlk, M., Mičolová, P., Kukleva, E., Nykl, P., Sakmár, M. (2017). Nanocarriers of 223Ra for TAT. 10th International Symposium on Targeted Alpha Therapy. Ispra: European Commission - Joint Research Centre.
- Valová, V., Kukleva, E., Mičolová, P., Kománková, L., Vlk, M., Kozempel, J. et al. (2017). Superparamagnetické 'core-shell' nanosondy. XXXIX. Pracovní dny Radiofarmaceutické sekce České společnosti nukleární medicíny. Praha: ČLS JEP.
- Vlk, M., Nykl, P., Sakmár, M., Málková, E., Kukleva, E., Mičolová, P., Lobaz, V, Šlouf, M et al. (2017). Stabilizace nanonosičů před značením 99mTc, 68Ga a 223Ra. XXXIX. Pracovní dny Radiofarmaceutické sekce České společnosti nukleární medicíny. Praha: ČLS JEP.
- Kukleva, E., Mičolová, P., Kozempel, J., Vlk, M., Sakmár, M. (2017). Nanočástice hydroxyapatitu značené 68Ga a 18F. XXXIX. Pracovní dny Radiofarmaceutické sekce České společnosti nukleární medicíny. Praha: ČLS JEP.
- Kozempel, J., Vlk, M., Mičolová, P., Kukleva, E., Málková, E., Sakmár, M., Nykl, P., Lobaz, V. et al. (2016). Nanohydroxyapatity - univerzální biokompatibilní nosiče pro radiofarmacii. Nukleární medicína. Praha: Česká lékařská společnost Jana Evangelisty Purkyně. ISSN 1805-1146.

2016

- Mičolová, P., Sakmár, M., Málková, E., Kukleva, E., Vlk, M., Kozempel, J. (2016). Oxid titaničitý, perspektivní nosič teranostických radionuklidů, příprava, značení, stabilita in vitro.. Nukleární medicína. Praha: Česká lékařská společnost Jana Evangelisty Purkyně. ISSN 1805-1146.
- Mičolová, P., Kukleva, E., Málková, E., Vlk, M., Nykl, P., Sakmár, M., Kozempel, J. (2016). Příprava, stabilizace a značení oxidu titaničitého 99mTc a 223Ra pro nukleární medicínu. Czech Chemical Society Symposium Series 14 (5). Praha: Česká společnost chemická, vol. 14, 218. ISSN 2336-7202.
- Mičolová, P., Málková, E., Kukleva, E., Vlk, M., Nykl, P., Sakmár, M., Kozempel, J. (2016). Příprava stabilizovaných nanočástic. XXXVIII. Pracovní dny radiofarmaceutické sekce České společnosti nukleární medicíny, Sborník.

2015

- Marešová, L.; Jandová, L.; Málková, E.; Mičolová, P.; Kukleva, E.; Nykl, P.; Vlk, M.; Kozempel, J. : In vivo stabilitní studie ^{223}Ra značeného nanohydroxyapatitu. In: Nukleární medicína. 2015, pp. 16. ISSN 1805-1146.
- Vlk, M.; Mičolová, P.; Málková, E.; Kukleva, E.; Nykl, P.; Sakmár, M.; Kozempel, J.: Příprava hydroxyapatitů jako teranostických nosičů, značení a stabilita in vitro. In: Nukleární medicína. 2015, pp. 15-16. ISSN 1805-1146.
- Mičolová, P.; Málková, E.; Kukleva, E.; Vlk, M.; Kozempel, J.: 223-Ra and 99m-Tc Labelled Titanium Dioxide Nanoparticles. In: Molecular and Supramolecular Carriers for Imaging and Therapy. 2015, pp. 39.
- Vlk, M.; Mičolová, P.; Málková, E.; Bajzíková, A.; Kukleva, E.; Kománková, L.; Sakmár, M.; Kozempel, J.: Radium-223 labelled nanocarriers for alpha radionuclide therapy. In: Molecular and Supramolecular Carriers for Imaging and Therapy. 2015, pp. 8.

- Mičolová, P.; Málková, E.; Kukleva, E.; Vlk, M.; Kozempel, J.: ^{99m}Tc and ^{223}Ra Labelled Hydroxyapatite nanoparticles as potential Theranostic agents for nuclear medicine. In: 9th Symposium on targeted Alpha Therapy. 2015, pp. 42.

- Kukleva, E.; Kozempel, J.; Vlk, M.; Mičolová, P.; Vopálka, D.: Příprava ^{227}Ac z ^{226}Ra ozařováním neutrony. In: Zborník recenzovaných príspevkov - Študentská vedecká konferencia PriF UK 2015. Bratislava: Univerzita Komenského, 2015, pp. 1007-1011. ISBN 978-80-223-3859-2.

- Mičolová, P.; Málková, E.; Kukleva, E.; Vlk, M.; Kozempel, J.: In vitro stability značených nosičů ^{223}Ra a ^{99m}Tc. In: Zborník recenzovaných príspevkov - Študentská vedecká konferencia PriF UK 2015. Bratislava: Univerzita Komenského, 2015, pp. 1053-1058. ISBN 978-80-223-3859-2.

2014

- Bajzíková, A.; Kozempel, J.; Vlk, M.; Kukleva, E.; Mičolová, P. Kontrola kvality eluátu ^{223}Ra. In: Nukleární medicína. 2014, pp. 18. ISSN 1805-1146.

- Kukleva, E.; Aksenov, N.; Kozempel, J.; Vlk, M.: Synthesis of complexes based on platinum. In: BOOKLET OF ABSTRACTS 17th Radiochemical Conference. 2014, pp. 455. 1. ISBN 978-80-01-05504-5.

- Kozempel, J.; Kománková, L.; Šebesta, F.; Vlk, M.; Kukleva, E.; Mičolová, P.: Effect of mobile phase salinity on the Ac-227/Ra-223 generator. In: BOOKLET OF ABSTRACTS 17th Radiochemical Conference. 2014, pp. 344. 1. ISBN 978-80-01-05504-5.

- Kukleva, E.; Kozempel, J.; Vlk, M.; Mičolová, P.; Vopálka, D.: Preparation of ^{223}Ra by neutron irradiation of ^{226}Ra. In: BOOKLET OF ABSTRACTS 17th Radiochemical Conference. 2014, pp. 276. 1. ISBN 978-80-01-05504-5.